UNIVERSITY OF CALIFORNIA
SANTA CRUZ

A MULTIFACETED INVESTIGATION OF FISH DISPERSAL IN THE EASTERN PACIFIC

A dissertation submitted in partial satisfaction
of the requirements for the degree of

DOCTOR OF PHILOSOPHY

In

ECOLOGY & EVOLUTIONARY BIOLOGY

By

Katherine E. Dale

June 2022

The Dissertation of Katherine E. Dale is approved:

_____
Professor Rita S. Mehta, chair

_____
Professor Giacomo Bernardi

_____
M. Timothy Tinker, Ph.D.

_____
Professor Mark H. Carr

_____
Michael J. Miller, Ph.D.

_____
Su Sponaugle, Ph.D.

_____
Peter Biehl
Vice Provost and Dean of Graduate Studies

Table of Contents

List of Figures and Tables

relatedness. As larvae near metamorphosis, phylogenetic signal increases, and larvae look more similar to those from the same clade. Characteristics below each axis are listed in order of decreasing loading strength (Supporting Information Table S2). Greatest body depth, GBD; predorsal length, PdL; snout-to-anus length, Sn-A; pectoral fin length, P1L; head length, HL; head width, HW; and eye radius, ER.

Figure 1.5 The relationship between log body length and log pectoral fin length varies among species. Here, we show a selected seven species that demonstrate the ontogenetic variation seen in pectoral fin length. Darker lines indicate more negative allometry. All species exhibited negative allometry or isometry, in which the relative size of pectoral fins decreases or remains proportional over development. Despite this general trend, the strength of this change varied among species, with the California moray (Gymnothorax mordax) losing its pectoral fin, and others, such as the bignose conger (Rhynchoconger nitens), retaining a large pectoral fin. Illustrations show the approximate size of the pectoral fin (red structure) for larvae close to metamorphosis, and are modified from Raju (1985) and Moser (1996).

Figure 1.6 Phylo-allometric PCA (aPCA) for 17 species of eels across three habitat categories. For each species, morphological traits were centred, scaled and log-transformed, then regressed against body length. This resulted in a set of seven regression slopes for each species, which were used as observations in a phylogenetically corrected allometric principal components analysis (aPCA).

Location in the morphospace indicates which characteristics show the most extreme size changes over growth for a species. For instance, the California moray (Gymnothorax mordax) experiences a complete loss of its pectoral fin over ontogeny. Snout-to-anus length, Sn-A; pectoral fin length, P1L; head width, HW; and eye radius, ER.

Figure 1.7 Morphological characteristics when larvae are halfway to transitioning can predict larval range. Here, morphology is represented in numerical form by pPC2 axis values from the median-size pPCA. Species with large larval ranges have long predorsal and snout-to-anus lengths when they are halfway to metamorphosis. The black line indicates the line of regression (R2 adj. = 0.207). Illustrations of median-length larvae are modified from Smith (1979), Moser (1996) and Raju (1985).

Figure 3.1 Adult California morays were sampled from 11 locations between southern California and southern Baja California peninsula, Mexico, including five offshore islands (Catalina Island, Isla San Martin, Isla San Martin & Isla San Jerónimo, Isla Guadalupe, and Isla Natividad). The two most probable biogeographic breaks in this region are at Punta Eugenia and Bahía Magdalena.

Figure 2.2 California morays show local adaptation in the face of high gene flow. a) Populations off coastal southern California/northern Mexico (Palos Verdes, San Diego, Isla San Martin/Isla San Jeronimo) appear to be under different selective pressures than those from populations such as Isla Natividad, Isla Guadalupe, and

Todos Santos. Catalina Island (Two Harbors area) and Las Barrancas are comprised primarily of F1 hybrids. b) When examining neutral loci, populations are indistinguishable, suggesting high gene flow. c) and d) When examining single-ancestry individuals (those with >0.9 probability of belonging to a single genetic cluster according to loci under selection), F_{ST} values show divergence for loci under selection (c; mean $F_{ST} = 0.012$) but are low for neutral loci (d; $F_{ST} < 0.0001$). The same list of loci under selection was used for both sets of analyses; the lower number of total loci for the single-ancestry analysis is due to filtering within the STACKS pipeline.

Figure 2.3. Discriminant Analysis of Principal Components (DAPC) analyses for loci under selection (n = 216) reveal that populations cluster together. a) Todos Santos was the most genetically distinct population. b) Removing the two Todos Santos individuals provided a more granular view of the remaining populations. As no environmental information was available for Todos Santos individuals, the coordinates from plot b were used in testing for correlations with environmental covariates. Lines in plot b indicate minimum spanning tree based on squared differences among groups.

Figure 2.4 a) Sea surface height (SSH), b) sea surface temperature (SST), c) sea surface temperature anomaly (SSTA) and d) the magnitude of SSTA during estimated year of settlement are predictors of DAPC axis 2 values (used as a proxy for genetic

haplotype). All environmental predictors were averaged across Oct-Mar, as leptocephali are most abundant in waters off Baja California and southern California during this period (S. Carter, pers. comm.).

Figure 2.5. Bootstrapping results for environmental covariate regressions indicate that for sea surface height, sea surface temperature, and sea surface temperature anomaly, trends were specific to settlement year (and not any other set of years). Bars below each density curve indicate the 2.75-97.5 percentiles for each set of bootstrapped results. Vertical bars indicate the true slope value for the original set of settlement years. Asterisks indicate statistically significant regressions whose slope value also falls outside of the 2.5-97.5% percentile range.

Figure 2.6 Larval *Gymnothorax mordax* have been found as far as the northern Gulf of California and South America, despite the adult range (shaded in blue) encompassing a much narrower geographic region. Far-ranging larvae support our prediction of high gene flow, with selection presumably occurring in the late larval or early settlement period. Data are from CalCOFI and IMECOCAL sampling programs and the Scripps Institution of Oceanography Marine Vertebrate collection and represent collections from 1957-2015.

Figure 3.1. Moray eels around Catalina Island show a subtle, but diverse, range of

hue, luminance, and pattern. These images have been corrected for white balance and exposure, but glare and injuries have not yet been masked out

Figure 3.2 Workflow for (A−C) image processing and (D−F) calibration and image analysis. (A) Raw, uncorrected original photograph including the 18% standard gray card used for white balance correction. (B) Photo after white-balance and exposure correction. (C) Glare, injuries, and background masked out with uniform white. (D) Each of the 13 clusters produced for each individual was described by a luminance (L*), green−red (a*) and blue−yellow (b*) value. (E) Countershading was calculated by measuring the luminance value for the ventral (v) and dorsal (d) side of the head (snout to parabranchial opening, 1), the mid-body (from parabranchial opening to vent, 2) and the tail (vent to tip of tail, 3). (F) We examined dominant spot size and pattern diversity using ImageJ

Figure 3.3 Environmental principal components analysis (PCA) showing Axes 1 and 2, which together explain 66.9% of environmental variation among traps. Axis 3 explained an additional 15.9%. The 4 sites chosen successfully capture the diverse array of habitats occupied by California morays, with Cat Harbor representing the most distinct site. Ellipses are calculated based on a multivariate normal distribution

Figure 3.4 Moray eel (A,B) hue and (C) luminance is predicted by environmental characteristics. Eels are redder, yellower, and lighter in sandy habitats with bare substrate. Alternatively, eels are greener, bluer, and darker in habitats with high substrate diversity, clearer water, high percentages of boulder, and high rugosity (see Table S2 for variable loadings). Triangles represent eels from Cat Harbor. Conditional R2 values represent variance explained by both fixed effects and trapping site. Point colors represent actual CIE Lab scores, with green−red (a*) and blue−yellow (b*) values shown at luminance (L*) of 25 (the mean across all individuals) to improve visualization

Figure 3.5 Countershading varies significantly between the head, middle body, and tail regions (repeated-measures ANOVA, post-hoc Tukey HSD test, $p < 0.0001$). Both within individual eels and across all eels, the head and tail show the most extreme degree of countershading (countershading ratio <1). This may be related to moray behavior of keeping the head (and occasionally tail) outside of crevices. Bar: median; box: interquartile range (IQR) spanning the 25th–75th percentiles; whiskers: 1.5× above/below IQR; dots: outliers. Dashed line at 1.0 indicates no countershading

Figure 4.1. Illustration of the five case-study fisheries, listed with importance and knowledge gaps. This set of five species represent a diverse array of life histories,

Table 1.1 List of species analyzed, along with the most prevalent common name, habitat category, number of specimens, median/maximum body lengths of specimens and larval range. Larval range was calculated by combining all available occurrence data on adults and larvae to obtain a single 'maximum' range. Habitat category abbreviations: OP, offshore pelagic; OB, offshore benthic; CB, coastal benthic.

Table 1.2 Posterior distributions for the best-performing model for each taxon. Asterixes indicate covariates whose 2.5-97.5 percentiles do not include zero, and thus could be considered important predictors of larval abundance.

Table 2.1 Sample and genetic information summaries for the 10 sampled populations.

Table 2.2 Pairwise F_{st} values calculated for neutral loci (a; n loci = 54,960) and loci under directional selection (b; n loci = 216). Green values represent more similar population pairs; red values represent more divergent population pairs. For both loci under selection and neutral loci, genetic connectivity patterns do not follow simple isolation-by-distance patterns. For example, the two populations from Catalina Island (Cat Harbor, which faces south, and the Two Harbors area, which faces north) and Palos Verdes all appear to be under different selective pressures, despite being located geographically close to one another.

Table 2.3 Nine of the loci under directional selection had “highly similar” significant matches with protein-coding sequences in BLAST. We extracted all BLAST matches with E-values <1E-10; one locus (ID 130717, that explains variation between Todos Santos and all other populations. within the first DAPC) had matches to several proteins. We examined each protein for its general function, typically on the molecular level, as well as organismal-level effects within teleost fishes. Proteins that fell into the 80th percentile for variation explained across DAPC axes are marked by a * (axis 1, loci under selection, all individuals) or † (axis 2, loci under selection, sans Todos Santos) (Fig. S1.2).

Table 3.1. Sample sizes for both eels and traps per site, along with the average number of eels captured per trap

Table 4.1. List of case-study fisheries. These species represent a diverse array of habitats and life history strategies.

A MULTIFACETED INVESTIGATION OF FISH DISPERSAL IN THE EASTERN PACIFIC

Katherine E. Dale

Abstract

The biodiversity of terrestrial and aquatic communities is driven by the ability of species to successfully disperse to and persist in different habitats. For many marine fishes, dispersal occurs via a planktonic larval form that resides in the surface layer of the ocean for a period of days to months before moving to juvenile habitats and metamorphosing. The period from hatching to soon after settlement is a critical period for fish, as it features high mortality rates.

In this dissertation, I investigate selective factors that influence larval dispersal, biogeography, and population persistence in the Eastern Pacific. In Chapter 1, I examined whether morphology of larval eels (order Anguilliformes) can predict larval geographic range, and found that morphological traits of intermediate-stage larvae predicted larval latitudinal range, as leptocephali with larger relative predorsal lengths and snout-to-anus lengths exhibited larger larval ranges. In Chapter 2, I used RAD sequencing to examine genetic structure of California morays (*Gymnothorax mordax*) and found that California morays exhibit local adaptation in the face of high gene flow, with selection likely taking place primarily during the late larval or early juvenile period. In Chapter 3, I used highly quantitative methods to test if skin coloration of California morays around Catalina Island, CA were correlated with their habitats. I found that eels were yellower and lighter in sandy habitats and that

countershading (surprising for a benthic, crevice-dwelling fish) was present on the head and tail. We hypothesize that selection on coloration is also occurring during the first few years after settlement. In Chapter 1, I used a long-term west coast ichthyoplankton dataset to examine what environmental factors are influencing larval distributions of five commercially-important taxa of fishes, as well as larval fish overall: Pacific sanddab (*Citharichthys sordidus*), California sheephead (*Semicossyphus pulcher*), cabezon (*Scorpaenichthys marmoratus*), rockfishes (*Sebastes* spp.) and sablefish (*Anoplopoma fimbria*). I found that Bayesian hierarchical modeling is an effect method to model larval fish abundance, and that sea surface height was the strongest environmental covariate.

Acknowledgements

I am eternally grateful that I decided to come to UC Santa Cruz for my PhD. My primary advisor, Rita Mehta, is one of the most supportive, insightful, and enthusiastic mentors I have worked with. I have a tendency to work in isolation, and Rita has taught me the importance of good communication, teamwork, and asking for help. I have learned a lot about mentoring, teaching, managing a lab, and supporting others from her! Rita has also taught me a lot of valuable skills in the fields of phylogenetics, evolution, and morphology – areas I didn't know much about before joining the lab.

As the last-remaining Tinker Lab graduate student at UCSC, I also owe a lot to Dr. Tim Tinker, my "nice Canadian supermodeller advisor." Tim provided me with a lot of life advice, particularly about being a scientist in both academia and a federal agency, and of course about all things modeling. Every time we met, I found myself furiously scribbling down notes – he is just brilliant, and I'm glad to have had the chance to learn about math, coding, and Bayesian statistics from him.

Many people warned me against having a large dissertation reading committee – but by some miracle, we had almost no scheduling conflicts, despite having folks in Halifax, Santa Cruz, and Japan! My committee consists of interesting folks with a diverse array of insights. Dr. Michael Miller is the world's expert on eel larvae, and it has been really fun to work with a long-time hero of mine. I look forward to collaborating with Mike in the future! It was also an honor to work with Drs. Sue Sponaugle and Mark Carr, whose collective research forms the backbone for much of

what we know about the early life history of fishes, especially in the Pacific. The genetics work would not have been possible without Dr. Giacomo Bernardi, who welcomed me into his lab and who was always willing to schedule a last-minute meeting with me to troubleshoot various analyses or lab work issues (of which there were many!).

The Mehta lab has been a constant area of support for me over the last few years. I am lucky to be genuine friends with my labmates. I want to give a special shoutout to Chris Law and Sarah Kienle, who were excellent role models. Chris, I'll eventually beat you in Catan and I still make the best pancakes! I am also grateful to Kelley Voss, my "lab twin" who has basically had the exact same timeline as I have (literally, we completed most PhD milestones within days of each other) and who has inspired me to be more politically active. I also want to thank the large crew of undergraduate and postgraduate interns who have assisted me. I learned a lot about successful mentorship from this incredible group! These include Sean McCollum, Adam Mercer, Nora Laszlo, Mary Gomes, Elena Pilch, Ryan Hallisey, Shannon Stoll, Brittany Sellers, Andrew Doan, Richard Urbina, Elena Carrillo, and Josh Mayo.

I want to dedicate this work to two incredible women who were taken from us too soon: My first and longest Santa Cruz housemate Ama Delevett, and my mother Pamela Dale. Ama was a rare bird and one of the most special people I have had the joy of knowing. She was a pillar of our community, a friend and supporter of everyone, and had one of the brightest burning souls of anyone I have ever met. Ama taught me to be present, to forgive, to connect, and to be a "yes" person. My mom

was a tremendously smart and accomplished woman and an early and vocal advocate for recycling and safe and supportive communities. Many have told me that I am very similar to her, sometimes eerily so … it seems that her drive and passion for the environment was passed along to me. I hope that she would be proud.

I will be the 7th "Dr. Dale" in my extended family once I graduate – so needless to say, my family have been major STEM role models! In particular, I am not sure where I would be without my dad, who unexpectedly found himself juggling a full-time job and three young kids single-handedly when my mom passed away. He has been a lifelong advocate of providing experiences (rather than material items) for his children, such as summer marine science programs, extracurricular activities, and yearly trips to Hawaii. He always encouraged us to be independent, read lots of books, and spend time outside exploring the woods and walking in the creek. As a member of the often monetarily beleaguered millennial generation, I am also grateful for his frugal nature and financial foresight, which enabled all of his children to attend college debt-free.

It may sound odd: But I want to extend a special thank you to my bikes and bike friends for keeping me sane, especially during 2020, which was an especially difficult year for me on a number of levels. I know bikes are just pieces of metal or carbon, but these machines have taken me on thousands of miles of amazing adventures and allowed me to connect with both old friends and an amazing heap of ones. #eelsandwheels forever!

I am grateful for all of the funding I have received in support of my dissertation work. These include: A NOAA-Sea Grant Fellowship in Population & Ecosystem Dynamics; a UC MEXUS Small Grant, a Lewis and Clark Fund Grant for Exploration and Field Research, an Achievement Rewards for College Scientists (ARCS) Foundation fellowship; several awards from the California-Nevada Chapter and Western Division of the American Fisheries Society; a Lerner-Gray Memorial Fund grant; a Wrigley Institute Graduate Summer Fellowship; a Myers Trust Research Award; a Friends of the Seymour Marine Discovery Center Student Research and Education Award; and yearly summer research support from the Ecology and Evolutionary Biology Department at UCSC. Santa Cruz is one of the most expensive places to live in the US – I am privileged to have had a department who was willing to support current graduate students over the summers, both with living and research costs.

Statement of Contribution

The text of this dissertation includes reprints of the following previously published material:

Chapter 1. Dale, K. E., Tinker, M. T., & Mehta, R. S. (2019). Larval morphology predicts geographical dispersal range of Eastern Pacific eels. *Biological Journal of the Linnean Society*, *128*(1), 107–121. https://doi.org/https://doi.org/10.1093/biolinnean/blz092

I conceived the project, performed all analyses, and wrote the manuscript. M. Tim Tinker contributed statistical advice. Rita S. Mehta provided guidance on theory and analyses. All authors discussed the results and edited the final manuscript.

Chapter 3. Dale, K. E., Hallisey, R., & Mehta, R. S. (2021). Coloration is related to habitat in *Gymnothorax mordax*, an elongate kelp forest predator. *Marine Ecology Progress Series*, *677*, 67–79.

I conceived and designed the project, oversaw field work, and led stastistical analyses and writing. Ryan Hallisey assisted with all field work, wrote parts of the manuscript, and ran a subset of statistical analyses. Rita S. Mehta provided funding for field work, assisted with field work, and provided guidance on project direction and analyses. All authors discussed the results.

Introduction

All marine fishes have evolved adaptations to the environments in which they are found. This results in phylogenetically related species having divergent geographic ranges, population structures, and morphological features. Selection during the early life stage of fish can determine which species (or individuals within a species) can survive in a given location. Even if propagules are successful in reaching potential juvenile habitats, further selection may occur after settlement when larvae remain vulnerable to predation, lack of prey availability, lack of suitable habitat, etc. Thus, larvae must be able to successfully disperse to adult habitats as well as contend with environmental conditions once they arrive.

Overview

In this dissertation, I investigated potential evolutionary drivers that may affect dispersal, biogeography, and survival of Eastern Pacific fishes. In Chapters 1-3, I focus on order Anguilliformes, the true eels. Anguilliformes, along with their other relatives in superorder Elopomorpha, have a unique, leaf-shaped, transparent larval form called a leptocephalus (Miller 2009). Leptocephali, which are unique to the Elopomorpha, exhibit the longest pelagic larval duration times of any fish larvae, with some species of eels having pelagic larval duration times of several months to more than a year (Miller 2002; Miller and Tsukamoto 2020). Accordingly, eel larvae can be potentially subject to seasonally varying water temperatures, shifts in oceanographic currents, and long-distance transport that may bring them out of the range of suitable

juvenile habitats. For the final chapter, I take a wider, more holistic view of environmental factors and their potential influence on larval fish distributions along California. I develop a hierarchical model to examine larval abundances of five case-study taxa. In comparison to eels, these case-study fishes have non-leptocephalus larvae, with shorter pelagic larval durations, smaller maximum body sizes, and more cylindrical body shapes.

The subtropical Eastern Pacific is a unique and challenging place to be a larval fish, particularly for marine eels, which are generally more common in warmer waters. While the region between Baja California Sur, Mexico, and southern California is ostensibly dominated by the cold-water, southward-flowing California Current, both seasonal changes and decadal oscillations can induce poleward nearshore transport, eddy formation, and an influx of warmer waters from the south (Shanks and Eckert 2005; Durazo 2015).

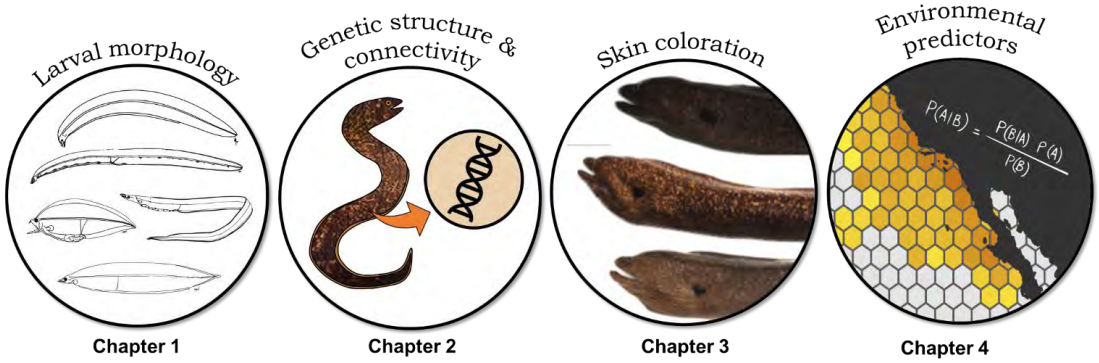

Outline of Chapters

In **Chapter 1**, I analyzed a set of eight morphological measurements recorded 395 Eastern Pacific leptocephali from 395 collected by researchers at the National

Oceanic and Atmospheric Administration's Southeast Fisheries Science Center. The 17 Anguilliform species included represented three adult habitats – coastal benthic (11 species), offshore pelagic (5 species), and offshore benthic (1 species). We investigated if groups of eels varied significantly from one another at their median or maximum larval body lengths, how scaling patterns for traits varied between species, and how interspecific diversity of larval body shapes varied for intermediate- and late-stage larvae. Further, we investigated whether morphological traits or scaling strength could predict larval latitudinal range, hypothesizing that species with large maximum body sizes, high aspect ratios, and negative allometry of body depth would have larger larval ranges. All analyses were performed within a phylogenetic framework to account for shared evolutionary history, using a pruned molecular phylogeny published by Santini et al. (2013).

After examining larval body shape across a diverse array of Anguilliform species, I narrow my focus to California's only muraenid, the California moray (*Gymnothorax mordax*). This species of moray has been shown to be in high abundances in southern California (Higgins and Mehta 2017), as well as having morphological features that make it a top kelp forest predator (Diluzio et al. 2017; Harrison et al. 2017; Higgins et al. 2018). A long-standing hypothesis has assumed that California morays in southern California are non-reproductive due to water temperatures (McCleneghan 1973). In **Chapter 2**, I used restriction-site associated sequencing (RADseq) to investigate this question, as well as determine if California morays have high gene flow or show population structure, identify signatures of

source and recipient populations, and identify potential environmental or oceanographic processes that may contribute to population structure. Based on previous studies of muraenids, it was hypothesized that California morays would show high genetic connectivity. I also hypothesized that populations in southern California would be primarily recipient populations with low genetic diversity, and that patterns of genetic diversity would correlate with El Niño Southern Oscillation conditions. In **Chapter 3**, I move from examining selection during dispersal to studying selection post-settlement. Using a highly quantitative approach, I characterized California moray skin coloration, described as hue, pattern, and luminance. I examined several potential mechanisms that may explain correlations between coloration and habitat. In **Chapter 4**, I end by taking a more holistic view of teleost fishes in the Eastern Pacific, examining how larval abundances shift in relation to various environmental factors. I constructed a three-part hierarchical model that accounts for sampling variation, observation variation, and spatial autocorrelation. In addition to examining all ichthyoplankton, I examined which environmental covariates best describe abundance trends for five case-study species: Pacific sanddab (*Citharichthys sordidus*), California sheephead (*Semicossyphus pulcher*), cabezon (*Scorpaenichthys marmoratus*), rockfishes (*Sebastes* spp.) and sablefish (*Anoplopoma fimbria*).

Biological Journal of the Linnean Society, 2019, **XX**, 1–15. With 7 figures.

Larval morphology predicts geographical dispersal range of Eastern Pacific eels

KATHERINE E. DALE*, M. TIMOTHY TINKER and RITA S. MEHTA

Department of Ecology and Evolutionary Biology, University of California, Santa Cruz, 130 McAllister Way, Santa Cruz, CA 95060, USA

Received 6 March 2019; revised 23 May 2019; accepted for publication 24 May 2019

The geographical range of many marine species is strongly influenced by the dispersal potential of propagules such as eggs and larvae. Here, we investigate morphological diversity and the effect of body shape on geographical range of leptocephali, the unique, laterally compressed larvae of eels (order Anguilliformes). We used phylogenetically informed analyses to examine the morphological variation of larvae for 17 Eastern Pacific eel species from three adult habitats. We also investigated whether morphological traits of leptocephali could predict larval latitudinal range, hypothesizing that body shape may influence passive dispersal via currents. We found that no two species shared the same multivariate growth trajectories, with the size and scaling of pectoral fin length and snout-to-anus length being particularly variable. Larvae with longer relative predorsal and snout-to-anus lengths at median sizes exhibited wider larval geographical ranges. Body aspect ratio and maximum body length at metamorphosis, two traits we hypothesized to be important for passive transport, were not significant predictors of maximal larval range. We discovered an increase in phylogenetic signal over larval development as eels approach metamorphosis, potentially due to similar selective pressures between related species (such as juvenile habitat or adult morphology). Lastly, we conclude that larval body shape is probably influenced by adult habitat and adult morphology.

ADDITIONAL KEYWORDS: Anguilliformes – dispersal – fish larvae – leptocephalus – morphology

INTRODUCTION

Understanding how species distributions change through space and time is central to ecological studies. In the marine realm, continued dispersal of propagules between or within populations is important in determining future persistence, the structure of communities and adaptation to changing environmental conditions (Roughgarden *et al.*, 1988; Carr, 1989; Moser & Watson, 2006). For many marine fishes, dispersal occurs primarily during a planktonic larval stage, which remains in the oceanic environment for some length of time before moving to and settling in juvenile habitats. The period between hatching and settlement is a crucial period in a fish's life and has been the focus of much work (e.g. Cowen & Sponaugle, 2009; Peck *et al.*, 2012; Llopiz *et al.*, 2014b).

Both extrinsic and intrinsic factors influence the dispersal and retention of propagules (Cowen & Sponaugle, 2009). Extrinsic pressures include the strength and direction of oceanic currents (Shanks & Eckert, 2005), oceanographic processes such as eddies, fronts and rings (Limouzy-Paris *et al.*, 1997), geographical features such as peninsulas (Ebert & Russell, 1988), and large-scale climate oscillations (Cowen, 1985; Knights, 2003; Llopiz *et al.*, 2014; Higgins *et al.*, 2017). Larval mobility is also influenced by factors intrinsic to larvae such as pelagic larval duration time (Shanks, 2009), swimming performance (Stobutzki & Bellwood, 1997; Müller *et al.*, 2008), ability to detect environmental cues (Gerlach *et al.*, 2007; Naisbett-Jones *et al.*, 2017) and growth rate (Wilson & Meekan, 2002). The interaction between these extrinsic and intrinsic factors may further impede or facilitate dispersal (e.g. Hunt von Herbing, 2002).

One such interaction is that between body shape and ocean currents, which has rarely been explored for larvae. In contrast, the biomechanical influence of adult body shape on organisms' abilities to move through fluids is well documented (e.g. Webb, 1988; Vogel, 1996). For instance, aspect ratio, defined as

*Corresponding author. E-mail: kdale@ucsc.edu

length divided by width, is a unitless metric often used to describe the structures by which animals move through water or air (Sambilay, 1990; Dong *et al.*, 2006). Structures such as bird wings and fish fins provide upward lift to the animal, but fluid vortices formed at the tips of these structures result in drag, a downward force that counteracts lift. Organisms that have evolved structures of high aspect ratio (i.e. long and thin) experience this tip-associated drag over a smaller area relative to their total size and are thus more efficient at moving through fluids. Structures of low aspect ratio (i.e. short and deep) are better adapted for quick manoeuvring but must contend with increased drag. Some fish species, such as plaice (*Pleuronectes platessa*), have evolved deep-bodied, dorso-laterally compressed larvae, whose lower aspect ratios may improve passive movement by currents (Ryland, 1962; Froese, 1990). However, recent work by Katz & Hale (2016) showed that most larval fish have higher aspect ratios (i.e. are longer and thinner) than their adult forms, a body shape which may improve respiration and swimming efficiency (Webb & Weihs, 1986). An exception to the pattern is the order Anguilliformes (true eels), which are typically less elongate than their parents (Katz & Hale, 2016). These studies encouraged us to investigate whether body shape could influence the dispersal range of anguilliform larvae.

In general, fish larvae are morphologically distinct from adults and display a wide diversity of body shapes. Larval fish must move through fluids at relatively small sizes, avoid predation, find and capture food, and navigate to suitable juvenile habitat, challenges which could potentially explain the evolution of diverse body shapes (Moser, 1981). Larvae of especially small sizes and low swimming speeds experience an environment dominated by viscous forces rather than inertial forces, and undulatory swimming is the most effective form of movement at this stage. Larger, faster larvae experience viscous forces only in a narrow boundary region adjacent to their bodies, and instead must contend with lateral inertial forces. The transition between fluid regimes represents a physical challenge for juvenile aquatic animals as they grow (Müller *et al.*, 2000; McHenry, 2005; Stevens *et al.*, 2018). Consequently, the majority of work on the relationship between body shape of larval fish and the environment has examined changes in growth rate and body shape between larvae and adults (Fuiman, 1983; Katz & Hale, 2016), the influence of morphological characteristics such as tail length on active locomotion/manoeuvring (Batty, 1984; Webb & Weihs, 1986; Voesenek *et al.*, 2018), and the physiological requirements of shape related to respiration, feeding and predator avoidance (Osse, 1989). However, we have little understanding of the patterns of morphological changes larvae undergo before they transition to their adult form, and how these patterns vary with phylogenetic relatedness.

Leptocephali, the larvae of true eels and their relatives (superorder Elopomorpha), are unusual among fish larvae. Despite their ecological and morphological diversity as adults, all elopomorphs share a transparent, leaf-shaped, laterally compressed larval form. Leptocephali, while generally less elongate than the adults of their species (Katz & Hale, 2016), still exhibit larger maximum body sizes than other fish larvae, with some taxa consistently reaching body lengths greater than 30 cm (Raju, 1985; Bohlke, 1989; Moser, 1996; Miller, 2009). This increased growth may be partially due to a long pelagic larval duration period, which ranges from 3 to 4 months in tropical species to potentially 1–3 years in the genus *Anguilla* (Brothers & Thresher, 1985; Bonhommeau *et al.*, 2010).

The Eastern Pacific harbours a remarkable diversity of anguilliforms. Among the most common midwater species are the slender snipe eels (family Nemichthyidae), which are extremely elongate as both adults and larvae. Adult slender snipe eels have an interesting skull morphology, with long, thin upper and lower jaws whose tips curve away from one another (Bohlke, 1989). Also in the midwater are the large-mouthed gulper eels (family Saccopharyngidae), a group whose divergent morphological traits have made its taxonomic placement difficult (Robins, 1989; Santini *et al.*, 2013). A group related to the Saccopharyngids are the bobtail eels (family Cyematidae), whose adults have forked tails and relatively short bodies. The leptocephali of these latter groups are deep-bodied with large jaws. Members of all three clades are cosmopolitan or semi-cosmopolitan (Bohlke, 1989; Moser, 1996). In contrast, many of the coastal and benthic eels in the Eastern Pacific are endemic to the region, including the dogface witch-eel (*Facciolella gilberti*), a deepwater benthic species; the California moray (*Gymnothorax mordax*), a rare example of a temperate moray; and the white-ring garden eel (*Heterconger canabus*), a burrowing species endemic to the Gulf of California. Leptocephali of coastal, shallow-water eels show less morphological diversity than midwater species, but can still range substantially in their maximum body lengths (Moser, 1996).

The leptocephali of all Anguilliformes vary in characteristics such as body depth, head shape and body length (Miller, 2009), but there has been no examination of whether these traits are related to the evolutionary history of clades within the Anguilliformes, factors related to larval survival, or adult life history. However, the conserved leptocephalus body form in Elopomorpha, despite the divergence in adult lifestyles, suggests that this larval form confers a selective advantage. Mimicry of gelatinous

zooplankton may contribute to the functional advantage of transparency and a leaf-like shape (Miller *et al.*, 2013; Greer *et al.*, 2016). Alternatively, we propose that the leptocephalus body shape could assist with dispersal to juvenile habitats. Species such as the European eel (*Anguilla anguilla*) and American eel (*Anguilla rostrata*) may travel thousands of kilometres prior to metamorphosis and are hypothesized to use both passive dispersal and active swimming to reach juvenile habitats (McCleave *et al.*, 1998; Wuenschel & Able, 2008; Bonhommeau *et al.*, 2009; Tsukamoto *et al.*, 2009; Rypina *et al.*, 2014). As *Anguilla* larvae mature and elongate, buoyancy decreases, allowing them to use active swimming to reach their ultimate destination (Tsukamoto *et al.*, 2009). Other species, particularly eels associated with nearshore habitats, also appear to utilize swimming or other behavioural adaptations to facilitate local retention (Miller, 2009; Miller *et al.*, 2011a).

The distinct body shapes and lengthy planktonic residence times of leptocephali provide an ideal platform for studying the relationship between shape and dispersal range. Furthermore, the temperate, highly dynamic Eastern Pacific is a unique place to study leptocephali, which are more commonly associated with warm water environments (Miller, 2009). To our knowledge, this work represents the first examination of morphological traits as predictors of larval transport in the Eastern Pacific.

Here, we use a comparative evolutionary framework to examine (1) how body shape and other morphological traits of leptocephali vary across adult habitats and between distinct ontogenetic stages, (2) whether the overall body shape or scaling patterns of larvae vary with respect to adult habitat and (3) whether the relative size or growth trajectories of morphological traits such as body shape can be used to predict larval range. We hypothesized that larvae with high body aspect ratios (long and thin) and larger body lengths at metamorphosis would have greater larval ranges, as would larvae that become increasingly long and thin over ontogeny. Additionally, we hypothesized that more closely related species would share similar morphology, irrespective of adult habitat type.

MATERIAL AND METHODS

We analysed a set of eight morphological measurements recorded on 395 specimens by researchers at the National Oceanic and Atmospheric Administration's Southeast Fisheries Science Center, part of an effort to create CalCOFI Atlas No. 33, an identification guide to larval fishes of the California Current (Moser, 1996). Specimens were preserved in formalin at capture and came from a variety of sampling programmes in the Eastern Pacific, which are described in Moser (1996). Morphological characteristics (measured in mm) were body length (BL; defined as the distance from the tip of the snout to the posterior margin of the hypural plate, equivalent to standard length), greatest body depth (GD), predorsal length (PdL), snout-to-anus length (Sn-A), head length (HL; defined as the distance from the tip of the snout to the posterior margin of the cleithrum), head width (HW), eye radius (ER) and pectoral fin length (P_1L) (Fig. 1). Species were included in the following analysis if they were represented by nine or more individuals and if specimen body lengths covered >50% of pre-metamorphosis body lengths. For the shorthead conger (*Bathycongrus macrurus*), bobtail snipe eel (*Cyema atrum*), Pacific worm eel (*Myrophis vafer*), slender snipe eel (*Nemichthys scolopaceus*), ringeye conger (*Paraconger californiensis*) and bignose conger (*Rhynchoconger nitens*), no information was available on body size at metamorphosis. Instead, data from the next most closely related species were used as a proxy. Of the 24 species for which data were recorded, 17 species across nine families fit our criteria. These 17 species were classified according to their adult habitat based on information available in FishBase (Froese & Pauly, 2018) and Atlas 33 (Moser, 1996). Species fell into three adult habitat categories: offshore pelagic, coastal benthic and offshore benthic (Table 1), defined

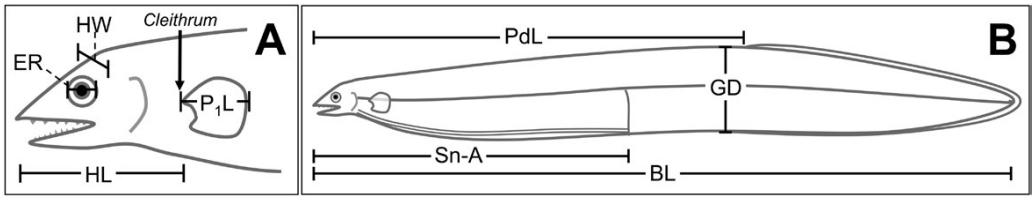

Figure 1. Morphological measurements for leptocephali analysed in this study for the head (A) and body (B). For details on how these measurements were taken, refer to CalCOFI Atlas 33 (Moser, 1996). Greatest body depth, GD; predorsal length, PdL; snout-to-anus length, Sn-A; pectoral fin length, P_1L; head length, HL; head width, HW; and eye radius, ER.

by depth range and lifestyle as reported in FishBase (Froese & Pauly, 2018). The offshore pelagic group encompassed five mesopelagic and bathypelagic species whose adults live in offshore waters at depths typically >200 m, and that are not associated with the benthos. Coastal benthic species were defined as having adult habitats that primarily fall within 20 km of the coast, in waters <200 m deep. This group included 11 reef-associated or fossorial species across Congridae, Muraenidae and Ophichthidae, the three most speciose anguilliform families. The offshore benthic group contained a single member, the benthopelagic dogface witch-eel (*Facciolella gilberti*), adults of which are associated with the benthic region of the continental slope (Bohlke, 1989).

All analyses were performed within a phylogenetic framework to account for shared evolutionary history, using a pruned molecular phylogeny published by Santini *et al.* (2013) (Supporting Information Fig. S1). Nine of the 17 species had exact matches in the tree; an additional six were represented by species within the same genus. Two species of conger eels, the shorthead conger (*Bathycongrus macrurus*) and shortsnout conger (*Chiloconger denatus*), were not represented by species or genus. Instead, we estimated the location of these species on the tree using members of the same subfamily. All analyses were completed in R 3.4.3 (R Core Team, 2016).

Morphological diversity between habitat categories and throughout development

We used both individual phylogenetically corrected analysis of variance (pANOVA) tests and phylogenetically corrected multivariate analysis of variance (pMANOVA) tests to examine whether morphological traits varied between the offshore pelagic and coastal benthic habitat groups (Garland *et al.*, 1993). The offshore benthic group was not included because it contained a single species. We chose to run individual pANOVAs in addition to pMANOVAs due to the collinearity of the morphological traits. We conducted both pMANOVAs and pANOVAs using the 'aov.phylo' tool in the R package 'geiger' (Harmon *et al.*, 2008), using an $\alpha = 0.05$ and 5000 simulations. For the pMANOVA, we used Pillai's trace test statistic due to its robustness towards departures from test assumptions, such as the presence of collinearity (Olson, 1979; Sheehan-Holt, 1998). Due to constraints within the function requiring a 1:1 match between the number of tree tips and data, we ran the pMANOVAs/pANOVAs on the morphological variables for the maximum-length and median-length larva of each species. Minimum-length larvae were not examined, as very small individuals were only available for a subset of species. Median-length individuals were those with body lengths closest to the estimated median body length between hatching and metamorphosis for each species.

Table 1. List of species analyzed, along with the most prevalent common name, habitat category, number of specimens, median/maximum body lengths of specimens and larval range

Common name	Scientific name	Habitat category	*N*	Median body length (mm)	Maximum body length (mm)	Larval range (°lat)
Slender snipe eel	*Nemichthys scolopaceus*	OP	22	122.1	263.1	81.0
Bobtail eel	*Cyema atrum*	OP	21	40.8	69.8	71.3
Sawtooth eel	*Serrivomer sector*	OP	60	34.8	63.7	62.5
Whiptail gulper eel	*Saccopharynx lavenbergi*	OP	10	25.1	40.4	53.8
Narrownecked oceanic eel	*Derichthys serpentinus*	OP	17	34.1	65.1	60.0
Dogface witch-eel	*Facciolella gilbertii*	OB	29	102.7	193.9	33.4
Gilbert's garden eel	*Ariosoma gilberti*	CB	21	114.2	227.2	48.1
Shorthead conger	*Bathycongrus macrurus*	CB	20	68.4	146.7	26.4
Shortsnout conger	*Chiloconger dentatus*	CB	13	70.5	128.3	32.2
Hardtail conger	*Gnathophis cinctus*	CB	11	66.2	123.1	46.7
Cape garden eel	*Heteroconger canabus*	CB	28	65.5	122.6	21.5
Ringeye conger	*Paraconger californiensis*	CB	17	53.9	133.3	46.6
Bignose conger	*Rhynchoconger nitens*	CB	22	70.6	126.3	31.7
Pacific worm eel	*Myrophis vafer*	CB	31	63.9	98.0	45.7
Pacific snake eel	*Ophichthus triserialis*	CB	9	47.3	123.0	52.7
Yellow snake eel	*Ophichthus zophochir*	CB	20	82.2	147.2	52.7
California moray	*Gymnothorax mordax*	CB	44	57.1	108.0	42.4

Larval range was calculated by combining all available occurrence data on adults and larvae to obtain a single 'maximum' range. Habitat category abbreviations: OP, offshore pelagic; OB, offshore benthic; CB, coastal benthic.

To further examine multivariate patterns of body shape at these two distinct ontogenetic stages, we used a phylogenetically corrected principal components analysis (pPCA) to collapse variation in seven size-corrected morphological characters (greatest body depth, predorsal length, snout-to-anus length, head length, head width, eye diameter and pectoral fin length), into two orthogonal axes (Revell, 2009). As in the pMANOVA, we ran the two pPCAs using the median- and maximum-length larvae of each species to numerically capture morphological variation at both intermediate and advanced ontogenetic stages. To compute the pPCAs, we first size-corrected the morphological traits by fitting a simple linear regression of each log-transformed trait against log body length. Residuals were then computed using the 'phyl.resid' function in the R package 'phytools' (Revell, 2012). We fitted pPCA models to the covariance matrix of residuals using the 'phyl.pca' function. The patterns of variation on the pPCA ordination were analysed by examining the strength with which the seven size-corrected traits loaded onto each pPCA axis.

To quantify how larval morphology varies over ontogeny, we performed simple linear regressions of each log-transformed morphological trait against log body length, incorporating all individuals within a species. The 95% confidence intervals for the slopes were used to interpret scaling patterns. If confidence intervals included a slope of 1, we considered the relationship to be isometric, where the morphological trait grew proportionally with body length. Slope intervals $>|1|$ represented positive allometry, where the trait's size stayed larger than expected in relation to body length. Slope intervals $<|1|$ indicated negative allometry, where the trait's size stayed smaller than expected in relation to body length. Negative slope values indicated that the trait decreased in size over ontogeny, whereas positive values indicated the trait increased in size over ontogeny (e.g. Gisbert *et al.*, 2002).

To determine which suites of traits underwent the most extreme size changes within each species, we generated a phylo-allometric PCA (aPCA) (Baliga & Mehta, 2018). Data were first centred, scaled and log-transformed for normality. For each species, we ran a linear regression of every log-transformed trait against log body length. These regressions resulted in a set of seven slopes for each species, which represented the log-linear relationships between body length and each morphological character. The multivariate distribution of these slopes was then calculated in a aPCA using the same 'phyl.pca' function used for the pPCA. All PCAs in this study were displayed using the 'phylomorphospace' function in the package 'phytools'.

Morphology as a predictor of larval range

The relative size or scaling trajectory of individual traits could help to explain differences in dispersal range. We examined larval geographical range using latitudinal range. Although midwater pelagic eels are distributed circumglobally, coastal eels are distributed primarily north–south, leaving latitude as the best comparative range metric amongst the three groups. We compiled latitudinal range information both for adults and for larvae, when available (Supporting Information Table S1). Adult and larval range are not necessarily equivalent. For example, some species may have large larval geographical ranges, but only recruit to and reproduce in a small portion of that area. Alternatively, adults of some species may be highly mobile, extending the adult range beyond that of the larvae. It is important to note that we used geographical species ranges as a proxy for dispersal, not dispersal distances for individual larvae. Although preferable, data on actual larval dispersal distance is not currently available for eels in the Eastern Pacific.

Ultimately, we decided the best estimate of larval range came from combining information on both adults and larvae to find the maximum possible range for each species. Importantly, this method assumes that if adults are found in a specific area, larvae must be able to reach that location as well. This hypothesis is probably appropriate for coastal benthic species with high adult site fidelity, but it is unknown how well this is supported for offshore pelagic species. Qualitative adult geographical data were obtained for most species using sources in Atlas 33 (Moser, 1996) and FishBase (Froese & Pauly, 2018). When encountering ambiguous locations (i.e. 'Ecuador'), we used the southernmost border of the country or region (Supporting Information Table S1). Information on species-specific larval range was significantly more limited than data on adult range. Leptocephali are uncommon in typical ichthyoplankton catch datasets, as larvae are able to avoid or escape the nets typically used in plankton sampling (Castonguay & Mccleave, 1987). Thus, larval range was compiled from two disparate sources. The first was Atlas 33 (Moser, 1996), which provided limited qualitative data for seven coastal benthic species. The second was the original catch location of specimens in the dataset, which is probably an underestimate of true range due to constraints on sampling coverage. We then combined data from all sources to obtain one 'maximum' latitudinal range value for each species (Fig. 2).

We tested if morphology at either median or maximum size could predict maximum latitudinal range using results of the two pPCAs, whose axes represent the general body shape of each species at intermediate and late-stage development. Axes 1 and

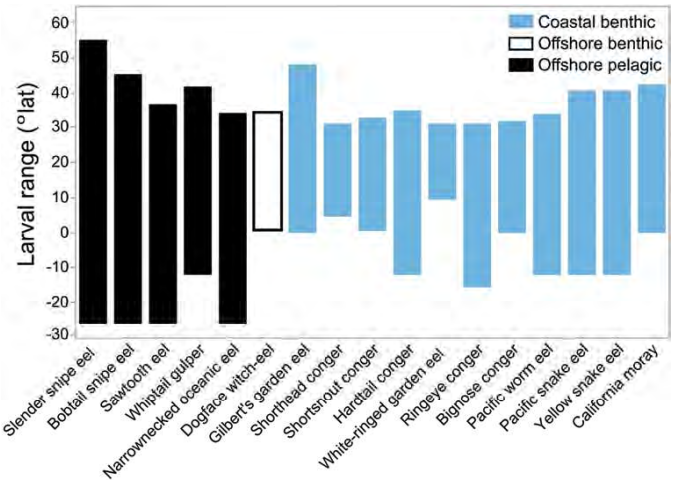

Figure 2. Larval latitudinal ranges for each of the species in this dataset. Larval range was calculated by combining all available geographic range data for both adults and larvae to obtain one 'maximum' value. This estimation assumes that if adults are found in a specific location, larvae must be able to disperse there as well.

2 (pPC1, pPC2) from each of these pPCAs were used as predictor variables in phylogenetic generalized least squares (PGLS) regressions (Grafen, 1989), in which larval range was the dependent variable. We additionally performed a PGLS regression using body length at metamorphosis (as reported in Atlas 33) as the predictor variable. PGLS regressions were run using the 'pgls' function in the R package 'caper' (Orme *et al.*, 2013).

To determine whether scaling patterns predict range, we ran further PGLS regressions on the axes derived from the aPCA and larval latitudinal range. The aPCA compressed the overall patterns of growth into a two-dimensional ordination representing variation in scaling strength for different traits. The coordinates on axes 1 and 2 (aPC1, aPC2) are numerical approximations of scaling strength and direction. PGLS analyses were performed with either aPC1 and aPC2 axis values treated as predictor variables and maximum larval range as the dependent variable.

RESULTS

In total, we analysed morphological data for 130 offshore pelagic individuals, 236 coastal benthic individuals and 29 offshore benthic individuals spread across 17 species. Our pMANOVAs did not detect significant differences in median- or maximum-length morphology between the offshore pelagic and coastal benthic groups ($F_{2,14} = 1.79$, 2.245; $P > 0.05$). Our pANOVAs on individual trait values were also insignificant. The lack of any significant difference between groups may be due to the wide variance in trait values within each group. Relative pectoral fin length, predorsal length and head width showed especially large variation across species at both minimum and maximum sizes. Estimated body lengths at metamorphosis as reported in Atlas 33 or estimated from specimens ranged from 4.04 cm (whiptail gulper, *Saccopharynx lavenbergi*) to 26.31 cm (slender snipe eel, *Nemichthys scolopaceus*). Offshore pelagic species, except for the slender snipe eel, had shorter maximum body lengths than coastal benthic or offshore benthic species. However, traits such as relative eye radius and body aspect ratio (body length divided by greatest body depth) were generally conserved within habitat groups (Fig. 3). Coastal benthic and offshore benthic species tended to have longer and more narrow bodies, while offshore pelagic species had shorter and deeper bodies. The exception was the offshore pelagic slender snipe eel, which exhibited the most elongate larvae in the dataset.

As indicated by the pPCA results, larvae from all three habitat categories were more morphologically diverse at median than at maximum size (Fig. 4). At median size, even closely related species did not cluster within the morphospace. As seen in the maximum pPCA, phylogenetic clustering increased as larvae approached metamorphosis. At both ontogenetic stages, relative pectoral fin length, eye radius, head length and head width explained 55.9–62.1% of the interspecific variation (Fig. 4; Supporting Information Table S2). The coastal benthic California moray and

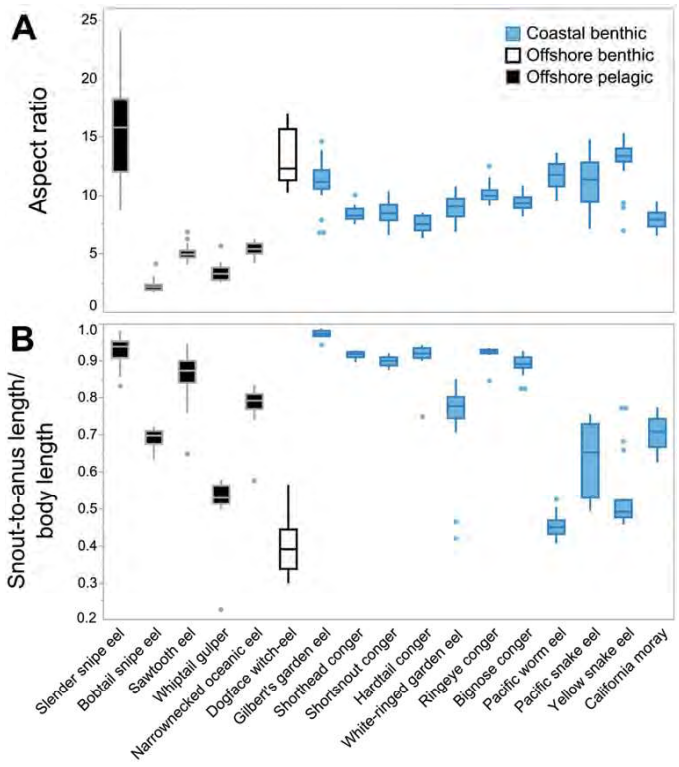

Figure 3. The diversity of body aspect ratios (A) and relative snout-to-anus lengths (B) for 17 species of eels across three habitat categories. Aspect ratio is calculated as body length/greatest body depth. Note that offshore pelagic and coastal benthic/offshore benthic species each converge on a different set of aspect ratios, with the notable exception of the slender snipe eel (*Nemichthys scolopaceus*), a highly elongate offshore pelagic species.

the offshore benthic dogface witch-eel were outliers at both ontogenetic stages.

SCALING PATTERNS ACROSS SPECIES

Growth patterns varied across species, with no two species exhibiting the same scaling pattern for all seven traits (Supporting Information Table S4). Greatest body depth was the only characteristic that demonstrated highly variable scaling patterns showing positive allometry (N = 1), isometry (N = 8) and negative allometry (N = 8), in addition to a wide variety of scaling strengths (slope values 0.66–1.35). However, our results indicated that for the majority of species (N = 16), body aspect ratio remained proportional or elongated as body length increased. A single offshore pelagic species (the bobtail snipe eel, *Cyema atrum*) scaled with positive allometry for greatest body depth, indicating that this species becomes increasingly deep-bodied with development. Of the seven morphological variables, pectoral fin length showed the widest variation in scaling strength, but almost all species showed negative allometry, in which the relative size of the pectoral fin decreased with growth (Fig. 5). The most extreme case was the California moray, whose pectoral fin transitioned from 10% of head length at hatching to non-existent at metamorphosis. The ringeye conger (*Paraconger californiensis*) was the only species to exhibit isometry and maintain a pectoral fin that was 17% of head length up to metamorphosis. All species converged on a pattern of strong negative allometry for head width, head length and eye radius, such that even species with very large maximum body sizes retained small heads and pectoral fins despite large increases in body length or depth.

The aPCA results revealed that species within the same habitat category diverge markedly in their

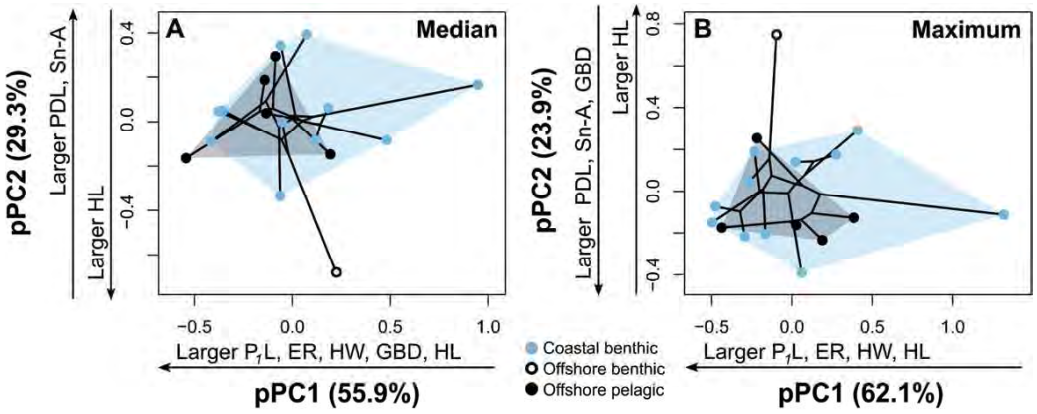

Figure 4. Phylogenetically corrected principal components analyses (pPCA) of larval morphology at median size and maximum size. PCAs were performed on the residuals of the relationships between each of the seven log-transformed characteristics and log body length. At median size, larvae do not cluster by relatedness. As larvae near metamorphosis, phylogenetic signal increases, and larvae look more similar to those from the same clade. Characteristics below each axis are listed in order of decreasing loading strength (Supporting Information Table S2). Greatest body depth, GBD; predorsal length, PdL; snout-to-anus length, Sn-A; pectoral fin length, P_1L; head length, HL; head width, HW; and eye radius, ER.

multivariate scaling patterns (Fig. 6). Pectoral fin length and eye radius loaded heavily on axis 1 of the aPCA and explained 60.9% of the variation in scaling strength. This trend was driven by the loss of the pectoral fin in the California moray. The remaining species primarily diverged along axis 2, which explained an additional 15.8% of the variation. Characteristics that loaded strongly on this axis were predorsal length, snout-to-anus length and eye radius (Supporting Information Table S3). Species did not cluster by adult habitat category in the aPCA, but species within the same family generally occupied a similar region of the phylomorphospace.

Morphology as a predictor of larval range

We found a significant negative relationship between axis 2 of the pPCA (representing larval predorsal length and snout-to-anus length at median size) and larval latitudinal range ($P = 0.019$, R^2 adj. = 0.28; Fig. 7). This indicated that species whose larvae have longer relative anterior body sections (predorsal length and snout-to-anus length) at approximately halfway to transitioning have larger larval ranges. We did not find any significant relationships between any other pPCA axis, body length at metamorphosis or multivariate scaling pattern (as represented by axes 1 and 2 from the aPCA).

DISCUSSION

In this study, we examined the morphological diversity and scaling patterns of leptocephalus larvae whose adults occupy disparate habitats in the eastern Pacific. We then used these traits to better understand how morphology relates to larval geographical range. Our comparative analyses show that (1) there are distinct morphological differences between the larvae of offshore pelagic, offshore benthic and coastal benthic species and that these differences are most pronounced at intermediate ontogenetic stages; (2) morphological traits of leptocephali show subtle to extreme changes over ontogeny; and (3) larvae with longer anterior body segment lengths at median size have larger latitudinal ranges.

The leptocephali in this dataset exhibited diverse growth patterns. Variance in the size of morphological traits was high enough within habitat groups that groups were not significantly different from one another, even when comparing single characteristics. However, our phylogenetically corrected pPCA found that larvae more closely clustered by clade at maximum rather than median size. An increase in phylogenetic signal over ontogeny suggests that selective pressures presumed to be similar between related species (such as juvenile habitat or adult morphology) may strengthen.

Larval aspect ratio appears to be somewhat related to adult morphology and thus to adult habitat. Body aspect ratio was conserved within habitat categories, apart from the offshore pelagic slender snipe eel, which had the highest body aspect ratio in our dataset. Adults of coastal benthic and offshore benthic species have elongate body plans adapted for fossorial or

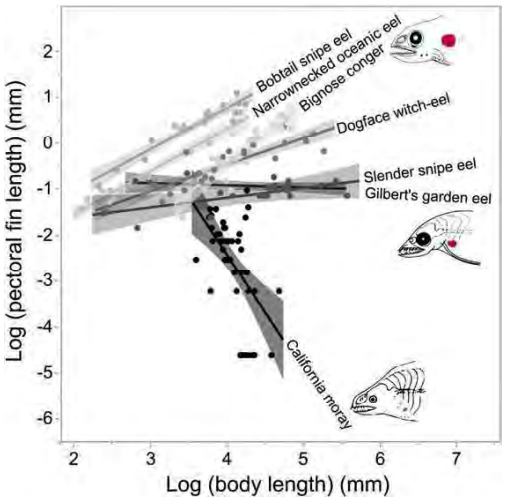

Figure 5. The relationship between log body length and log pectoral fin length varies among species. Here, we show a selected seven species that demonstrate the ontogenetic variation seen in pectoral fin length. Darker lines indicate more negative allometry. All species exhibited negative allometry or isometry, in which the relative size of pectoral fins decreases or remains proportional over development. Despite this general trend, the strength of this change varied among species, with the California moray (*Gymnothorax mordax*) losing its pectoral fin, and others, such as the bignose conger (*Rhynchoconger nitens*), retaining a large pectoral fin. Illustrations show the approximate size of the pectoral fin (red structure) for larvae close to metamorphosis, and are modified from Raju (1985) and Moser (1996).

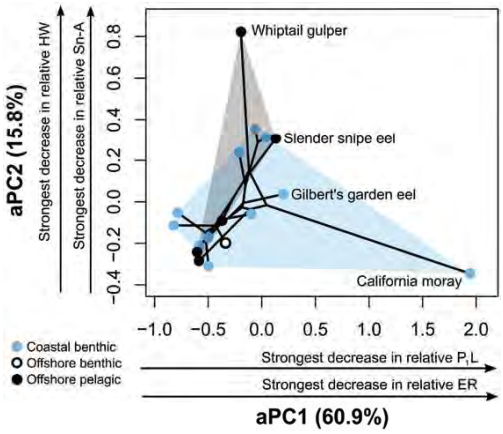

Figure 6. Phylo-allometric PCA (aPCA) for 17 species of eels across three habitat categories. For each species, morphological traits were centred, scaled and log-transformed, then regressed against body length. This resulted in a set of seven regression slopes for each species, which were used as observations in a phylogenetically corrected allometric principal components analysis (aPCA). Location in the morphospace indicates which characteristics show the most extreme size changes over growth for a species. For instance, the California moray (*Gymnothorax mordax*) experiences a complete loss of its pectoral fin over ontogeny. Snout-to-anus length, Sn-A; pectoral fin length, P_1L; head width, HW; and eye radius, ER.

crevice-dwelling lifestyles. Similarly, their leptocephali all have high aspect ratios. In other traits, leptocephali do not resemble adults. For example, large-jawed whiptail gulpers also have large jaws as larvae, but while adult whiptail gulpers are highly elongate, their larvae are short and deep-bodied. This mismatch could be due to evolutionary/physical constraints, where an elongate larval body plan may not be able to support large larval jaws, but this remains to be further tested. Although we did not have direct data on jaw size, only the dogface witch-eel occupied the pPCA morphospaces in the region defined by long heads and low body depths, providing tentative support for this hypothesis.

The scaling patterns of traits such as pectoral fin length, predorsal length and snout-to-anus length were highly variable, and no two species showed the same set of scaling patterns for all traits. This was surprising given that some species, such as the Pacific snake eel (*Ophichthus zophochir*) and yellow snake eel (*Ophichthus triserialis*) are in the same genus and live in the same habitat as adults. The two snake eels primarily diverged in head length and snout-to-anus length. Pectoral fin length also explained a high level of variance in scaling patterns among species, a trend that was driven by the California moray, which completely loses its pectoral fin over larval development. All members of the family Muraenidae have lost their pectoral fins as adults (Smith, 1979). As the only muraenid in our dataset, the California moray again demonstrates that loss of the pectoral fin during the larval stage is an unusual trait among Eastern Pacific eel families. Alternatively, the ringeye conger (*Paraconger californiensis*), shortsnout conger (*Chiloconger dentatus*) and shorthead conger (*Bathycongrus macrurus*) retained pectoral fins that were 26–30% of their head length at metamorphosis. Offshore pelagic species had even larger pectoral fins relative to body length, with the exception of the slender snipe eel (*Nemichthys scolopaceus*). Pectoral fins probably do not improve swimming performance of adult eels, which use undulation along their body lengths to move (Tytell & Lauder, 2004). Studies

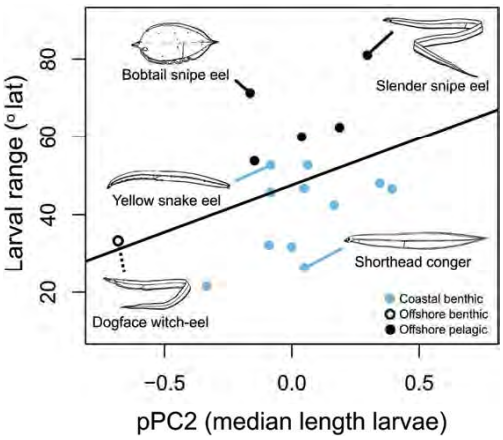

Figure 7. Morphological characteristics when larvae are halfway to transitioning can predict larval range. Here, morphology is represented in numerical form by pPC2 axis values from the median-size pPCA. Species with large larval ranges have long predorsal and snout-to-anus lengths when they are halfway to metamorphosis. The black line indicates the line of regression (R^2 adj. = 0.207). Illustrations of median-length larvae are modified from Smith (1979), Moser (1996) and Raju (1985).

of zebrafish (*Danio rerio*) larvae have shown that movement of pectoral fins improves respiration (Green *et al.*, 2011), but eels have low respiration rates, as the majority of their bodies are made up of non-metabolically active glycosaminoglycans (Bishop & Torres, 1999). The example of the California moray leads us to hypothesize that adult body plan influences pectoral fin development more than respiratory or locomotory needs during the larval stage.

In contrast, the relative size and scaling pattern of head characteristics (eye radius, head length and head width) were highly conserved across and within groups. Leptocephali retain large eyes throughout development potentially due to the importance of vision in finding and consuming food (Taylor *et al.*, 2011, 2015; Grace & Taylor, 2017). The large, rod-dominated eyes of leptocephali are unusual among fish larvae, and probably assist with feeding on particulate matter or gelatinous material in low-light conditions (Taylor *et al.*, 2011). Paralleling our finding that larval body shapes exhibit a stronger phylogenetic signal at later developmental stages, the retinal structure of elopomorph leptocephali has been shown to diverge with ecological niche as larvae approach metamorphosis (Taylor *et al.*, 2015).

The dogface witch-eel was a morphological outlier in our pPCAs due to its long head and very short snout-to-anus length. However, in other traits and in larval range, this single offshore benthic species aligned well with the coastal benthic group. This species appears to have evolved from a clade of coastal benthic eels (Supporting Information Fig. S1), suggesting that throughout its evolutionary history, the dogface witch-eel may have faced similar selective pressures towards dispersal as coastal benthic eels, such as an obligatory migration to juvenile habitat. However, its position as an outlier in our analyses also suggests that its derived benthopelagic lifestyle has strongly influenced both its larval and its adult morphology.

Morphology as a predictor of range size

We initially hypothesized that among the larvae in this study, species with relatively higher body aspect ratios (long and thin) or positive allometry for aspect ratio would have larger larval ranges. We also hypothesized that larvae with large maximum body lengths at metamorphosis, or rapid growth over ontogeny, would be able to escape the limitations of viscous fluid regimes and more effectively disperse via currents. These hypotheses were not supported for any habitat group. Surprisingly, relative predorsal fin length and snout-to-anus length at intermediate size were the strongest predictors of larval geographical range. Given these observations, we propose that longer relative anterior body segments may facilitate swimming in elongate larval forms. This hypothesis may be especially valid for leptocephali, whose large sizes place them in a fluid regime controlled by inertial rather than viscous forces. Previous studies have suggested that the tail provides a major source of power for larval fishes (Batty, 1984; Osse *et al.*, 1997). However, propulsive forces from the tail would be more beneficial to non-leptocephalus larval shapes which possess a caudal peduncle and tail fin. Leptocephali, like adult eels, utilize their entire bodies to swim; thus, longer predorsal lengths and snout-to-anus lengths may improve swimming ability through reduced drag and increased body propulsion (Lighthill, 1970, 1971; Tytell & Lauder, 2004; Katz & Hale, 2016). We found the relationship between predorsal length and snout-to-anus length and larval range to be true across a range of habitat categories, aspect ratios and maximum body sizes, indicating that it is the relative length of these segments in comparison to total body length (not the degree of elongation) that predicts geographical range. Tentative support for the swimming hypothesis comes from the catadromous eels in the genus *Anguilla*, which make long migrations (500–6000 km) as larvae. Leptocephali of Japanese eels (*Anguilla japonica*) have snout-to-anus lengths of 36–60% of total length

(Kuroki *et al.*, 2010) while American and European eels (*A. rostrata*, *A. anguilla*) have snout-to-anus lengths of 72–85% of total length (Bohlke, 1989). American and European eels have longer relative snout-to-anus lengths and undergo longer migrations as larvae than Japanese eels (McCleave *et al.*, 1987; Tsukamoto, 1992; Aoyama *et al.*, 2003). However, even though leptocephali in the present study are not known to undertake long migrations, species with larval ranges >60° latitude had snout-to-anus lengths that were 73–98% of total length, substantially larger than those in the genus *Anguilla*. These long anterior lengths suggest that an improved swimming ability may be more advantageous to eel species in the Eastern Pacific than previously thought.

Leptocephali of all three habitat groups may be passively transported substantial distances from the coast. Once in the open ocean, it is assumed that offshore pelagic species can metamorphose without any further migration, due to the relative homogeneity of the deep ocean and their pelagic lifestyle. In contrast, coastal benthic and offshore benthic species must travel to juvenile rearing sites while they are still leptocephali (Able & Fahay, 1998; Bell *et al.*, 2003; Wuenschel & Able, 2008; Miller *et al.*, 2011b). Thus, improved swimming abilities could be advantageous for species with limited juvenile habitat availability. However, our results show that offshore pelagic species with longer predorsal lengths and snout-to-anus lengths also have larger larval ranges, indicating that offshore pelagic species may undertake larger movements as larvae than previously assumed. While leptocephali are not common prey for other animals (Miller *et al.*, 2015), improved swimming ability may also allow larvae to escape predation.

An important caveat to the link between body shape and the physical environment is that many pre- or post-settlement factors limit recruitment and eventual survival of larvae (Carr & Syms, 2006). Intuitively, improved swimming abilities would allow larvae to disperse farther. However, the coastal benthic eels examined here had the narrowest ranges of all study species, implying that additional environmental and physiological constraints, particularly on processes surrounding settlement and recruitment, probably limit species' ranges more than the dispersal distance of a single individual. Under environmental and physiological constraints, increased larval dispersal distances would be ineffective at expanding a species' range, as any advantage obtained from dispersing farther would be nullified by the inability of the individual to survive to reproduce. This phenomenon has been shown for some species of marine invertebrates, whose adult range is constrained by sea surface temperature (Sanford *et al.*, 2006). The California moray may experience a similar constraint on adult range: California moray larvae successfully disperse and recruit to populations in southern California (the northernmost extent for this species), but are hypothesized to be mostly non-reproductive as adults due to water temperature inhibiting gonadal development (McCleneghan, 1973), a phenomenon supported by evidence from other basins (Miller & Robinet, 2018). Therefore, the interaction between temperature and reproductive physiology may ultimately restrict the range of the California moray. In contrast to coastal benthic species, the offshore pelagic group has access to a much larger area of suitable habitat for settlement due to the relative homogeneity of the deep ocean. Many of the offshore pelagic species in this study are found worldwide, suggesting that habitat availability contributes strongly to geographical range.

Improved information on larval distributions, pelagic larval duration times, spawning locations and the interaction between these factors could help to refine the relationship between morphology and geographical range. Pelagic larval duration times of individual larvae, in particular, can provide us with more insight into the effects of growth rate on larval ranges and survivorship. Importantly, we examined the overall geographical range reported for the species rather than the individual dispersal distance of a species' larva. Additionally, there were several mismatches between reported larval range and those reported for adults in this study. It is unclear if these range disparities are due to lack of sampling or biological mechanisms (e.g. adult migration). Systematic sampling for adults and larvae would strengthen the conclusions of our study, as would obtaining age data from larvae to assess pelagic larval duration time. Spawning location has also been shown to affect dispersal patterns of leptocephali in other regions (McCleave, 1993; Miller *et al.*, 2011b) and represents a large gap in our current knowledge of Eastern Pacific eels, especially with regard to offshore species. If a species spawns throughout its entire range, overall geographical range will appear large even if the dispersal distance of an individual larva is small. Similarly, growth rates, sea surface temperatures and current patterns, all of which are highly variable across space and time, may influence where fish settle (Norcross & Shaw, 1984; Miller *et al.*, 1988; Houde, 1989).

In this study, we found that adult body shape and adult habitat appear to influence the body shape of larvae, with phylogenetic signal increasing as larvae approach metamorphosis. Additionally, our finding that morphological traits at median size can predict geographical range leads us to ask whether this pattern is taxonomically widespread and that longer anterior body segments in other fish clades also have the capacity to improve dispersal, through swimming or other mechanisms.

ACKNOWLEDGMENTS

We thank William Watson, Sherri Carter and others at the National Oceanic & Atmospheric Administration Southwest Fisheries Science Center for providing morphological data. Members of the Mehta lab group and two anonymous reviewers provided comments on earlier drafts of the manuscript. We thank Vikram Baliga for statistical advice.

AUTHOR CONTRIBUTIONS

K.E.D. conceived the project, performed all analyses, and wrote the manuscript. M.T.T. contributed to statistical advice. R.S.M. provided guidance on theory and analyses. All authors discussed the results and edited the final manuscript.

REFERENCES

Able KW, **Fahay MP. 1998.** *The first year in the life of estuarine fishes in the middle Atlantic Bight.* New Brunswick: Rutgers University Press.

Aoyama J, **Wouthuyzen S**, **Miller MJ**, **Inagaki T**, **Tsukamoto K. 2003.** Short-distance spawning migration of tropical freshwater eels. *Biological Bulletin* **204:** 104–108.

Baliga VB, **Mehta RS. 2018.** Phylo-allometric analyses showcase the interplay between life-history patterns and phenotypic convergence in cleaner wrasses. *The American Naturalist* **191:** E129–E143.

Batty RS. 1984. Development of swimming movements and musculature of larval herring (*Clupea harengus*). *Journal of Experimental Biology* **110:** 217–229.

Bell GW, **Witting DA**, **Able KW. 2003.** Aspects of metamorphosis and habitat use in the conger eel, *Conger oceanicus*. *Copeia* **2003:** 544–552.

Bishop RE, **Torres JJ. 1999.** *Leptocephalus* energetics: metabolism and excretion. *The Journal of Experimental Biology* **202:** 2485–2493.

Bohlke EB, **ed. 1989.** Part 9, Volume 2. Leptocephali. In: *Fishes of the Western North Atlantic.* New Haven: Sears Foundation for Marine Research, 657–1055.

Bonhommeau S, **Castonguay M**, **Rivot E**, **Sabatie R**, **Le Pape O. 2010.** The duration of migration of Atlantic *Anguilla* larvae. *Fish and Fisheries* **11:** 289–306.

Bonhommeau S, **Le Pape O**, **Gascuel D**, **Blanke B**, **Tréguier AM**, **Grima N**, **Vermard Y**, **Castonguay M**, **Rivot E. 2009.** Estimates of the mortality and the duration of the trans-Atlantic migration of European eel *Anguilla anguilla* leptocephali using a particle tracking model. *Journal of Fish Biology* **74:** 1891–1914.

Brothers EB, **Thresher RE. 1985.** Pelagic duration, dispersal, and the distribution of Indo-Pacific coral-reef fishes. In: Reaka ML, ed. *The ecology of coral reefs.* Washington: National Oceanic and Atmospheric Administration, 53–70.

Carr MH. 1989. Effects of macroalgal assemblages on the recruitment of temperate zone reef fishes. *Journal of Experimental Marine Biology and Ecology* **126:** 59–76.

Carr MH, **Syms C. 2006.** Recruitment. In: Allen LG, Pondella DJ, Horn MH, eds. *The ecology of marine fishes: California and adjacent waters.* Berkeley: University of California Press, 411–427.

Castonguay M, **Mccleave JD. 1987.** Vertical distributions, diel and ontogenetic vertical migrations and net avoidance of leptocephali of *Anguilla* and other common species in the Sargasso Sea. *Journal of Plankton Research* **9:** 195–214.

Cowen RK. 1985. Large scale pattern of recruitment by the labrid, *Semicossyphus pulcher*: causes and implications. *Journal of Marine Research* **43:** 719–742.

Cowen RK, **Sponaugle S. 2009.** Larval dispersal and marine population connectivity. *Annual Review of Marine Science* **1:** 443–466.

Dong H, **Mittal R**, **Najjar FM. 2006.** Wake topology and hydrodynamic performance of low-aspect-ratio flapping foils. *Journal of Fluid Mechanics* **566:** 309–343.

Ebert TA, **Russell MP. 1988.** Latitudinal variation in size structure of the west coast purple sea urchin: a correlation with headlands. *Limnology and Oceanography* **33:** 286–294.

Froese R. 1990. *Growth strategies of fish larvae.* Unpublished D. Phil. Thesis, Universität Hamburg.

Froese R, **Pauly D. 2018.** *FishBase*. Available at: http://www.fishbase.org.

Fuiman LA. 1983. Growth gradients in fish larvae. *Journal of Fish Biology* **23:** 117–123.

Garland TJ, **Dickerman AW**, **Janis CM**, **Jones JA. 1993.** Phylogenetic analysis of covariance by computer simulation. *Systematic Biology* **42:** 265–292.

Gerlach G, **Atema J**, **Kingsford MJ**, **Black KP**, **Miller-Sims V. 2007.** Smelling home can prevent dispersal of reef fish larvae. *Proceedings of the National Academy of Sciences USA* **104:** 858–863.

Gisbert E, **Merino G**, **Muguet JB**, **Bush D**, **Piedrahita RH**, **Conklin DE. 2002.** Morphological development and allometric growth patterns in hatchery-reared California halibut larvae. *Journal of Fish Biology* **61:** 1217–1229.

Grace MS, **Taylor SM. 2017.** Species-specific development of retinal architecture in elopomorph fishes: adaptations for harvesting light in the dark. *Bulletin of Marine Science* **93:** 339–353.

Grafen A. 1989. The phylogenetic regression. *Philosophical Transactions of the Royal Society B* **326:** 333–371.

Green MH, **Ho RK**, **Hale ME. 2011.** Movement and function of the pectoral fins of the larval zebrafish (*Danio rerio*) during slow swimming. *The Journal of Experimental Biology* **214:** 3111–3123.

Greer AT, **Woodson CB**, **Guigand CM**, **Cowen RK. 2016.** Larval fishes utilize Batesian mimicry as a survival strategy in the plankton. *Marine Ecology Progress Series* **551:** 1–12.

Harmon L, **Weir J**, **Brock C**, **Rich G**, **Challenger W. 2008.** GEIGER: investigating evolutionary radiations. *Bioinformatics* **24:** 129–131.

Higgins BA, **Pearson D**, **Mehta RS. 2017.** El Niño episodes increase California moray recruits around Santa Catalina Island. *Journal of Fish Biology* **90:** 1570–1583.

Houde ED. 1989. Comparative growth, mortality, and energetics of marine fish larvae: temperature and implied latitudinal effects. *Fishery Bulletin* **87:** 471–495.

Hunt von Herbing I. 2002. Effects of temperature on larval fish swimming performance: the importance of physics to physiology. *Journal of Fish Biology* **61:** 865–876.

Katz HR, **Hale ME. 2016.** A large-scale pattern of ontogenetic shape change in ray-finned fishes. *PLoS ONE* **11:** 1–7.

Knights B. 2003. A review of the possible impacts of long-term oceanic and climate changes and fishing mortality on recruitment of anguillid eels of the Northern Hemisphere. *Science of the Total Environment* **310:** 237–244.

Kuroki M, **Fukuda N**, **Yamada Y**, **Okamura A**, **Tsukamoto K. 2010.** Morphological changes and otolith growth during metamorphosis of Japanese eel leptocephali in captivity. *Coastal Marine Science* **34:** 31–38.

Lighthill MJ. 1970. Aquatic animal propulsion of high hydromechanical efficiency. *Journal of Fluid Mechanics* **44:** 265–301.

Lighthill MJ. 1971. Large-amplitude elongated-body theory of fish locomotion. *Proceedings of the Royal Society B* **179:** 125–138.

Limouzy-Paris CB, **Graber HC**, **Jones DL**, **Röpke AW**, **Richards WJ. 1997.** Translocation of larval coral reef fishes via sub-mesoscale spin-off eddies from the Florida current. *Bulletin of Marine Science* **60:** 966–983.

Llopiz J, **Cowen R**, **Hauff M**, **Ji R**, **Munday P**, **Muhling B**, **Peck M**, **Richardson D**, **Sogard S**, **Sponaugle S. 2014.** Early life history and fisheries oceanography: new questions in a changing world. *Oceanography* **27:** 26–41.

McCleave JD. 1993. Physical and behavioural controls on the oceanic distribution and migration of leptocephali. *Journal of Fish Biology* **43:** 243–273.

McCleave JD, **Brickley PJ**, **O'Brien KM**, **Kistner Da**, **Wong MW**, **Gallagher M**, **Watson SM. 1998.** Do leptocephali of the European eel swim to reach continental waters? Status of the question. *Journal of the Marine Biological Association of the United Kingdom* **78:** 285–306.

McCleave JD, **Kleckner RC**, **Castonguay M. 1987.** Reproductive sympatry of American and European eels and implications for migration and taxonomy. In: American Fisheries Society Symposium, **1:** 286–297.

McCleneghan K. 1973. *The ecology and behavior of the California moray eel* Gymnothorax mordax *(Ayres, 1859) with descriptions of its larva and the leptocephali of some other East Pacific Muraenidae.* Unpublished D. Phil. Thesis, University of Southern California.

McHenry MJ. 2005. The mechanical scaling of coasting in zebrafish (*Danio rerio*). *Journal of Experimental Biology* **208:** 2289–2301.

Miller MJ. 2009. Ecology of Anguilliform leptocephali: remarkable transparent fish larvae of the ocean surface layer. *Aqua-BioScience Monographs* **2:** 1–94.

Miller TJ, **Crowder LB**, **Rice JA**, **Marschall EA. 1988.** Larval size and recruitment mechanisms in fishes: toward a conceptual framework. *Canadian Journal of Fisheries and Aquatic Sciences* **45:** 1657–1670.

Miller MJ, **Dubosc J**, **Vourey E**, **Tsukamoto K**, **Allain V. 2015.** Low occurrence rates of ubiquitously present leptocephalus larvae in the stomach contents of predatory fish. *ICES Journal of Marine Science* **70:** 883–891.

Miller MJ, **Norman MD**, **Tsukamoto K**, **Finn JK. 2013.** Evidence of mimicry of gelatinous zooplankton by anguilliform leptocephali for predator avoidance. *Marine and Freshwater Behaviour and Physiology* **45:** 375–384.

Miller MJ, **Robinet T. 2018.** Life history and morphology of eel larvae in the Gulf of Guinea of western Africa: revisiting Jacques Blache's research (1960–1977) 40 years later. *Reviews in Fish Biology and Fisheries* **28:** 355–379.

Miller MJ, **Wouthuyzen S**, **Ma T**, **Aoyama J**, **Suharti SR**, **Minegishi Y**, **Tsukamoto K. 2011a.** Distribution, diversity, and abundance of garden eel larvae off west Sumatra, Indonesia. *Zoological Studies* **50:** 177–191.

Miller MJ, **Yoshinaga T**, **Aoyama J**, **Otake T**, **Mochioka N**, **Kurogi H**, **Tsukamoto K. 2011b.** Offshore spawning of *Conger myriaster* in the western North Pacific: Evidence for convergent migration strategies of anguilliform eels in the Atlantic and Pacific. *Naturwissenschaften* **98:** 537–543.

Moser HG. 1981. Morphological and functional aspect of marine fish larvae. In: Lasker R, ed. *Marine fish larvae: morphology, ecology, and relation to fisheries.* Seattle: Washington Sea Grant Program, 89–131.

Moser HG, ed. **1996.** *The early stages of fishes in the California current region.* La Jolla: National Oceanic and Atmospheric Administration.

Moser HG, **Watson W. 2006.** Ichthyoplankton. In: Allen LG, Pondella DJ, Horn MH, eds. *The ecology of marine fishes: California and adjacent waters.* Berkeley: University of California Press, 269–319.

Muller UK, **van den Boogaart JGM**, **van Leeuwen JL. 2008.** Flow patterns of larval fish: undulatory swimming in the intermediate flow regime. *Journal of Experimental Biology* **211:** 196–205.

Müller UK, **Stamhuis EJ**, **Videler JJ. 2000.** Hydrodynamics of unsteady fish swimming and the effects of body size: comparing the flow fields of fish larvae and adults. *The Journal of Experimental Biology* **203:** 193–206.

Naisbett-Jones L, **Putman N**, **Stephenson J**, **Ladak S**, **Young K. 2017.** A magnetic map leads juvenile European eels to the Gulf stream. *Current Biology* **27:** 1–5.

Norcross BL, **Shaw RF. 1984.** Oceanic and estuarine transport of fish eggs and larvae: a review. *Transactions of the American Fisheries Society* **113:** 153–165.

Olson CL. 1979. Practical considerations in choosing a MANOVA test statistic: a rejoinder to Stevens. *Psychological Bulletin* **86:** 1350–1352.

Orme D, **Freckleton R**, **Thomas G**, **Petzoldt T. 2013.** *The caper package: comparative analysis of phylogenetics and evolution in R. R package, Version 5.2.* Available at: http://CRAN.R-project.org/package=caper.

Osse JWM. 1989. Form changes in fish larvae in relation to changing demands of function. *Netherlands Journal of Zoology* **40:** 362–385.

Osse JWM, **van den Boogaart JGM**, **van Snik GMJ**, **van der Sluys L. 1997.** Priorities during early growth of fish larvae. *Aquaculture* **155:** 249–258.

Peck MA, **Huebert KB**, **Llopiz JK. 2012.** Intrinsic and extrinsic factors driving match-mismatch dynamics during the early life history of marine fishes. *Advances in Ecological Research* **47:** 177–302.

R Core Team. **2016.** *A language and environment for statistical computing*. Vienna: R Foundation for Statistical Computing. Available at: https://www.R-project.org/.

Raju SN. 1985. Congrid eels of the eastern Pacific and key to their leptocephali. *NOAA Technical Report NMFS* **22:** 1–19.

Revell LJ. 2009. Size-correction and principal components for interspecific comparative studies. *Evolution* **63:** 3258–3268.

Revell LJ. 2012. Phytools: an R package for phylogenetic comparative biology (and other things). *Methods in Ecology and Evolution* **3:** 217–223.

Robins CR. 1989. The phylogenetic relationships of the anguilliform fishes. In: Böhlke EB, ed. *Fishes of the Western North Atlantic*. New Haven: Yale University Press, 9–23.

Roughgarden J, **Gaines S**, **Possingham H. 1988.** Recruitment dynamics in complex life cycles. *Science* **241:** 1460–1466.

Ryland JS. 1962. The swimming speeds of larval plaice. *Journal of Experimental Biology* **40:** 285–399.

Rypina II, **Llopiz JK**, **Pratt LJ**, **Lozier MS. 2014.** Dispersal pathways of American eel larvae from the Sargasso Sea. *Limnology and Oceanography* **59:** 1704–1714.

Sambilay V Jr. **1990.** Interrelationships between swimming speed, caudal fin aspect ratio and body length of fishes. *Fishbyte* **8:** 16–20.

Sanford E, **Holzman SB**, **Haney RA**, **Rand DM**, **Bertness MD. 2006.** Larval tolerance, gene flow, and the northern geographic range limits of fiddler crabs. *Ecology* **87:** 2882–2894.

Santini F, **Kong X**, **Sorenson L**, **Carnevale G**, **Mehta RS**, **Alfaro ME. 2013.** A multi-locus molecular timescale for the origin and diversification of eels (Order: Anguilliformes). *Molecular Phylogenetics and Evolution* **69:** 884–894.

Shanks AL. 2009. Pelagic larval duration and dispersal distance revisited. *Biological Bulletin* **216:** 373–385.

Shanks AL, **Eckert GL. 2005.** Population persistence of California current fishes and benthic crustaceans: a marine drift paradox. *Ecological Monographs* **75:** 505–524.

Sheehan-Holt JK. 1998. MANOVA simultaneous test procedures: the power and robustness of restricted multivariate contrasts. *Educational and Psychological Measurement* **58:** 861–881.

Smith DG. 1979. Guide to the leptocephali (Elopiformes, Anguilliformes, and Notacanthiformes). *NOAA Technical Report NMFS Circular* **424:** 39.

Stevens LM, **Blob RW**, **Mayerl CJ. 2018.** Ontogeny, morphology and performance: changes in swimming stability and turning performance in the freshwater pleurodire turtle, *Emydura subglobosa*. *Biological Journal of the Linnean Society* **125:** 718–729.

Stobutzki I, **Bellwood D. 1997.** Sustained swimming abilities of the late pelagic stages of coral reef fishes. *Marine Ecology Progress Series* **149:** 35–41.

Taylor SM, **Loew ER**, **Grace MS. 2011.** A rod-dominated visual system in leptocephalus larvae of elopomorph fishes (Elopomorpha: Teleostei). *Environmental Biology of Fishes* **92:** 513–523.

Taylor SM, **Loew ER**, **Grace MS. 2015.** Ontogenic retinal changes in three ecologically distinct elopomorph fishes (Elopomorpha: Teleostei) correlate with light environment and behavior. *Visual Neuroscience* **32:** 1–13.

Tsukamoto K. 1992. Discovery of the spawning area for Japanese eel. *Nature* **356:** 789–791.

Tsukamoto K, **Yamada Y**, **Okamura A**, **Kaneko T**, **Tanaka H**, **Miller MJ**, **Horie N**, **Mikawa N**, **Utoh T**, **Tanaka S. 2009.** Positive buoyancy in eel leptocephali: an adaptation for life in the ocean surface layer. *Marine Biology* **156:** 835–846.

Tytell ED, **Lauder GV. 2004.** The hydrodynamics of eel swimming. *The Journal of Experimental Biology* **207:** 1825–1841.

Voesenek CJ, **Muijres FT**, **Leeuwen JL Van. 2018.** Biomechanics of swimming in developing larval fish. *Journal of Experimental Biology* **221:** 1–14.

Vogel S. 1996. *Life in moving fluids: the physical biology of flow.* Princeton: Princeton University Press.

Webb PW. 1988. Simple physical principles and vertebrate aquatic locomotion. *American Zoologist* **28:** 709–725.

Webb PW, **Weihs D. 1986.** Functional locomotor morphology of early life history stages of fishes. *Transactions of the American Fisheries Society* **115:** 115–137.

Wilson DT, **Meekan MG. 2002.** Growth-related advantages for survival to the point of replenishment in the coral reef fish *Stegastes partitus* (Pomacentridae). *Marine Ecology Progress Series* **231:** 247–260.

Wuenschel MJ, **Able KW. 2008.** Swimming ability of eels (*Anguilla rostrata*, *Conger oceanicus*) at estuarine ingress: contrasting patterns of cross-shelf transport? *Marine Biology* **154:** 775–786.

SUPPORTING INFORMATION

Additional Supporting Information may be found in the online version of this article at the publisher's website.

Figure S1. Time-calibrated phylogenetic tree of eel species in this dataset. The tree was constructed using phylogenetic information from Santini *et al.* (2013).
Table S1. Adult and larval geographic range values and source literature for each of the 17 species examined.
Table S2. Loadings for the median and maximum phyloallometric PCAs (pPCAs) which were performed using median-length and maximum-length larva for each species. Also shown is the variance explained by each axis.
Table S3. Axis loadings from the phyloallometric PCA (aPCA). Also shown is the variance explained by each axis.
Table S4. Scaling patterns for seven characteristics across 17 species. All characteristics are size-corrected by body length.

Chapter 2

California moray eels exhibit local adaptation in the face of high gene flow

Katherine E. Dale[1], Giacomo Bernardi[1], Arturo Ramírez-Valdez[2,3], Daniel B. Wright[1], Jorge Rosales Casian[4], Rita S. Mehta[1]

[1]University of California, Santa Cruz, CA

[2]Facultad de Ciencias Marinas, Universidad Autónoma de Baja California, Ensenada, Baja California, Mexico

[3]Scripps Institution of Oceanography, University of California San Diego, La Jolla, CA

[4]Centro de Investigación Científica y de Educación Superior de Ensenada, Baja California

Abstract

We examined population connectivity across nearly the entire adult range of a subtropical Eastern Pacific fish species, the California moray (*Gymnothorax mordax*). Our objectives were to determine if California morays have high gene flow or show distinct population structure across different parts of their range, identify signatures of populations sources/recipient populations, and examine which environmental or oceanographic processes may contribute to structuring populations. We used restriction site-associated sequencing (RADseq) to examine genetic diversity across 252 individuals from 11 locations We used satellite data on sea surface temperature,

sea surface temperature anomaly, and sea surface height to examine whether environmental characteristics at the time of settlement were correlated with patterns of local adaptation. We found high gene flow across all populations, though a small subset of loci showed strong signs of local adaptation. Patterns of local adaptation were correlated with sea surface temperature, sea surface temperature anomaly, and sea surface height at the time of settlement, but not with geographic distance. Genes under selection have been implicated in teleost eye development, reproduction, and stress. Despite high gene flow, the California moray exhibits local adaptation with phenotype-environment mismatches during the late larval/early juvenile stages, ultimately constraining the range of the species. is consistent with

Introduction

Many marine reef fishes have a planktonic larval form that allows for population connectivity even across large geographic areas (Leis 1991). The highest rate of mortality in marine fishes occurs during this pelagic residence period and immediately following settlement, as larvae must find appropriate settlement habitats, find food, avoid predation (Sifa and Mathias 1987; Leggett and Deblois 1994; Garrido et al. 2015) Selection during the pelagic larval period or following settlement can thus ultimately constrain the geographic range of marine species and limit connectivity (Sanford et al. 2003, 2006; Marshall et al. 2010; Pinsky et al. 2020). Larval fish with traits such as increased growth rates, stronger swimming abilities, or higher tolerances for colder/warmer water may be more likely to reach and establish

primarily recipient populations (Leis 2018). Once they arrive, there could be a phenotype-environment mismatch if the individual is maladapted (Marshall et al. 2010). Under this framework, it would be expected that recipient populations to exhibit a lower genetic diversity than source populations, as individuals with lower fitness are "filtered out" before reaching reproduction age (Sotka 2012). However, a greater level of genetic diversity can be maintained for recipient populations with slow rates of population decay, such as for long-lived species or recipient populations with some amount of local reproduction (Gaggiotti and Smouse 1996).

In addition to inherent biological factors, abiotic characteristics of the environment such as the strength and direction of oceanic currents, oceanographic processes such as eddies and upwelling, geographic features such as islands and peninsulas, and large-scale climate oscillations can all influence larval mortality and dispersal (Cowen and Sponaugle 2009). One region with complex oceanographic patterns is the northeastern Pacific between the Baja California Peninsula, Mexico and southern California, USA. Two biogeographic provinces span this area: The warm-temperate San Diegan province and the subtropical Cortez province (Horn et al. 2006). There is a dramatic increase in sea surface temperatures moving south across these provinces, from an average of 15°C in California to an average of 23°C in southern Baja California. In the south, warmer waters from off the coast of central America arrive to mix with the southward flowing, cold-water California Current. The location of the biogeographic break between the two provinces varies for different species complexes, with Punta Eugenia and Bahía Magdalena being

commonly-cited cutoffs (Fig. 1; Robertson & Cramer 2009, Ruiz-Campos et al. 2010, Briggs & Bowen 2012).

In general, the subtropical western Pacific is dominated by the strong, cold-water California Current. However, seasonal, yearly, and decadal variations can cause the California Current to weaken or move offshore. For instance, during El Niño Southern Oscillation (ENSO) events and to a lesser extent during winter months from November to March, the coastal northward-flowing Davidson Current strengthens (Hickey 1979; Durazo 2015). This allows propagules from northern Baja California to be advected northward to California (Shanks and Eckert 2005). This phenomenon was most recently observed in the 2014-15 "warm blob" and 2015-16 ENSO events, during which many unusual fish species were recorded in southern California (Walker et al. 2020). The southern region of the San Diegan province south of Punta Eugenia also experiences seasonal changes, with a winter-spring dominated by the cold California Current and summer-fall that experiences warm northward currents from central Mexico (Durazo 2015). Therefore, seasonal or decadal shifts in oceanographic patterns can lead to population size fluctuations, or, at minimum, the arrival of unusual vagrants (Cowen 1985; Davis 2000; Lluch-Belda et al. 2005; Higgins et al. 2017).

Shifts in environmental conditions can also act as a strong selective pressure. Although the potential for genetic connectivity in the western Pacific is high, many marine organisms this region show surprisingly robust population structure, even when examining only a small subset of genetic markers. These trends are best

explained by local retention, negligible adult movement, geographic barriers, and species' interactions with abiotic factors, rather than geographic distance or pelagic larval duration time (Huang and Bernardi 2001; Bernardi et al. 2003; Sivasundar and Palumbi 2010; Paterson et al. 2015; Garcia et al. 2020; Mejía-ruíz et al. 2020). This is true even for species with long pelagic larval duration times, such as California spiny lobster (*Panulirus interruptus*) which remains planktonic for nearly a year (Iacchei et al. 2013). At the same time, some island communities appear to be recipient populations reliant on larvae arriving during ENSO events (Cowen 1985; Higgins et al. 2017). Thus, in the oceanographically complex eastern Pacific, there could be a variety of selective pressures on behavior, morphology, and physiology during both the critical pelagic residence period and post-settlement.

One Eastern Pacific fish species whose population connectivity has been suggested to depend on ENSO is the California moray eel (*Gymnothorax mordax*). The California moray is the only common muraenid found off California, and has a geographic range stretching from the California Bight to the southern end of Baja California, Mexico (Dale et al. 2021). Morays have an unusual larval form called a leptocephalus thatandthat is shared with other members of superorder Elopomorpha, which consists of the orders Anguilliformes (true eels) and Elopiformes (tarpon, bonefish, and relatives) These flattened, leaf-shaped, transparent larvae are larger than virtually any other fish larvae, and remain in the pelagic environment for long periods of time (Miller 2009). Although the pelagic larval duration (PLD) of the California moray is unknown, aging studies of other morays suggest a pelagic

residence of at least 45-80 days (Brothers and Thresher 1985; Bishop et al. 2000; Huang et al. 2018). While PLD is not as strong a predictor of dispersal distance and population connectivity as previously thought (Shanks 2009; Weersing and Toonen 2009; Selkoe and Toonen 2011; Leis et al. 2013), species with PLD times >45 days (such as anguilliform eels) often have broad ranges (Lester and Ruttenberg 2005). Previous genetic connectivity studies of morays in the Pacific have found no population structure (Reece et al. 2010, 2011; Huang et al. 2018; Ribout et al. 2018; Li et al. 2021). no population structure

Past work has shown that morays have a number of morphological adaptations that allow them to eat a variety of prey types including larger prey than expected; they are also long-lived and have minimal adult movement (Diluzio et al. 2017; Harrison et al. 2017; Higgins and Mehta 2018; Higgins et al. 2018; Mehta et al. 2020). In the 1970s, examinations of California moray gonads from individuals around Catalina Island in the California Channel Islands led to a long-standing hypothesis that the moray population in southern California may be comprised of nonreproductive individuals whose gonadal development is limited by cold water (McCleneghan 1973). Further work on otoliths showed that 30 of 33 individuals examined settled at Catalina Island during ENSO events (Higgins et al. 2017).

The adult range of the California moray spans two biogeographic provinces, a north-to-south sea surface temperature gradient of ~10°C, and strong seasonal patterns that vary between the southern and northern parts of their range. Thus, it would not be surprising if environmental conditions at the edges of their range were

influencing reproduction and dispersal patterns. Under this framework, the California moray could be an interesting example of an ecologically important fish species that has successfully established populations primarily reliant on the arrival of external larvae.

Here, we set out to 1) determine if the California moray has high gene flow across its range or shows population structure, 2) identify signatures of source and recipient populations, and 3) identify potential environmental or oceanographic processes may contribute to population structure. Based on previous studies of muraenids, we hypothesized that California morays would show high genetic connectivity. We also hypothesized that populations in southern California would be primarily recipient populations with low genetic diversity due to environment-phenotype mismatches, and that patterns of genetic diversity would correlate with ENSO conditions.

Methods

Sampling

Adult California morays (*Gymnothorax mordax*) were captured at five coastal sites and six islands between southern California, USA, and southern Baja California Sur, Mexico (Fig. 1; Table 2.1). All morays from Catalina Island, San Diego, Isla San Martin, and Las Barrancas were captured inusingin custom-made vinyl-coated wire traps (36” x 11” x 9”) deployed in depths < 20 m, primarily in boulder/cobble habitats. 15 eels from Palos Verdes (62.5%) were also trapped using this method.

Traps were baited by placing frozen anchovies or fish scraps into perforated plastic bottles, which allow the bait to be smelled but not accessed. Traps were set in the late afternoon and retrieved the following morning. Morays were lightly anesthetized using tri-methylsulfate (dosage 90 mg/L) before taking morphological measurements. We measured standard length (tip of the rostrum to end of the tail), head length (tip of the rostrum to buccopharyngeal opening), and body length (tip of the rostrum to anus). A 20 mg tissue sample was removed from the rear portion of the dorsal fin and stored in 90% ethanol. Morays were then placed in a bucket of fresh seawater to recover. Nine morays from Palos Verdes (37.5%) were obtained through South Coast Bio-Marine LLC using wire-frame traps. Morays from California were sampled under California Department of Fish and Wildlife permit #S-190830002-19086-001.

Morays from Isla Guadalupe, Isla San Jerónimo, Isla Natividad, and Punta Abreojos were obtained as bycatch via Mexican the spiny lobster fishery, who use baited wire-frame traps. Due to close geographic proximity and a small sample size (n = 3), individuals from Isla San Jerónimo were combined with Isla San Martin. Morays were frozen and transported to the US under Mexican export permit #SGPA/DGVS/01325/20. We conducted the same measurements and tissue sampling on moray bycatch. The two samples from Todos Santos were obtained from the Scripps Institution of Oceanography ichthyology tissue collection (specimens SIO 09-293, 11-328). Specimens were obtained in 2009 and 2011 via fishing bycatch. No detailed morphological information was available for Todos Santos specimens.

RAD library preparation

DNA was extracted and purified using Qiagen DNeasy Blood & Tissue kits (Qiagen, Inc) following standard protocols for subsampled tissue. We used restriction-associated DNA sequencing (RADseq) to examine population connectivity. RADseq is a powerful, low-coverage method that can be used to examine genome-wide genetic diversity in non-model organisms. A restriction enzyme is used to cut the nuclear genome at specific restriction sites; the sequences of these restriction sites can then be compared across individuals to assess genetic similarity. We constructed RAD libraries following Miller et al. (2007) and Baird (2008), using the enzyme Sbf1 for digestion. An initial concentration of 10 ng/uL of nuclear DNA was added from each individual for a total of 100 ng of starting material. After initial digestion and adding unique Illumina barcodes, samples were multiplexed and sheared to 500 bp using a Biorupter Sonicator. Non-tagged DNA was removed using Dynabeads (Invitrogen 11206D). All other purification and size-selection steps were completed using SPRI beads (Deangelis et al. 1995). Preparation for Illumina sequencing was completed using NEBNext reagents (New England Biolabs). Final amplification PCR was performed using a reaction volume of 16.6 uL and 10 amplification cycles. Libraries were sequenced at UC Berkeley QB3 Genomics using an Illumina NovaSeq SP platform using a 100SR/10× protocol.

Data filtering and genotype calling

We filtered out poor quality reads using a custom Perl script, selecting sequences with phred scores > Q33 and a minimum length of 80 bp. Individuals with ≤ 10 MB of data were removed. To identify and genotype single nucleotide polymorphisms (SNPs) in the remaining individuals, we used STACKS2 (Catchen et al. 2011, 2013). STACKS2 was then used to construct an initial catalog of consensus loci with *cstacks* using the top 10 most data-rich individuals from each population; for Todos Santos (n = 2) and Isla Guadalupe (n = 7), we included all individuals. The final catalog was constructed using 89 individuals. We then aligned the individual samples to the catalog with *sstacks*. In constructing stacks, we allowed for a maximum of three nucleotide mismatches between individuals (-M = 3) and required a minimum stack depth of three (-m = 3). We used *populations* to remove loci that were not present in ≥80% of individuals and to generate population statistics for downstream analysis.

Data analysis

Analysis using LOSITAN (Antao et al. 2008) confirmed that loci under directional selection were those with heterozygosity ≥ 0.025 and Φ_{st} values ≥ three standard deviations above the mean. We again ran *populations* for putative loci under selection and the remaining neutral loci. Within-population genetic diversity values (F_{is}) were produced by STACKS2 for all populations. We calculated pairwise Weir and Cockerham F_{st} values for both loci under selection and neutral loci using the 'pairwise.WCfst' function in R package 'hierfstat' (Goudet 2005). The Weir and Cockerham estimate is unbiased with regards to sample size.

We used STRUCTURE 2.3.4 (Pritchard et al. 2000) to identify haplotype clusters for both loci under selection and neutral loci. STRUCTURE assumes unlinked loci and panmixia. We used a parameter set of 10,000 burn-in reps and 100,000 reps from K=1 to K=10. To determine the most useful value of K for describing the dataset, we used the Evanno method as implemented through Structure Harvester (Earl and vonHoldt 2012).

To examine the relative strength of local adaptation versus gene flow, we first needed to remove any swamping effect of having many potentially genetically similar sampling sites. From the STRUCTURE analysis of loci under selection, we extracted what we termed "single-ancestry" individuals: Any individual that was identified as having a > 0.90 probability of belonging to a single genetic cluster. We reran *populations* on this subset, with each individual mapped to its genetic cluster rather than its original population. We then reran STRUCTURE on both the initial set of loci under selection and neutral loci and recalculated pairwise F_{st} values.

To additionally examine genetic divergence, we ran several Discriminant Analysis of Principal Components (DAPC) analyses using the 'dapc' function in R package 'adegenet' (Jombart 2008). DAPC is useful as it minimizes distances within populations, maximizes distances between populations, and collapses variation into several principal axes. We first ran a DAPC on neutral loci. We then constructed two DAPCs on loci under selection: First, for all individuals, and second without the two individuals from Todos Santos. We used the function 'xvalDapc' in package 'adegenet' to perform cross-validation and identify that we should retain 30 principal

components. We extracted the sequences of loci that explained ≥ 80% of variability along each axis.

We sent sequences for loci under selection through BLAST (https://blast.ncbi.nlm.nih.gov/Blast.cgi) to search the GenBank nucleotide database for "highly similar" matches to existing sequences, both protein-coding sequences as well as sequences without annotation. We extracted all protein-coding matches with E-values < 1^{-10}. We then conducted a literature search to examine the potential function of these genes in teleost fishes.

Environmental predictors of genetic divergence

First, we tested for simple isolation-by-distance between sampling sites. For this, we used a Mantel test between a matrix of genetic distances and a matrix of geographic distances, examining if the original correlation between matrices fell within a reference distribution generated by 5,000 permutations on the data.

We hypothesized that oceanographic conditions at the time of settlement would be predictive factors of genetic divergence. Age of each individual was estimated using the Von Bertalanffy growth curve built in Mehta et al. (2020), which found that head length is the strongest predictor of age. We did not have head length data for the two individuals from Todos Santos thus excluded them from environmental analyses. To obtain predicted settlement year, we subtracted estimated age from the year the individual was trapped.

Sea surface temperature (SST), sea surface temperature anomaly (SSTA), sea surface height (SSH), and the magnitude of Ekman transport (EKM) were selected for analysis. SST, SSTA, and SSH as these variables are proxies for El Niño Southern Oscillation events. EKM is a proxy for upwelling, an oceanographic process characteristic of the California Current system. We extracted monthly composite satellite data for SST, SSTA, and EKM from ERDDAP (dataset IDs: SST = erdMWsstdmday_LonPM180; SSTA = jplMURSST41anommday; EKM = erdlasFnTran6_LonPM180). SST and SSTA were available from 2002-present and for 91% of individuals' settlement years. EKM data was available from 1967-present but was only available for 46.7% of settlement years/locations. Monthly SSH data was extracted from PO.DACC (DOI: 10.5067/DYNTO-1D1M1) and were available from 1992-2010, encompassing 77.3% of individuals' settlement years. Data for all variables was averaged over a 6-month period from July-December, corresponding to the timeframe in which muraenid leptocephali are most abundant in coastal waters between Baja and southern California (Fig. S2.1).

We used DAPC axis values as a proxy for local adaptation trends. We used the DAPC on loci under selection, without the excluded Todos Santos individuals. We then ran a series of linear regressions for SST, SSH, and EKM, with each environmental variable as the predictor and DAPC axis 1 and 2 values as the response. To test if the resulting trends were particular to settlement year (and not any other set of years), we bootstrapped each regression by first assigning each individual a random year from within the support of each environmental dataset, then reran the

regression and extracted the slope. We completed 10,000 permutations of each regression, then examined if the original slope fell within the 2.5-97.5% percentiles of the bootstrapped slope values. We noted that the SSTA trend did not appear to be linear. Thus, for SSTA we used a Generalized Additive Model (GAM) to test the relationship between SSTA and the DAPC axes. The GAM was run using a Gaussian distribution family and a REML smoothing parameter estimation method with $k = 3$ basis functions. We ran a similar bootstrapping procedure with SSTA, extracting the first coefficient rather than the slope.

Higgins et al. (2017) used Oceanic Niño Index values to classify individuals as settling during ENSO, La Niña, or Neutral conditions and found that California morays around Catalina Island appeared to settle during ENSO events. To reexamine this trend with our data, we extracted ONI values (https://origin.cpc.ncep.noaa.gov/products/analysis_monitoring/ensostuff/ONI_v5.php) and classified each individual's settlement conditions following the protocol in Higgins et al. (2017): Over the course of each year, if ONI values remained >0.5 for a 6-month period, we considered it an ENSO year; if ONI values remained < -0.5 for a 6-month period, we considered it a La Niña year; any year where neither condition was met was classified as Neutral. We then ran an ANOVA between the three settlement conditions to examine if morays were settling more frequently in one of the three conditions.

To determine whether there were signatures of filtering between dispersal and adulthood, we extracted larval occurrence data for *Gymnothorax mordax*. Data were

obtained from the Scripps Institution of Oceanography Marine Vertebrate collection (https://sioapps.ucsd.edu/collections/mv/), the California Cooperative Oceanic Fisheries Investigation (CalCOFI; www.calcofi.org), and the Investigaciones Mexicanas de la Corriente de California (IMECOCAL; https://imecocal.cicese.mx/wp/). The latter two are ichthyoplankton sampling programs that have been collecting fish larvae in the California Current since 1950 and 1992, respectively.

Results

Genetic characteristics

We extracted and sequenced DNA from 10 locations. 252 individuals had >10 MB of high-quality data and were retained (Table 2.1). The final catalog contained 188,511 loci. An average of 55,745 stacks were created per individual (range: 12,026-104,828). Mean effective per-sample coverage was 12.3 (std dev = 8.2). Average polymorphism across all populations was 46% (range: 21-66%; Table 2.1). When examining all loci, average F_{is} was 0.0001, indicating fewer heterozygotes than expected within each population. K=2 was found to be an appropriate number of clusters for describing the dataset.

Neutral loci

54,960 loci were classified as neutral loci. When considering neutral loci, between-group genetic diversity was very low (Table 2.2; mean F_{st} = 0.0002). Similar to F_{st}

values, STRUCTURE analyses revealed that for neutral loci, California morays have very high gene flow, with no signal of genetic drift (Fig. 2.2a-b). All individuals had a ≥ 93.7% probability of belonging to a single haplotype. DAPC results revealed little population structure (Fig. S2.2.

Loci under selection

After filtering, 216 loci were found to be under directional selection. Pairwise F_{st} values for loci under selection were substantially higher (Table 2.2; mean $F_{st} = 0.40$). STRUCTURE analyses confirmed that population structure emerges when examining this subset of loci. Two haplotypes emerged (Fig. 2.2): A "coastal southern California/northern Baja" haplotype, consisting of Palos Verdes, San Diego, and Islas San Martin/San Jerónimo and a "Guadalupe/Todos Santos" haplotype consisting of Isla Guadalupe, Todos Santos, and Catalina Island (Cat Harbor). Interestingly, Catalina Island (Two Harbors area) and Punta Abreojos consisted of 73.6% and 100% F1 hybrids, respectively. The "single-ancestry" analysis reinforced differences between neutral loci and loci under selection, by removing the potential effect of having many sampling sites included in the analysis (Fig. 2.2c-d). We classified 91 individuals (36.1%) as "single-ancestry," with a STRUCTURE probability of ≥ 0.90 probability of belonging to a single genetic cluster, with 75 individuals in the "coastal southern California/northern Baja" group and 15 in the "Guadalupe/Todos Santos" group. Mean pairwise F_{st} was < 0.0001 for neutral loci and 0.012 for loci under selection.

The DAPC analysis on loci under selection revealed a complementary story to the STRUCTURE output. When considering loci under selection, Todos Santos was the most distinct population (Fig. 2.3a), with axis-1 explaining most of the genetic variation between Todos Santos and all other populations. After removing the two Todos Santos individuals and rerunning the DAPC, we found that axis-1 explained variation between Isla San Martin/Isla San Jerónimo and all other populations, while axis-2 explained differences between the remaining populations (Fig. 2.3b). There were 15 loci that were in the 80^{th} percentile for variance explained along axes 1 and 2 for the two DAPCs on loci under selection (Fig. S2.3). These loci explained genetic variation along each axis. Polymorphisms at these loci are presumed to explain most of the genetic divergence along each axis.

19 loci under selection had significant matches within the GenBank database. Nine matches corresponded specifically to protein-coding genes in BLAST (Table 2.3), including two of the loci identified as explaining a substantial amount of variance along the DAPC axes (Fig. S2.3). Two loci matched with multiple protein-coding sequences; in these instances, we examined all protein matches whose E-values were $< 1^{-10}$. We found that functions in teleost fishes primarily related to embryonic development (particularly of the eyes), immune system function, and cellular function. Several genes were also associated with development of female reproductive structures.

Environmental predictors of genetic divergence

Simple isolation-by-distance did not explain local adaptation trends (Mantel statistic $R = -0.03$, $p = 0.53$). Certain populations that were geographically distant showed similar patterns of local adaptation, such as Catalina Island (Two Harbors area) and Las Barrancas. Other population pairs that were closer together, such as Catalina Island (Two Harbors area) and Palos Verdes, showed strong differences in local adaptation trends (Fig. 2.2a-b).

We were interested in examining if environmental conditions at the time of settlement were predictive of genetic haplotype. We collated environmental data for sea surface temperature (SST), sea surface temperature anomaly (SSTA), sea surface height (SSH), and Ekman transport (EKM) (Fig. S2.1. Average estimated age of morays was 11.5 years old (SD = 4.67), and average year of settlement was 2007 (SD = 4.78). SST, SSTA, and SSH all showed significant relationships between DAPC axis 2 values, but not DAPC axis 1 values ($p < 0.001$, Fig. 2.4, Table S2.4). Bootstrapping results confirmed that these trends were specific to settlement years (Fig. 2.6a-c). While there was a slight significant positive correlation between EKM and genetic diversity ($p = 0.03$), bootstrapping showed that this trend was not unique to settlement years (Fig. 2.6d). In general, individuals from coastal southern California/northern Baja population tended to settle in years with cooler overall sea surface temperatures, more typical sea surface temperatures, and lower sea surface heights. In contrast, individuals from southern Baja (Las Barrancas, Punta Abreojos, and Isla Natividad) tended to settle in warmer and more extreme sea surface temperatures and higher sea surface heights. Results from analysis using Oceanic

Niño Index values showed that across all populations, morays settled equally in both La Niña and ENSO years (Fig. S2.5, ANOVA $F_{2,20} = 1.66$, $p = 0.22$).

We collated 55 occurrences of California moray leptocephali captured in the eastern Pacific (Fig. 2.7). Capture dates ranged from 1957-2015 from 14 separate cruises. 53.3% of larvae were captured well outside of the recognized adult range in the Gulf of California (18%), the Mexican Pacific (9%), or off Central/South America (26%). We confirmed with the original identifiers that *Gymnothorax mordax* identifications were correct (S. Carter & S.P.A. Jiménez Rosenberg, pers. comm.).

Discussion

In this study, we found that the California moray exhibits high gene flow across populations. Despite this, there was surprisingly strong evidence of local adaptation for a small subset of loci. Based on correlations with environmental covariates, function of loci under selection, and a disconnect between larval and adult geographic ranges, we hypothesize that selection is primarily occurring during the late larval or early juvenile period, based on several lines of evidence. This work indicates that population structure can exist even for organisms with high gene flow, and that phenotype-environment mismatches during the dispersal period can constrain the ranges of species (Marshall et al. 2010).

Other studies on population connectivity in morays found similar patterns of high gene flow. For instance, four species of Pacific-wide morays were found to have high gene flow across the entire Pacific (Reece et al. 2010, 2011). However, the

studies by Reece et al. utilized highly conserved regions of the nuclear and mitochondrial genomes, making significant signals of local adaptation unlikely. The long pelagic larval duration (PLD) time of these morays was cited as a potential explanation for high gene flow. A study on the tidepool snake moray (*Uropterygius micropterus*) found no correlation between genetic diversity and PLD; however, there was a significant effect of sea surface temperature on growth rate/PLD times across an SST gradient of ~6°C (Huang et al. 2018). Finally, two studies that used slightly expanded sets of nuclear and mitochondrial markers also found high gene flow in two species of morays in the western Pacific (Ribout et al. 2018; Li et al. 2021). Although this collection of studies examined genetic connectivity through a limited set of genetic markers, they converge on the same conclusion: Morays have high dispersal and high gene flow, even across large geographic regions. Only a few migrants per generation is enough supersede genetic drift (Strathmann et al. 2002; Burgess et al. 2016). Thus, we can assume that dispersal is high among moray populations.

Though our study is the first to use RADseq on a moray eel, several RADseq studies have been conducted on catadromous eels in the genus *Anguilla*. For example, though American and European eels (*Anguilla rostrata* and *A. anguilla*) have a mostly homogenized genome, selection occurs on a subset of loci (Pujolar et al. 2014; Pavey et al. 2015; Babin et al. 2017). Selection on even a small subset of loci has resulted in strikingly different ecotypes in the American eel (Pavey et al. 2015). In parallel to our study, loci under selection in American eels has also been correlated with latitude, longitude, and sea surface temperature (Babin et al. 2017). These

RADseq studies support the hypothesis that local adaptation can be maintained despite high gene flow through divergent selection on phenotypes or genotype-dependent habitat choice, selective pressures which act on every generation cycle.

The source of California morays inhabiting the most northern end of their range has been a persistent life history question that adds insight into the factors that maintain biodiversity in southern California kelp forest communities. STRUCTURE results indicate that most of individuals from the northern side of Catalina Island (Two Harbors area) and Punta Abreojos are first generation hybrids between the two primary haplotypes identified by STRUCTURE. A large number of first generation hybrids, with no second generation hybrids, supports the long-time hypothesis that morays around Catalina have minimal local reproduction (McCleneghan 1973). However, this historical hypothesis stated that sea surface temperature is limiting gonadal development or reproduction around Catalina, a conclusion which is not supported by our results Punta Abreojos experiences moderately warm SST conditions and also appears to be entirely comprised of first generation hybrids. Long-term trapping around Catalina Island has primarily taken place in the summer; observing gonads during other points throughout the year could help elucidate effects of sea surface temperature on gonadal development. Muraenid leptocephali appear to be most common in waters between the Baja Peninsula and southern California from July to December, so spawning may be occurring later in the year than sampling has typically occurred (Fig. S2.1).

Although populations in southern California/northern Baja would be the closest potential source populations for the hybrids around Two Harbors, nearly all individuals from these populations fall into a single genetic haplotype for loci under selection. Instead, we hypothesize that Las Barrancas may be a more probable source population, as individuals of both haplotypes reside there (Fig. 2.2). Oceanographic patterns during the winter could allow for northward transport from areas south of Punta Abreojos (Durazo 2015). However, admixture plots from STRUCTURE should be interpreted with care, as assumptions about the number of clusters and underlying model can bias results (Novembre 2016; Lawson et al. 2018).

STRUCTURE, DAPC, and pairwise F_{ST} results suggest that the two individuals from Todos Santos are under significantly different selective pressures than populations above Bahía Magdalena. This supports the hypothesis that Bahía Magdalena marks the transition between the San Diegan and Cortez provinces for Eastern Pacific morays (Dale et al. 2021). Potential gene flow between Las Barrancas and Catalina Island also weakens Punta Abreojos as a biogeographic break. However, gene flow remains high enough between Todos Santos and populations above Bahía Magdalena to remove signal of genetic drift, and these results should be confirmed with additional individuals from below Bahía Magdalena.

We hypothesize that selection is primarily occurring in the late larval or early juvenile stage. Larval occurrence data show that California morays have a high capacity for dispersal, with larvae often captured outside of the known adult range, such as in the Gulf of California and South America (Dale et al. 2021). Three

hypotheses could explain the disconnect between larval range and known adult range. First, adult fish may move to or from spawning or settlement areas. However, based on long-term mark-recapture data from Catalina Island, adult morays appear to have extremely high site fidelity, rarely moving even short distances to adjacent coves (Mehta et al. 2020). Second, adults may be present in areas outside of their known range but have not been observed due to their elusive nature. At least for the Gulf of California and parts of western Mexico, fish communities have been reasonably well-documented, with surveys increasing in frequency over the last decade (Nevárez-Martínez et al. 2008; Rodríguez-Romero et al. 2008; López-Martínez et al. 2010; López-Pérez et al. 2013). Data from these surveys include many species of morays, but California morays have not been recorded. Third, larvae that disperse to new regions are not able to recruit or survive to adulthood due to a phenotype-environment mismatch at the recipient location. Our data are consistent with this final hypothesis.

We found that environmental conditions around the late larval or early settlement period predict local adaptation trends. Interestingly, a study of three Eastern Pacific fish and invertebrate species also showed that kelp, oceanographic flow, and sea surface temperature explained weak genetic structuring (Selkoe et al. 2010). Here, we hypothesized that morays in southern California would settle primarily in ENSO conditions based on Higgins et al. (2017). We used both sea surface height and Oceanic Niño Index values as proxies for ENSO conditions. Contrary to our original hypothesis, our results show a more nuanced story, in which

morays north of Punta Eugenia typically settle in cooler and less anomalous sea surface temperatures and lower sea surface heights, conditions which are more characteristic of winter months or La Niña events. Thus, northward dispersal may be aided by either seasonal or decadal oceanographic oscillations. In contrast, morays south of Punta Eugenia (Isla Natividad, Punta Abreojos, and Las Barrancas) tended to settle in overall warmer temperatures, more extreme temperatures (either warmer or cooler than typical conditions), and higher sea surface heights. Durazo (2015) found that coastal regions south of Punta Eugenia experience two distinct interannual climate regimes, with the winter/spring characterized by cold, fresher waters and the summer/fall characterized by warm, saltier waters. At the same time, larval catch data shows that eel leptocephali are most common from July to December, encompassing both regimes. In support of a bimodal pattern of settlement conditions, the GAM of the relationship between SST anomaly and DAPC axis 2 showed that morays in southern Baja typically settled in conditions that are anomalously warmer or cooler than average.

One important caveat to our study is that we estimated age based on data from Catalina Island individuals. Presumably, morays from environments with higher sea surface temperatures will experience higher growth rates, and thus, age estimates based on head length would vary. Future work should examine otoliths from Baja individuals to obtain better age estimates and calculate population-specific growth curves.

In addition to growth rate, sea surface temperature is known to influence swimming performance of larval fish (Downie et al. 2020). One locus under selection, encoding the calcium-sensing protein synaptotagmin 12 (syt12), is upregulated in exercising vertebrates, including juvenile Atlantic salmon (*Salmo salar*) (Fernández-Chacón et al. 2001; Mes et al. 2020). Eel leptocephali are understood to be active and capable swimmers who use swimming to avoid being swept offshore, transverse strong currents, and reach settlement habitat (Miller & Tsukamoto 2020). Selection for strong swimming ability, especially in cooler temperatures, may be important for California morays moving northward.

Eel leptocephali are also unusual among fish larvae for having large, rod-dominated eyes, which may assist with feeding on particulate matter or gelatinous material in low-light conditions (Taylor et al. 2011, 2015). Interestingly, four of the protein-coding genes under selection are associated with eye development in zebrafish, including one gene directly implicated in rod differentiation and retina development (Kitambi and Hauptmann 2007; Xie et al. 2019). Many larval fishes have well-developed eyes and likely feed by sight – our data indicate that eyesight may be under selection in morays (Blaxter 1975). Turbidity variations likely exist along the range of the California moray, as different parts of the range vary in upwelling and productivity. Improved low-light vision in more turbid waters could be an advantage for larval fish that feed visually (Leis 2018)

Other loci under selection have also been linked to development in teleost fishes. These include the genes vcam1a and cntn1a. Vcam1a is involved with

lymphatic system development in zebrafish embryos (Yang et al. 2015). Cntn1a is a cell adhesion molecule that is most likely involved with early axon growth and development in zebrafish (Haenisch et al. 2005; Takeuchi et al. 2017), as well as potentially myelination and central nervous system regeneration (Schweitzer et al. 2007). The locus that matched with cntn1a fell into the 80th percentile for explaining variance across DAPC axis 1 (loci under selection; all individuals); this axis described differences between Todos Santos and all other populations. Thus, we hypothesize that Todos Santos individuals experienced selection related to nervous system development or regeneration, in addition to proteins whose functions have not yet been characterized.

The locus that explained the most variation along DAPC axis 2 (loci under selection; no Todos Santos) matched with several proteins. The functions of these proteins are involved with development of oocytes/ovarian follicles, eye development, and blood vessel development in teleosts, in addition to proteins only studied at the cellular level. This DAPC axis was correlated with SST, SSTA, and SSH. Thus, we hypothesize a link between environmental conditions at settlement and functions related to this gene, such as development of reproductive, sensory, or circulatory structures. Unfortunately, RADseq provides no information on gene upregulation/downregulation. Additionally, the vast majority of loci were uncharacterized. Studies on gene function and mRNA specifically in Anguilliformes would be useful areas for further research.

Author Contributions

RSM and KED conceived the project. KED, ARV, RSM, and JRC collected samples. KED, DBW, and GB performed laboratory work and bioinformatic analyses. KED wrote the initial manuscript. All authors discussed results and reviewed/contributed towards the final manuscript.

Acknowledgements

This project would not have been possible without assistance from fishing cooperatives in Mexico. We especially thank T. Camacho Bareño and his family for their hospitality in Las Barrancas; J.J. Cota-Nieto and the SCPP Punta Abreojos SC de RL in Punta Abreojos; R. Martinez and the SCPP Buzos y Pescadores SC de RL for Isla Natividad samples; SCPP Abuloneros y Langosteros for Isla Guadalupe samples; and I. Gonzalez Zacarías, D. Rosales, and B. Cervantes from Rocas San Martin, SPR de RL, and A. Valenzuela Toro (Isla San Martin). Sampling off coastal California was facilitated by J. Ross of South Coast Bio-Marine (Palos Verdes) and P. Zerofski and R. Hallisey (San Diego). Catalina Island field teams from 2017-2019 were instrumental in obtaining samples from around Catalina Island. Thank you to M. Cronin for lab work assistance. Larval identifications were performed by S. Carter & S.P.A. Jiménez Rosenberg. Funding was provided to KED through a University of California Institute for Mexico and the United States Small Grant, a Lewis and Clark Fund Grant, an Achievement Rewards for College Scientists

(ARCS) Foundation fellowship and NMFS/Sea Grant Population and Ecosystem Dynamics Graduate Fellowship Award #NA20OAR4170467. Funding was provided to RSM through a UCSC COR Grant and a Hellmanâ€™s Fellowship.

Tables & Figures

Table 2.1. Sample and genetic information summaries for the 10 sampled populations.

	Punta Abreojos	Isla Natividad	Isla Guadalupe	Isla San Martin & Isla San Jerónimo	San Diego	Palos Verdes	Catalina Island (Cat Harbor)	Catalina Island (Two Harbors
	33	21	7	28	20	24	12	87
	413-925	424-1156	447-922	465-1009	491-1008	452-1032	419-1025	394-1149
	1,106,260	1,146,573	1,609,272	4,922,533	4,636,993	3,770,595	3,002,036	2,159,626
	4428	3941	4365	32,400	27,835	21,858	12,642	13,326
	40%	34%	27%	66%	60%	58%	42%	62%
	0.0006	0.0006	0.0008	0.0012	0.0011	0.0010	0.0009	0.0006
	0.0006	0.0006	0.0008	0.0012	0.0012	0.0010	0.0010	0.0006
	0.0000	0.0000	0.0000	0.0002	0.0002	0.0001	0.0002	0.0001

Site	Todos Santos	Las Barrancas
N samples	2	18
Standard length range (mm)	972	610-1195
Total sites	3,227,119	1,887,758
Polym. loci	6,876	9135
% Polym.	21%	48%
Obs. hetero.	0.0011	0.0010
Pi	0.0012	0.0010
F_{is}	0.0001	0.0002

Table 2.2. Pairwise F_{st} values calculated for neutral loci (a; n loci = 54,960) and loci under directional selection (b; n loci = 216). Green values represent more similar population pairs; red values represent more divergent population pairs. For both loci under selection and neutral loci, genetic connectivity patterns do not follow simple isolation-by-distance patterns. For example, the two populations from Catalina Island (Cat Harbor, which faces south, and the Two Harbors area, which faces north) and Palos Verdes all appear to be under different selective pressures, despite being located geographically close to one another.

a. Neutral loci	Catalina Island (Two Harbors	Catalina Island (Cat Harbor)	Palos Verdes	San Diego	Isla San Martin & Isla San	Isla Guadalupe	Isla Natividad	Punta Abreojos	Las Barrancas
Todos Santos	1E-03	6E-04	7E-04	5E-04	6E-04	1E-03	1E-03	7E-04	5E-04
Las Barrancas	1E-04	1E-04	7E-05	1E-04	7E-05	-1E-05	6E-06	6E-05	
Punta Abreojos	6E-05	1E-04	8E-05	7E-05	2E-05	2E-05	3E-05		
Isla Natividad	4E-06	1E-04	6E-05	8E-05	4E-05	9E-05			
Isla Guadalupe	6E-05	2E-04	-3E-05	-1E-04	-6E-05				
Isla San Martin & Isla San Jerónimo	6E-05	7E-05	8E-05	1E-04					
San Diego	1E-04	9E-05	9E-05						
Palos Verdes	1E-04	7E-05							
Catalina Island (Cat Harbor)	2E-04								

b. Loci under selection	Catalina Island (Two Harbors	Catalina Island (Cat Harbor)	Palos Verdes	San Diego	Isla San Martin & Isla San	Isla Guadalupe	Isla Natividad	Punta Abreojos	Las Barrancas
Todos Santos	0.89	0.48	0.62	0.43	0.22	0.38	0.70	0.80	0.53
Las Barrancas	0.52	0.22	0.33	0.29	0.29	0.31	0.30	0.38	
Punta Abreojos	0.14	0.44	0.40	0.38	0.36	0.56	0.33		
Isla Natividad	0.37	0.33	0.34	0.31	0.31	0.40			
Isla Guadalupe	0.68	0.29	0.37	0.27	0.24				
Isla San Martin & Isla San	0.50	0.26	0.29	0.24					
San Diego	0.52	0.26	0.26						
Palos Verdes	0.48	0.31							
Catalina Island (Cat Harbor)	0.56								

Table 2.3. Nine of the loci under directional selection had "highly similar" significant matches with protein-coding sequences in BLAST. We extracted all BLAST matches with E-values <1E-10; one locus (ID 130717, that explains variation between Todos Santos and all other populations. within the first DAPC) had matches to several proteins. We examined each protein for its general function, typically on the molecular level, as well as organismal-level effects within teleost fishes. Proteins that fell into the 80th percentile for variation explained across DAPC axes are marked by a * (axis 1, loci under selection, all individuals) or † (axis 2, loci under selection, sans Todos Santos) (Fig. S2.3).

Accession No.	**Homolog species in BLAST**	**E-value**	**Putative gene**	**Function (general)**	**Function (teleosts)**
XM_035383633.1	*Anguilla anguilla*	7.0E-16	Connector enhancer of kinase suppressor of Ras 1 (cnksr1)*	Scaffold/adaptor protein; regulator of Ras signalizing pathways	--
XM_035423455.1	*Anguilla anguilla*	2.0E-10	Contactin-1a-like (cntn1a)†	Myelination; central nervous system regeneration (Schweitzer et al. 2007)	Early axon growth in zebrafish embryos (Haenisch et al. 2005). Expressed more strongly in zebrafish larvae than adults, primarily in brain (Takeuchi et al. 2017)
XM_035410368.1	*Anguilla anguilla*	1.0E-22	Gap junction alpha-4 protein-like (gja4)*	Creates gap junctions. Regulates ovarian follicle development	Stimulates oocyte growth and ovarian follicle development in teleosts (Chang

				(Simon et al. 1997)	et al. 1999; Beato et al. 2020)
XM_027926232.1	*Marmota flaviventris*	5.0E-12	Photoreceptor-specific nuclear receptor subfamily 2 group E member 3 (nr2e3)	Control transcription by binding to other ligands	Rod photoreceptor differentiation in zebrafish (Kitambi and Hauptmann 2007); retina development in zebrafish (Xie et al. 2019)
XM_035389236.1	*Anguilla anguilla*	9.0E-15	Polyglutamine binding protein 1 (pqbp1)	Head and eye development; bone formation; cartilage development	--
XM_035405517.1	*Anguilla anguilla*	3.0E-14	Proline-rich protein 12-like (prr12)	DNA binding; transcriptional coactivator	Eye developmennt (zebrafish larvae); ovary and neural structures in brain and eyes (zebrafish adults) (Resendes 2022)
XM_035390895.1	*Anguilla anguilla*	2.0E-21	Protein phosphatase (ptc7)	Regulates biosynthesis of the ubiquinone, coenzyme Q	--
XM_035382989.1	*Anguilla anguilla*	1.0E-03	Peptidyl-tRNA hydrolase 2 (pth2)	Hydrolizes N-substituted aminoacyl-tRNAs	Upregulated in response to schooling and social environments in zebrafish (Anneser et al. 2020)
XM_035390855.1	*Anguilla anguilla*	5.0E-22	Ras-related protein Rab-36 (rab36)*	Protein transport and vesicular activity; spatial distribution of lysosomes and formation of macropinosomes (Chen et al. 2010)	Unclear; unrelated to immune response to bacterial infection in channel catfish (Chen et al. 2010; Wang et al. 2014)

XM_035405426.1	*Anguilla anguilla*	7.0E-11	SMG1 nonsense mediated mRNA decay associated PI3K related kinase (smg1)	Degradation of irregular mRNAs	Depletion of this gene does not appear to influence zebrafish development (Wittkopp et al. 2009). May be related to immune defense in adult rainbow trout (Wang et al. 2019)
XM_035400514.1	*Anguilla anguilla*	5.0E-22	Sorting nexin 5 (snx5)*	Intracellular trafficking	Embryonic development of eyes, blood vessels, and hematopoeietic precursor cells in zebrafish (Yoo et al. 2006; Olena et al. 2015)
XM_005059390.2	*Ficedula albicollis*	1.0E-23	Serine/threonine kinase 38 (stk38)	Phosphorylates OH group of serine/threonine sidechains in proteins	Innate immune response in grass carp (Xu et al. 2019)
XM_040163796.1	*Gasterosteus aculeatus*	3.0E-10	Synaptotagmin XII (syt12)	Synaptic vesicle protein that acts as a Ca^{2+} sensor in the regulation of neurotransmitter release	Upregulated in response to exercise in juvenile Atlantic salmon (Mes et al. 2020)
XM_035420413.1	*Anguilla anguilla*	2.0E-20	Vascular cell adhesion molecule 1a (vcam1a)	Cell-cell recognition; leukocyte-endothelial cell adhesion	Lymphatic development in zebrafish embryo; similar effects were not seen in mice (Yang et al. 2015)
XM_035428230.1	*Anguilla anguilla*	2.0E-25	Zinc finger and BTB domain containing 22b (zbtb22b)*	Regulation of transcription by RNA polymerase II	--

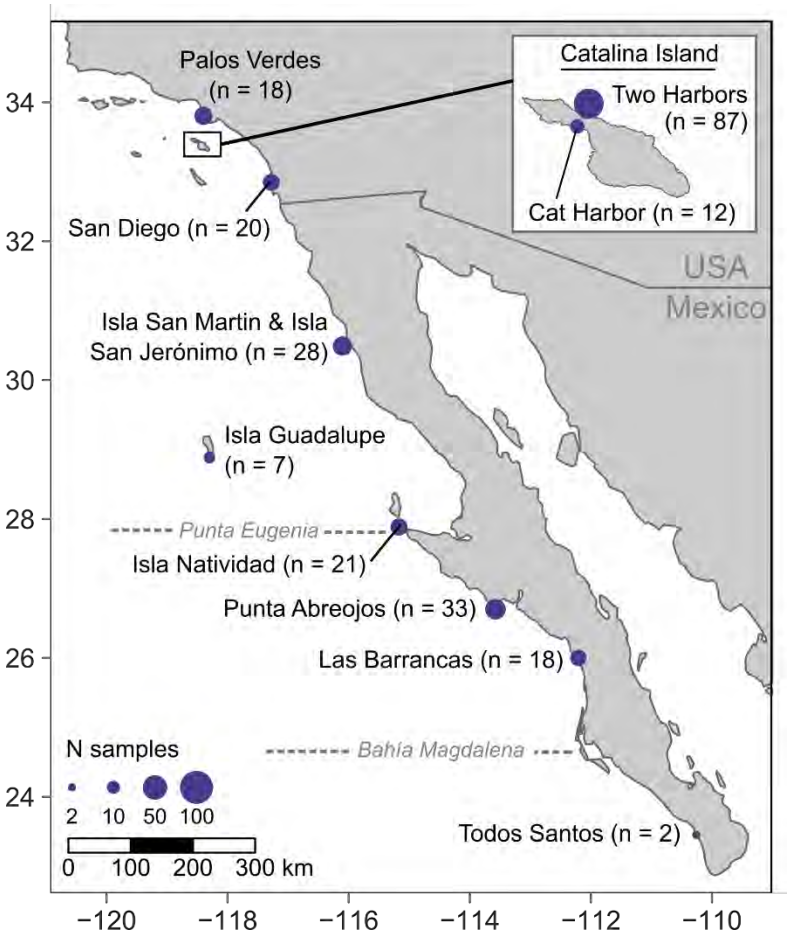

Figure 2.1. Adult California morays were sampled from 11 locations between southern California and southern Baja California peninsula, Mexico, including five offshore islands (Catalina Island, Isla San Martin, Isla San Martin & Isla San Jerónimo, Isla Guadalupe, and Isla Natividad). The two most probable biogeographic breaks in this region are at Punta Eugenia and Bahía Magdalena.

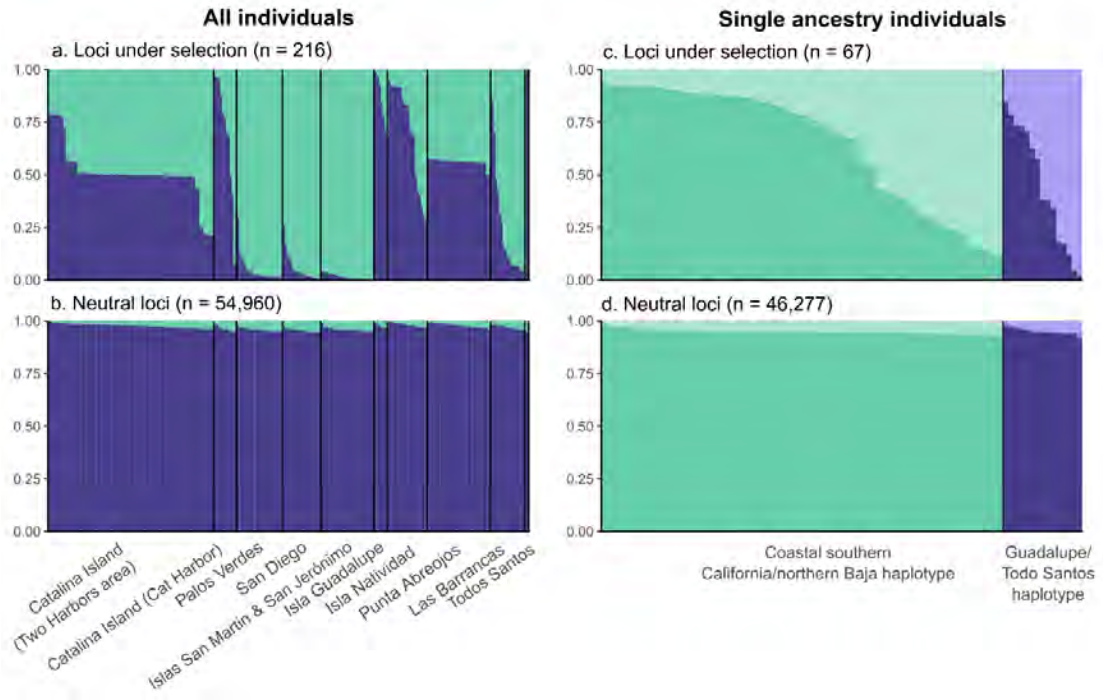

Figure 2.2. STRUCTURE plots showing genetic relatedness for K = 2. Each bar represents an individual; individuals that share more of the same color are assumed to be more genetically similar. a) Populations off coastal southern California/northern Mexico (Palos Verdes, San Diego, Isla San Martin/Isla San Jeronimo) appear to be under different selective pressures than those from populations such as Isla Natividad, Isla Guadalupe, and Todos Santos. Catalina Island (Two Harbors area) and Las Barrancas are comprised primarily of first generation hybrids. b) When examining neutral loci, populations are indistinguishable, suggesting high gene flow. c) and d) When examining single-ancestry individuals (those with >0.9 probability of belonging to a single genetic cluster according to loci under selection), F_{ST} values show divergence for loci under selection (c; mean $F_{ST} = 0.012$) but are low for neutral

loci (d; $F_{ST} < 0.0001$). The same list of loci under selection was used for both sets of analyses; the lower number of total loci for the single-ancestry analysis is due to filtering within the STACKS pipeline.

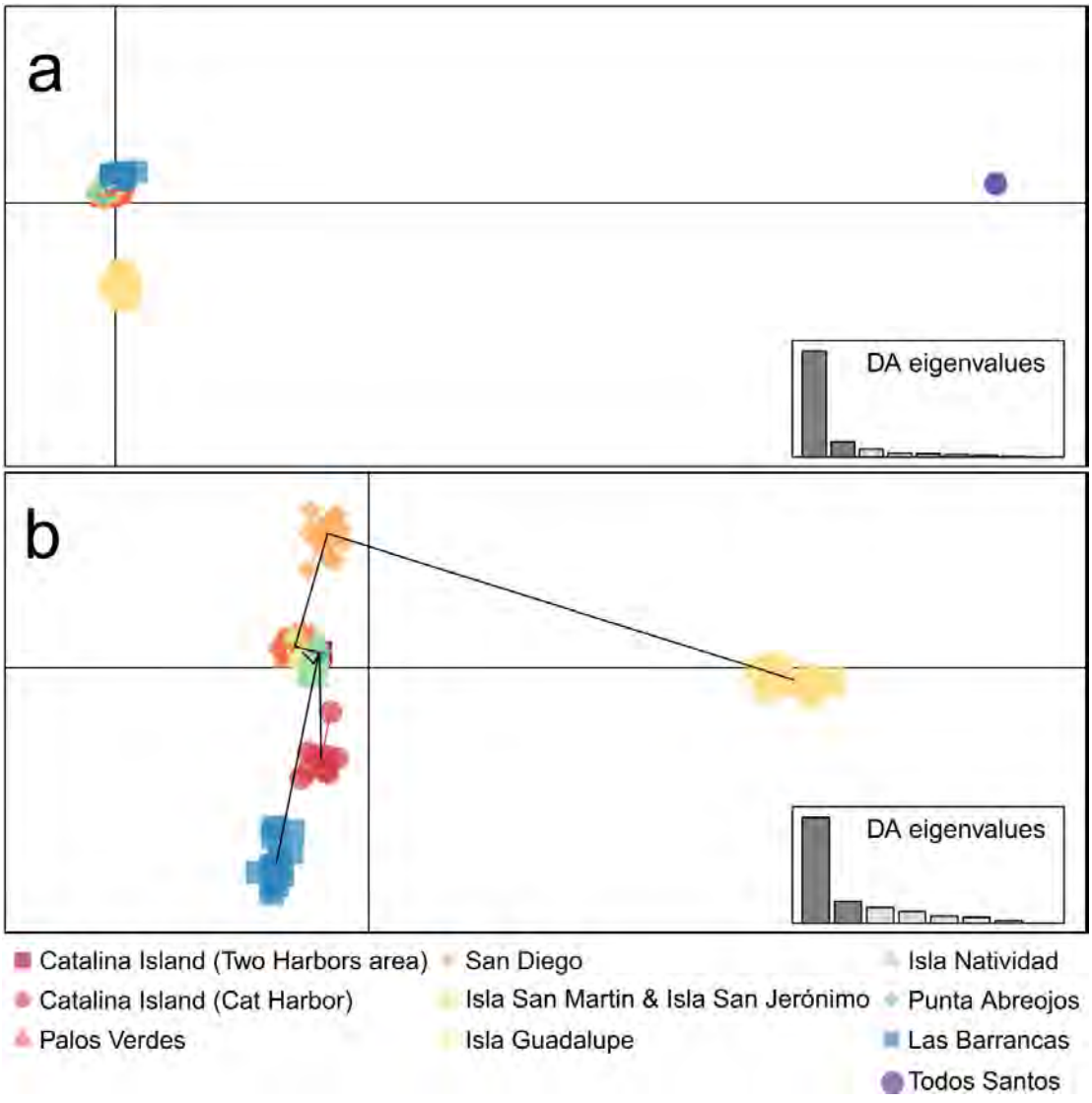

Figure 2.3. Discriminant Analysis of Principal Components (DAPC) analyses for loci under selection (n = 216) reveal that populations cluster together. a) Todos Santos was the most genetically distinct population. b) Removing the two Todos Santos individuals provided a more granular view of the remaining populations. As no environmental information was available for Todos Santos individuals, the coordinates from plot b were used in testing for correlations with environmental covariates. Lines in plot b indicate minimum spanning tree based on squared differences among groups.

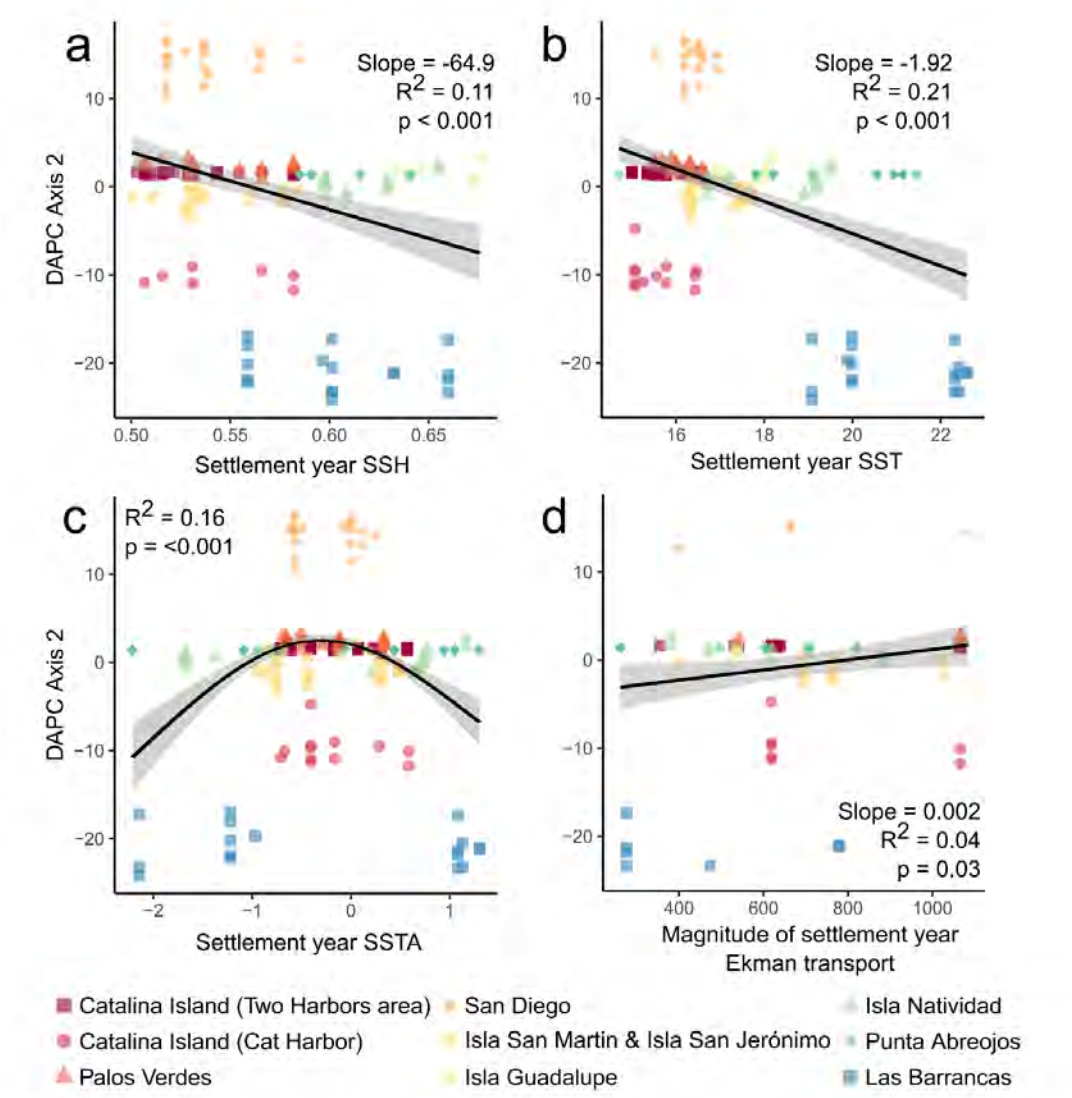

Figure 4. There are significant relationships between environmental covariates and genetic diversity. a) Sea surface height (SSH), b) sea surface temperature (SST), c) sea surface temperature anomaly (SSTA) and d) the magnitude of SSTA during estimated year of settlement are predictors of DAPC axis 2 values (used as a proxy for genetic haplotype). All environmental predictors were averaged across Oct-Mar,

as leptocephali are most abundant in waters off Baja California and southern California during this period (S. Carter, pers. comm.).

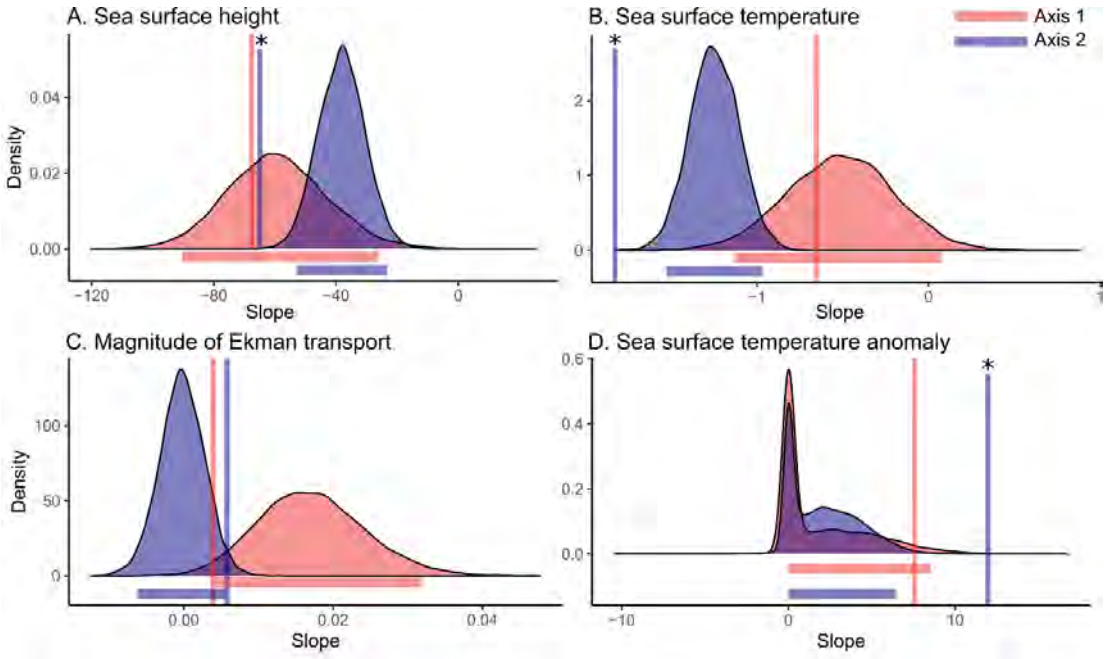

Figure 2.5. Bootstrapping results for environmental covariate regressions indicate that for sea surface height, sea surface temperature, and sea surface temperature anomaly, trends were specific to settlement year (and not any other set of years). Bars below each density curve indicate the 2.75-97.5 percentiles for each set of bootstrapped results. Vertical bars indicate the true slope value of the relationship between the environmental covariate and genetic diversity for the original set of settlement years. Asterisks indicate statistically significant regressions whose slope value also falls outside of the 2.5-97.5% percentile range.

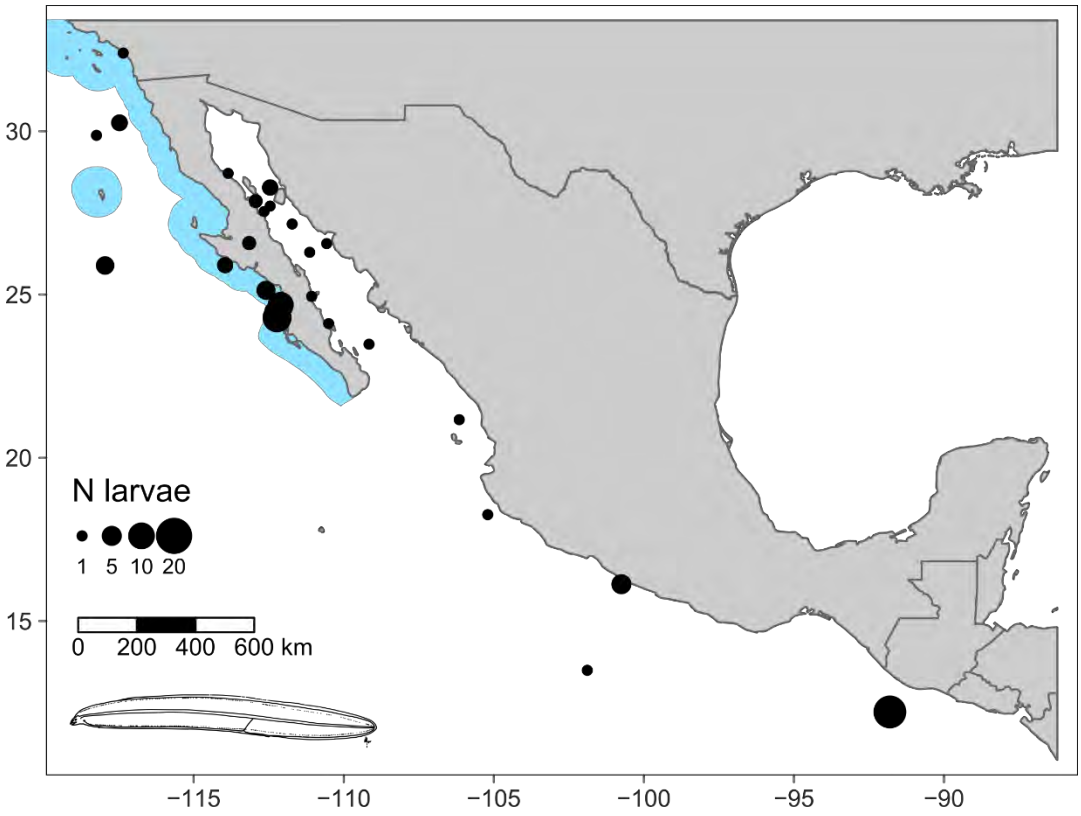

Figure 2.6. Larval *Gymnothorax mordax* have been found as far as the northern Gulf of California and South America, despite the adult range (shaded in blue) encompassing a much narrower geographic region. Far-ranging larvae support our prediction of high gene flow, with selection presumably occurring in the late larval or early settlement period. Data are from CalCOFI and IMECOCAL sampling programs and the Scripps Institution of Oceanography Marine Vertebrate collection and represent collections from 1957-2015. No morphological data is available for most individuals.

Vol. 677: 67–79, 2021
https://doi.org/10.3354/meps13873

MARINE ECOLOGY PROGRESS SERIES
Mar Ecol Prog Ser

Published October 28

Coloration is related to habitat in *Gymnothorax mordax*, a kelp forest predator

Katherine E. Dale*, Ryan Hallisey, Rita S. Mehta

University of California, Santa Cruz, CA 95060, USA

ABSTRACT: Animal coloration serves a variety of functions, including communication and camouflage. We quantified hue, luminance, countershading, and pigmentation pattern of the California moray eel *Gymnothorax mordax* and determined whether coloration was correlated with the environmental variables of the kelp forest ecosystem. The California moray is an elongate, predatory, crevice-dwelling fish that does not rapidly change color. We photographed morays trapped at a variety of depths in 4 environmentally diverse sites around the Two Harbors isthmus on Catalina Island, California, USA. Depth, substrate type, cover type, horizontal visibility, and reef rugosity were recorded for the environment surrounding each trapped eel. We found that eels were lighter, redder, and yellower in shallow habitats with high percentages of sand, bare substrate, and seagrass. In habitats with greater substrate diversity, clearer water, and a higher percentage of boulder, morays were darker, greener, and bluer. Despite their benthic, crevice-dwelling behavior, we found that all individuals exhibited countershading, which was most extreme at the head and tail. Pigment spots became larger and more uniform in size as standard length increased, but few other size- or age-related color changes were found. We found little evidence that coloration is correlated with foraging success and instead speculate that coloration is established post-settlement in smaller size classes not examined in this study. This work shows that California morays exhibit a range of colorations and that hue and luminance are correlated with environmental variables in the Two Harbors region of Catalina Island.

KEY WORDS: Fish · Hue · Pigmentation pattern · Countershading · Muraenidae

1. INTRODUCTION

Coloration is used across the animal kingdom for a variety of purposes, including inter- and intra-specific communication, thermoregulation, and defense (Caro 2005, Cuthill et al. 2017). The term 'coloration' includes hue (the wavelength of reflected light), luminance (degree of lightness), countershading (ratio of dorsal to ventral luminance), and pigmentation pattern. Previous studies have examined coloration for both terrestrial and aquatic organisms (Cuthill 2019), primarily examining how coloration can be used as a predator avoidance mechanism (e.g. Eterovick et al. 1997, Johnsen & Sosik 2003, Cournoyer & Cohen 2011, Orton et al. 2018). Within fishes, coloration has been examined primarily for tropical species that are fusiform, rapidly change color, or those that have distinct color polymorphisms (Barry & Hawryshyn 1999, Marshall 2000, Gilby et al. 2015, Tyrie et al. 2015, Phillips et al. 2017). Bright colorations with many hues are more common in tropical ecosystems, where higher, more consistent light levels and increased water clarity may have allowed for the development of more dramatic colorations (Marshall 2000, Stevens & Merilaita 2009). A smaller subset of work has examined coloration in temperate fishes. Previous studies have shown correlations between coloration of fishes and abiotic environmental characteristics without explicitly examining background matching, such as for arc-eye hawkfish *Para-*

*Corresponding author: kdale@ucsc.edu

cirrhites arcatus with multiple color polymorphisms (Whitney et al. 2018), Eurasian perch *Perca fluviatilis* in pelagic/littoral lake habitats (Kekäläinen et al. 2010), and coastrange sculpin *Cottus aleuticus* on different stream substrates (Whiteley et al. 2011). A study on King George whiting *Sillaginodes punctata* found that lower light conditions were correlated with brighter hues and more extreme countershading (Meakin & Qin 2012), while studies on threespine stickleback *Gasterosteus aculeatus* (Reimchen 1989) and brown trout *Salmo trutta* found a positive trend or no trend between coloration and water clarity/canopy cover (Westley et al. 2012).

Studies of coloration of aquatic predators are rare, though some work exists for penguins, seals, and cetaceans (Wilson et al. 1987, Caro et al. 2011, 2012). Few studies have examined coloration in predatory fishes, though Nassau groupers *Epinephelus striatus* apparently use rapid patterning changes to avoid detection by prey (Watson et al. 2014). Countershading, an aspect of coloration in which the ventral portion of an animal's body is lighter than the dorsum, may be an additional camouflaging tactic towards catching prey. When an animal is viewed from above or below, countershading may conceal an organism's shadow or break up the outline of an animal's body shape (Ruxton et al. 2004).

In this study, we examined coloration and its relation to habitat characteristics in a benthic, piscivorous, temperate reef fish with an extreme body plan. The California moray eel *Gymnothorax mordax* Ayers, 1859 is the only coastal moray species found off the coast of California, ranging from Point Conception, CA, USA, to southern Baja, Mexico (Fitch & Lavenberg 1971). They occupy most of Catalina Island's diverse coastal habitats, from kelp-dominated systems to sandy bays. As long-lived kelp forest predators capable of eating large prey whole, morays are thought to experience very little predation as adults (Higgins & Mehta 2018).

Similar to other reef-dwelling eels, California morays are primarily crevice-dwelling and nocturnal, characteristics that help organisms avoid detection by diurnal predators and prey without relying on coloration (Gilbert et al. 2005). Unlike the fusiform or deep-bodied fishes typically focused on in coloration studies, highly elongate fishes with reduced fins such as eels tend to roll/twist their bodies along the anterior–posterior axis exposing their ventrum as they swim through the water column (Donatelli et al. 2017). Natural history observations of adult California morays suggest a wide variety of colorations (Fig. 1) but no rapid color changes. In captivity, however, individuals of varying lengths (320–760 cm) have exhibited shifts to lighter colorations over the course of several months to years (R. Mehta unpubl. data), a morphological color change possibly driven by ontogenetic changes, diet, or UV light (Chen et al. 1994, Leclercq et al. 2010, Sköld et al. 2016).

Residence in a diverse range of habitats, high site fidelity, an elongate body plan, and lack of rapid color-changing ability make California morays an interesting model for quantitatively examining coloration in a predatory fish. Here, we first aimed to use robust quantitative methods to characterize the variation in coloration for California moray eels in Two Harbors, CA, hypothesizing that eels would exhibit a gradient of colorations rather than distinct polymorphisms. We did not expect morays to exhibit countershading, as background matching in the water column or shape concealment does not seem to be advantageous for these nocturnal, benthic crevice-dwelling predators with a flexible body. Secondly, we examined whether hue, luminance, countershading, or pigmentation pattern were related to habitat. We hypothesized that morays would be greener and yellower in environments with more seagrass and sand, respectively, that overall body luminance would be darker in deeper and more rugose environments, and that pattern diversity would be positively related to substrate and cover diversity. Lastly, we hypothesized that coloration

Fig. 1. Moray eels around Catalina Island show a subtle, but diverse, range of hue, luminance, and pattern. These images have been corrected for white balance and exposure, but glare and injuries have not yet been masked out

would be correlated with feeding success, body condition, or mortality of adult eels.

2. MATERIALS AND METHODS

2.1. Sampling sites and trapping procedure

Eel trapping and environmental sampling took place on the western end of Santa Catalina Island, California, from June 26 to August 11, 2019. We sampled 4 sites: West Big Fisherman's Cove (West BFC), Intakes (located between Big Fisherman's Cove and Blue Cavern Point), Cat Harbor, and 4th of July Cove (Fig. S1 in the Supplement; www.int-res.com/articles/suppl/m677p067_supp.pdf). Three of the sites are within State Marine Conservation Areas (SMCA), with West BFC and Intakes falling within the Blue Cavern Onshore SMCA and Cat Harbor falling within the Cat Harbor SMCA. A previous study suggested that Intakes and 4th of July Cove have significantly different substrate types from one another (Higgins & Mehta 2018), while our qualitative observations from previous fieldwork suggested that Cat Harbor was shallower, sandier, and more turbid than the reef-dominated sites.

Eels were captured using custom-made double-chambered wire mesh traps with dimensions 36′ × 11′ × 9′ (~91 × 28 × 23 cm), which select for eels approximately 400–1200 mm in length. Traps were baited using a perforated water bottle containing 2 to 3 frozen anchovies. Each night, we set 4–6 traps at one of the 4 sites at depths between 2 and 10 m, the range of depths at which California morays are most common (Higgins & Mehta 2018). Each evening, we rotated the site at which traps were deployed. After 12–14 h of soak time, we checked each trap while on SCUBA for the presence of eels. Underwater environmental surveys were conducted around any trap in which eels were caught.

2.2. Environmental surveys

Underwater environmental surveys recorded trap depth, cover/substrate type, rugosity (i.e. substrate complexity), and horizontal visibility around each trap. When possible, each procedure was conducted 4 times per trap along each of the cardinal headings, then averaged.

To examine cover and substrate type, we conducted a uniform point of contact (UPC) survey following California Reef Check protocols (Freiwald et al. 2019). For each trap, the substrate size (sand, cobble, boulder, or reef) and cover type (articulated coralline algae, crustose coralline algae, red algae, encrusting red algae, brown algae, other brown algae, green algae, seagrass, or none) were recorded every 1 m along a 10 m transect (Freiwald et al. 2019). We then computed the proportion of each of the 4 substrate types and 9 cover types per trap. We additionally calculated 2 diversity indices for both substrate and cover using a Shannon-Wiener index (Shannon 1948).

Rugosity was measured using the linear distance method (Risk 1972, Luckhurst & Luckhurst 1978). A chain of known length was rolled out along each 10 m transect following the contour of the reef as closely as possible. We then recorded the surface distance along the transect that the chain reached. To calculate rugosity (R) index , we used the following equation:

$$R = \frac{C}{D} - 1 \quad (1)$$

Where C is the length of the chain fully extended and D is the average surface distance covered along the reef. Higher R values indicate a more rugose reef.

Horizontal visibility was measured using the black disc method (Montes-Hugo et al. 2003). This method is advantageous when measurements are taken at varying light levels, as its reflectiveness depends less on above-surface conditions (Montes-Hugo et al. 2003). One diver swam away from the trap while holding a 30 cm diameter black disc attached to the end of the transect line that was clipped to a trap. The second diver remained at the trap and recorded the distance at which the black disc was no longer discernible from the background.

Due to the strongly colinear nature of the environmental data, we ran a principal component analysis (PCA) to reduce the dimensionality of the habitat data. First, we checked every environmental variable for normality by examining quantile-quantile plots. Then we applied a log transformation to depth, horizontal visibility, and rugosity and an arcsine transformation to the proportions for the 4 substrate types and 9 cover types. We then centered and scaled all values using the 'scale' function in R and imputed 3 missing depth values using the 'imputePCA' function in R package 'missMDA' (Josse & Husson 2016). We then performed a PCA using the 'PCA' function in package 'FactoMineR' (Lê et al. 2008). We extracted PCA components that explained >80% of variation, corresponding to the first 3 axes. PCA coordinates were used as numerical representations of the overall habitat of each trap.

2.3. Moray measurements and photography

Once traps were brought to the surface, morphological data and photographs were taken for all eels. Morays were anesthetized in a solution of approximately 90 mg of tricaine methanesulfonate (MS-222) per liter of seawater. Although MS-222 has previously been shown to cause uniform darkening in skin luminance in small fishes (Wojan et al. 2019), anaesthetization was required to conduct measurements on eels, and MS-222 is preferable to clove oil in that it works rapidly (Wojan et al. 2019, R. Mehta unpubl. data). No qualitative changes in coloration were observed due to anesthesia. Eels were submerged and handled for only a few minutes, and this handling was consistent across all individuals. To ensure that each eel was only included once throughout our trapping efforts, we inserted a passive integrated transponder (PIT) tag (BIOMARK© MK165) into the tail muscle using 16-gauge injector needles (BIOMARK© #N165). For any successive catches in a site, we first scanned each individual with a PIT tag reader (BIOMARK© #601) to identify new individuals for our data set. The 15-digit serial number associated with each tag was used to link images, environmental data, and morphological data. We measured standard length (SL), body length (BL), and head length (HL) in mm. We calculated age using a previously developed von Bertalanffy head length–age curve (Mehta et al. 2020). We tested whether SL and age varied across sites by first log-transforming SL to meet assumptions of normality, then using an analysis of variance (ANOVA) test.

Each moray was photographed in a standard setting over a whiteboard with a scale bar using an Olympus Tough TG-5 camera in RAW setting (Fig. 2A). All photos were taken with fixed ISO 100 and aperture f/8.0 under natural lighting as suggested in Gray et al. (2011). In 79% of photos, we included a calibration grey card with 18% standard reflectance, which allowed coloration to be compared across all individuals. If the image did not contain a grey card, it was corrected using an image of a grey card taken in equivalent lighting conditions. We conducted white balance and exposure corrections using the MICA toolbox (Troscianko & Stevens 2015), a plug-in available for ImageJ (Rueden et al. 2017). A multi-spectral image was first generated for each RAW file, which corrected exposure and white balance using the 18% grey standard (Fig. 2B). We used GIMP 2.10 (The GIMP Development Team 2019) to mask out glare, reflection from the whiteboard, and shadows with a uniform white background (Fig. 2C). Only 10–15% of the body surface was masked out for any individual and typically occurred on the most extreme dorsal and ventral edges of the head and mid-body. We saved this new image as a JPEG.

2.4. Quantifying coloration

We quantified hue and luminance and conducted all statistical analyses in R 3.6.1 (R Core Team 2016). Hue and luminance were calculated through the function 'kMeansList' in R package 'colordistance'

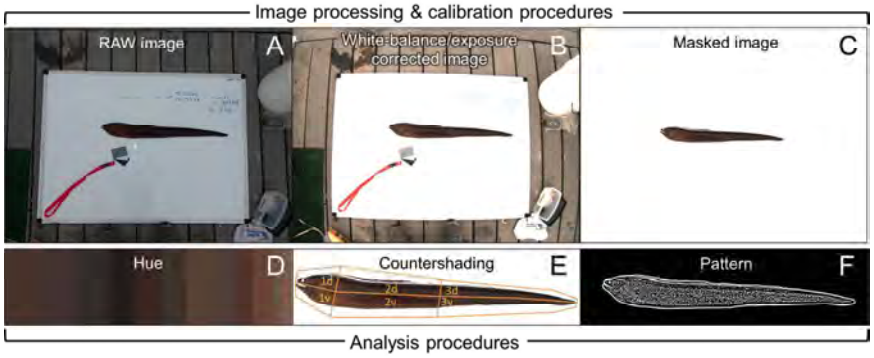

Fig. 2. Workflow for (A–C) image processing and (D–F) calibration and image analysis. (A) Raw, uncorrected original photograph including the 18% standard gray card used for white balance correction. (B) Photo after white-balance and exposure correction. (C) Glare, injuries, and background masked out with uniform white. (D) Each of the 13 clusters produced for each individual was described by a luminance (L^*), green–red (a^*) and blue–yellow (b^*) value. (E) Countershading was calculated by measuring the luminance value for the ventral (v) and dorsal (d) side of the head (snout to parabranchial opening, 1), the mid-body (from parabranchial opening to vent, 2) and the tail (vent to tip of tail, 3). (F) We examined dominant spot size and pattern diversity using ImageJ

(Weller & Westneat 2019). We converted from sRGB values to CIE Lab colorspace using a 'D65' standard daylight reference white. CIE Lab colorspace is typically recommended for coloration analyses because it is perceptually uniform (Weller & Westneat 2019). We chose to use K-means clustering over alternative methods because we were interested in extracting dominant color palette information for each individual to compare against environmental variables rather than comparing between individuals. Each of the clusters' centers were defined by a luminance value $L^\star$, a green–red value $a^\star$, and a blue–yellow value $b^\star$ along with the proportion of pixels in each cluster (Fig. 2D). Clusters were calculated by iteratively sampling 20 000 pixels from the image until convergence. Pure white values were ignored, but the $L^\star$, $a^\star$, and $b^\star$ channels were otherwise unbounded. We found that 13 clusters minimized total within-cluster sum-of-squares values while maintaining low runtimes. We then ran a PCA on each CIE Lab channel using the 'PCA' function in package 'FactoMineR' (Lê et al. 2008). We used values from the first PC axis as an overall $L^\star$, $a^\star$, and $b^\star$ value for each eel. We tested for coloration polymorphisms in hue and luminance using a Hartigan's dip test for multimodality (Hartigan & Hartigan 1985), using R package 'diptest.' We also examined whether coloration variables were correlated with one another through a series of linear regressions.

We analyzed countershading for the head (snout to parabranchial opening), the mid-body (from parabranchial opening to vent), and the tail (vent to tip of tail) (Fig. 2E). Each of these sections was further divided into a dorsal and ventral portion along the geometric midline of the fish. The luminance of the dorsal and ventral regions of each section was then quantified using the 'Pattern Color & Luminance Measurements' tool in the MICA Toolbox. We calculated a countershading ratio value for each of the 3 sections and the overall body by dividing the dorsal luminance by the ventral luminance. Countershading ratio values closer to 0 indicate more extreme countershading, values around 1 indicate no countershading, and values above 1 indicate reverse countershading. Countershading values for each body section were determined to be normally distributed through examinations of quantile-quantile plots. We tested whether countershading ratio values were significantly less than 1 (i.e. countershading present) using a 1-sample 1-tailed *t*-test. A repeated measure ANOVA test was used to determine if countershading varied among the 3 body regions within each individual, followed by a Tukey honest significant difference (HSD) test to examine which regions were driving differences.

Size-corrected dominant spot size and spot size diversity were quantified using the pattern and luminance measurements tool in the MICA Toolbox. Briefly, this tool uses a bandpass filtration method to determine the relative proportion of different pattern sizes across the entire body, termed 'pattern energy' (Fig. 2F). We ran this tool on the masked images with a filtration size range of 2–688 px, progressing by a factor of $\sqrt{2}$. We extracted the pixel size at which pattern energy was highest, equivalent to the dominant spot size. This spot size was converted from px to cm using the scale bar in each photograph. To size-correct dominant spot size, we ran a linear regression between SL and dominant spot size, then extracted the residuals of this relationship, thereby removing the effect of BL. Additionally, we calculated a spot size diversity index by dividing the sum of pattern energies by the maximum pattern energy. Low spot size diversity values indicated that a single spot size dominated the overall pattern.

To test if sites represented distinct suites of colorations, we ran 2 multivariate ANOVA (MANOVA) tests with the 3 hue values, 4 countershading values, and 2 pattern indices as predictor variables and site as the dependent variable. As Cat Harbor represented the most extreme habitat, we ran an additional MANOVA testing for differences just between Cat Harbor and the other 3 sites.

2.5. Relationship between coloration and habitat

To determine whether habitat is correlated with coloration, we ran a series of linear regressions between each of 6 response variables (PCA Axis 1 values for $L^\star$, $a^\star$, $b^\star$; countershading ratio across the entire body; size-corrected dominant spot size; and spot size diversity) and 5 predictors (environmental PCA Axes 1, 2, and 3, age, and log-transformed SL). Age and length were tested separately because growth rates of California morays have been shown to decline with age, such that age and SL are uncoupled in individuals >15 yr old, with head length being the more accurate predictor of age (Mehta et al. 2020). We did not run a regression analysis between dominant spot size and log-transformed SL since dominant spot size was already size-corrected. We categorized trapping site as a random effect. Regressions were estimated using restricted maximum likelihood (ReML) using the function 'lme' in R package 'nlme' package (Pinheiro et al. 2019). Conditional R^2 values were cal-

culated by the function 'rsquared' in R package 'piecewiseSEM' (Lefcheck 2016).

2.6. Correlation between coloration and foraging success

We used body condition as a first metric of foraging success. We calculated mathematical relationship between mass and SL for eels from the present study as well as 2163 eels captured around Catalina Island from 2015–2018 (Mehta et al. 2020). An expected mass was then calculated for each eel. The difference between the expected mass and observed mass formed the condition index for each individual, where positive values indicated that an individual was heavier for its length than expected. We then tested for significant linear relationships between all coloration variables and body condition.

As a second metric of foraging success, we examined whether coloration was correlated with the presence of gut contents or the number of prey items consumed. To determine recent feeding success, we manually palpated prey items from the stomach into the oral cavity, then recorded total number of prey items (Hyslop 1980). This method reflects prey recently consumed as complete digestion of fish prey representing 12% of moray mass is roughly 11–12 d (R. Mehta unpubl. data). We ran a series of logistic regressions with all coloration variables, age, and SL as predictor variables, and the presence of gut contents as the response variable. We ran a similar set of linear regressions with the number of prey items consumed as the response variable.

3. RESULTS

3.1. Moray sampling and environmental surveys

A total of 120 eels were photographed from 4 sites around Two Harbors, Catalina Island (Table 1). Eels captured ranged in length from 410–1118 mm (mean 674 mm). Age (calculated via HL) ranged from 7.8–23.3 yr (mean 11.3 yr). Log-transformed SL and age was not significantly different between sites (ANOVA, $F_{3,116}$ = 1.76 and $F_{3,115}$ = 1.43, respectively; both $p > 0.05$; Table S1).

Habitat surveys were completed on 57 traps (Table 1). The 4 sites exhibited variation in environmental features (Fig. 3). Cat Harbor was the most distinct of the 4 sites, characterized by sandy, shallow, highly turbid habitat with low rugosity. 4th of July was the least rugose and had the lowest substrate diversity. Cover was primarily comprised of brown algae and cobble. Conversely, Intakes had high rugosity, high substrate diversity, and high coverage diversity, with a mixture of reef and boulder. Habitat

Table 1. Sample sizes for both eels and traps per site, along with the average number of eels captured per trap

Site	N eels	N traps	Age range (yr)	Size range (mm)	N eels with gut contents
4th of July	30	14	7.8–19.4	442–1018	7
Cat Harbor	32	15	7.8–23.3	414–1118	8
Intakes	26	11	9.1–19.4	556–922	6
West Big Fisherman's Cove	32	17	7.9–19.0	415–1004	5

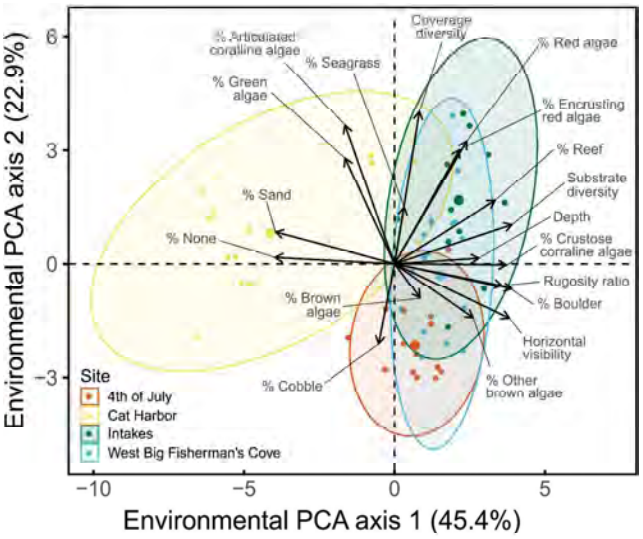

Fig. 3. Environmental principal components analysis (PCA) showing Axes 1 and 2, which together explain 66.9% of environmental variation among traps. Axis 3 explained an additional 15.9%. The 4 sites chosen successfully capture the diverse array of habitats occupied by California morays, with Cat Harbor representing the most distinct site. Ellipses are calculated based on a multivariate normal distribution

in West BFC resembled both 4th of July and Intakes. Axes 1, 2, and 3 of the environmental PCA together described 84.0% of variation among trap environments (Fig. 3, Table S2).

3.2. Quantifying coloration

We quantified 4 aspects of coloration: hue, luminance, countershading, and pattern. Hue and luminance were represented by the first principal components analysis for $L^\star$ (dark to light), $a^\star$ (green to red), and $b^\star$ (blue to yellow) value, which have a maximum range of −100 to 100. Eels varied from 1.5 to 80.0 in the $L^\star$ channel, −6.5 to 50.5 in the $a^\star$ channel, and −7.5 to 38.8 in the $b^\star$ channel. All 3 channels were strongly correlated with one another ($p < 0.0001$; Table S3). Neither hue nor luminance was correlated with age or SL ($p > 0.05$). We found no evidence of distinct polymorphisms in hue or luminance (Hartigan's dip test, $p > 0.05$); instead, eels fell along a gradient for each channel (Fig. 4). We tested whether sites represented different suites of colorations through 2 MANOVAs, first between all sites, and second between Cat Harbor and all other sites.

Eels showed an average countershading ratio (CR) of 0.95 across all body regions, and countershading was significantly less than one in all body regions (1-tailed t-test, df = 370, $p < 0.0001$). Countershading values were normally distributed. CR varied significantly between the head (snout to branchial opening), mid-body (gill opening to vent), and tail (vent to tip of tail) (Fig. 5). This trend occurred both within individual eels and when averaged across all eels (repeated measures ANOVA, $F_{2,245} = 60.17$, $p < 0.0001$; Table S1), with all regions being significantly different from one another (Tukey HSD test, SE = 0.02, $p < 0.0001$). The head showed the most extreme degree of countershading (mean CR = 0.85), followed by the tail region (mean CR = 0.93). Countershading of the tail was positively related to SL so that longer eels had more extreme countershading in their tails ($p < 0.01$, slope = −0.2; Table S3). However, age was not significantly related to tail countershading ($p > 0.05$). On average, the mid-body region showed reverse countershading, in which the dorsal side was lighter than the ventral side (mean CR = 1.07). However, the mid-body region also exhibited the greatest variation in CR values, with a SD of 0.22, nearly twice that of the head (SD = 0.12) and tail (SD = 0.15).

Pattern results confirmed that moray pigmentation is best described as 'mottled' rather than 'uniform' or 'disruptive' (Barbosa et al. 2008), with pattern energies forming a curve rather than a staircase or flat line (Fig. S2). We determined that spots remained proportionally very small in relation to overall body

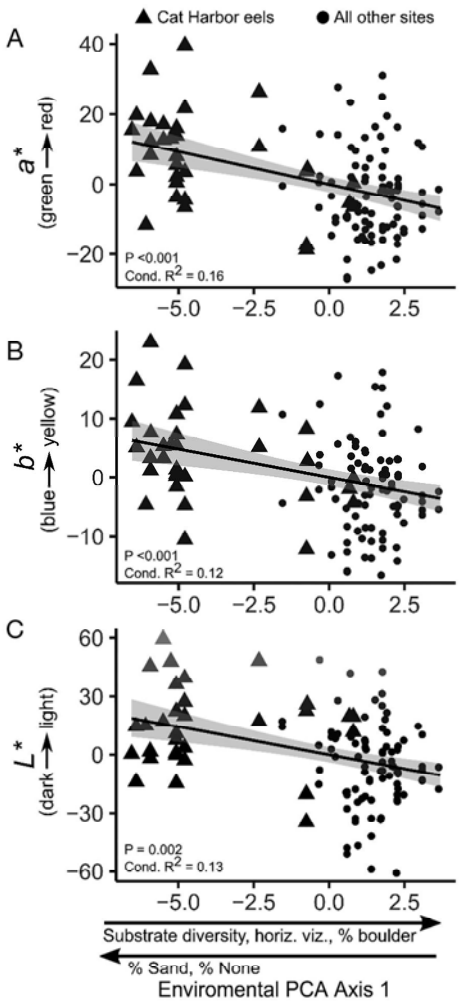

Fig. 4. Moray eel (A,B) hue and (C) luminance is predicted by environmental characteristics. Eels are redder, yellower, and lighter in sandy habitats with bare substrate. Alternatively, eels are greener, bluer, and darker in habitats with high substrate diversity, clearer water, high percentages of boulder, and high rugosity (see Table S2 for variable loadings). Triangles represent eels from Cat Harbor. Conditional R^2 values represent variance explained by both fixed effects and trapping site. Point colors represent actual CIE Lab scores, with green–red ($a^\star$) and blue–yellow ($b^\star$) values shown at luminance ($L^\star$) of 25 (the mean across all individuals) to improve visualization

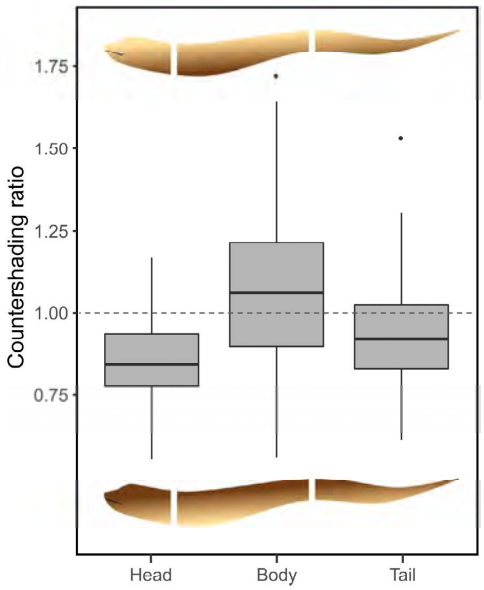

Fig. 5. Countershading varies significantly between the head, middle body, and tail regions (repeated-measures ANOVA, post-hoc Tukey HSD test, $p < 0.0001$). Both within individual eels and across all eels, the head and tail show the most extreme degree of countershading (countershading ratio <1). This may be related to moray behavior of keeping the head (and occasionally tail) outside of crevices. Bar: median; box: interquartile range (IQR) spanning the 25th–75th percentiles; whiskers: 1.5× above/below IQR; dots: outliers. Dashed line at 1.0 indicates no countershading

length, even for large individuals (linear regression, $p < 0.001$, slope = 0.005; Table S3). Spot size diversity was negatively correlated with SL, indicating that as eels grow, their spots become more uniform in size ($p < 0.001$, slope = −0.001; Table S3). Additionally, dominant spot size was negatively correlated with spot size diversity, in that individuals with larger spots had lower spot size diversity ($p < 0.001$). However, no other correlations were seen between coloration variables.

When considered separately, all 4 sites were indistinguishable from one another in terms of coloration except for countershading of the head (MANOVA, $F_1 = 5.42$, $p = 0.02$; Table S4). When Cat Harbor was compared separately from the other sites, a^* and pattern spot size distinguished Cat Harbor from all other sites (MANOVA, $F_1 = 3.71$ vs. 1.02, $p < 0.001$ vs. $p = 0.004$; Table S4), with Cat Harbor eels being redder and having a slightly higher pattern of spot size diversity.

3.3. Relationship between coloration and habitat

Hue (a^* and b^*) and luminance (L^*) were significantly correlated by environmental PC axis 1 ($p < 0.05$), representing habitat (Table S3). Eels in habitats with greater substrate diversity, clearer water, greater percentages of boulder, and greater rugosity were greener, bluer, and darker (Fig. 4). Conversely, eels were redder, yellower, and lighter in shallow habitats with high percentages of sand and bare substrate (Fig. 4). Since we found that countershading varied between body regions, we tested for environmental correlations for each section individually. However, none of the countershading variables, size-corrected dominant spot size, or spot size diversity were correlated with habitat as represented by the 3 environmental PC axes ($p > 0.05$).

3.4. Correlation between coloration and foraging success

We tested for the effect of coloration on body condition and predation success. Only 27 eels (22.5%) from all 4 sites had stomach contents (Table 1). We found no relationship between any of the 6 coloration variables (hue, luminance, average countershading across the entire body, and pattern) and the 3 metrics of foraging success (body condition, the presence of gut contents, or the number of gut contents) ($p > 0.05$). Instead, age and SL were the strongest predictors of foraging success. Longer, older eels were in better condition, more frequently had prey in their stomachs, and had more prey items in their stomachs ($p < 0.05$; Table S3, Fig. S3).

4. DISCUSSION

4.1. Quantifying coloration

We found that California morays exhibit a gradient of colorations rather than distinct polymorphisms, and there is strong correspondence between hue and luminance and environmental variables. A few of our initial hypotheses were supported: eels were lighter and yellower in areas with high percentages of sand and bare substrate, while eels in rugose environments with clear water, high substrate diversity and high percentages of boulder were darker and bluer. Although the environmental surveys did not measure coloration of the actual habitat, we hypothesize that sand is yellower than other types of substrate

and thus has some correspondence with moray hue. However, we found no correlation between seagrass and hue, nor between pattern diversity and substrate/cover diversity. Similarly, while red hues appear darker underwater due to rapid wavelength attenuation through water (Jerlov 1976, Johnsen 2002), California morays were redder in shallower environments. One potential explanation may be the strong correlation between the a^* and b^* channels: eels that were yellower were also redder. Consequently, we hypothesize that California morays have several strategies to avoid detection by predators and prey depending on habitat: individuals in areas with an abundance of potential hiding places may depend more on behavior to avoid detection, but individuals in sand-dominated habitats with fewer crevices, like Cat Harbor, may rely more on coloration.

Although the MS-222 likely affected all eels similarly, Gray et al. (2011) demonstrated that this anesthetic can decrease overall coloration variation. Future studies examining fitness or communication as it relates to eel coloration should consider the effects of MS-222 on overall color variation. Future work examining fitness consequences or intraspecific communication should attempt to photograph eels prior to and after anesthesia to determine if there are differences in coloration.

We show that California morays have a mottled pigmentation pattern. Our initial hypothesis that mottling might be a form of concealment in habitats with a diverse array of substrate and cover types was unsupported. An alternative hypothesis could be that morays in temperate ecosystems are more frequently mottled. However, among subtropical and temperate species in the genus *Gymnothorax*, pigmentation pattern varies from uniform, with little patterning (e.g. *G. prasinus*, *G. unicolor*) to disruptive, with reticulations, spots, or bars (e.g. *G. minor*, *G. prionodon*, *G. ypsilon*) (Froese & Pauly 2019). Only a few species (*G. porphyreus*, *G. obesus*) qualitatively exhibit the same type of mottling as the California moray.

In California morays, it appears that controls on pigmentation cause smaller spots to coalesce into larger spots of more uniform size as BL increases but that spot size remains proportionally very small in comparison to overall BL. Similar changes in pigmentation patterns have been observed in *G. favagineus*, whose spot number increases with length while relative spot size remains constant (Chen et al. 1994). In zebrafish, reaction-diffusion or mechanical mechanisms could be responsible for skin patterns in fish across development, including spots that coalesce over time (Caballero et al. 2012, Watanabe & Kondo 2015). In addition to genetic controls (Kelsh 2004), growth rate, body shape, interactions between pigment cells, and epigenetics all affect the rate and type of pattern development (McClure & McCune 2003, Caballero et al. 2012) in fishes.

Countershading, one of the traits we investigated as part of the suite of coloration traits, is often associated with fish species having a fusiform shape and residing in the water column (Ruxton et al. 2004), where it is hypothesized to assist with camouflaging organisms when viewed from above or below in low turbidity environments. Other eels with different life histories exhibit countershading, such as European eels *Anguilla anguilla* in the migratory, pelagic silver eel phase (Pankhurst & Lythgoe 1982) and a heterenchelyid mud eel *Pythonichthys* cf. *macrurus* which exhibits an unusual infaunal, flatfish-like lifestyle (Martinez & Stiassny 2017). However, California morays are benthic, nocturnal, non-migratory, and do not maintain a constant body posture when in the water column, and we did not expect to find strong countershading. While we found that the countershading is not as striking as in European eels or *P. macrurus*, all individual morays examined exhibited countershading and that location on the body, rather than habitat, predicted countershading intensity. We also observed reverse countershading in the middle region of the body. Variations in countershading intensity across the 3 body regions may correspond with the amount of time morays expose each body section during the day, as morays frequently protrude their heads, and occasionally tails, out of crevices. Alternatively, countershading variations across the length of the body (including reverse countershading in the mid-body) could assist with shape concealment of this elongate fish in the water column. Fish that are primarily active at dawn/dusk have been shown to exhibit countershading, despite the low-light environment, with countershading potentially providing camouflage through shape concealment (Nemtzov et al. 1993). These results suggest that there may be functional advantages of countershading even for benthic, elongate, crevice-dwelling organisms.

4.2. Correlation between coloration and foraging success

Our results indicate that coloration is not correlated with either body condition or the presence/number of prey items. Instead, we found that age and SL

were the strongest predictors of body condition, presence of gut contents, and number of prey items. Past work has shown that as California morays grow, they can consume proportionally larger prey and have larger bite forces (Higgins et al. 2018). Thus, body size appears to be a bigger influence on foraging success than coloration.

We viewed coloration through a human-based system and did not measure the visual systems of potential prey or predators of eels, and thus, biological conclusions regarding the benefit of coloration are not possible. Modeling the visual systems of predators and prey is ultimately required for assessing how morays appear to other organisms in the system (Endler 1990, Olsson et al. 2018). Current evidence suggests that while color vision may be more common in marine fishes than previously thought, the extent and type of color vision in fish is likely limited (Levine & MacNichol 1982, Marshall & Vorobyev 2003, Marshall et al. 2019). California morays feed primarily on kelp bass *Paralabrax clathratus* (Higgins et al. 2018). Kelp bass possess double cones, which indicates some ability to distinguish colors during the daytime (Schwassmann 1968), though they may also be used for detecting luminance differences (Lythgoe 1980, Pignatelli et al. 2010). Along with color vision, fish differ in their achromatic vision (i.e. ability to distinguish between luminance signals), predominantly used for detecting edges and patterns (Siebeck et al. 2014). It appears that for some fish, the visual processing pathways for hue and luminance are linked (Siebeck et al. 2014), but fish likely vary widely and may adapt to different environmental conditions (Carleton et al. 2020). While no studies quantify achromatic vision for morays, studies on serranids related to kelp bass show that this clade of fishes is relatively sensitive to luminance differences (Caves et al. 2017) but fall well below human abilities.

4.3. Selection on morays <400 mm

Coloration selection in eels in size classes smaller than those selected by our traps is the most likely explanation for the correlation between coloration and the environment. Unfortunately, it is also the selective force for which we have the least evidence. Traps used in this study target eels >400 mm, corresponding to morays approximately 7 yr and older. Thus, trap selectivity precluded us from examining how early coloration is established. It is unknown what mechanisms may influence coloration of smaller eels, though predation or post-settlement color change are the most likely. While adult California moray eels likely have very few natural predators around Catalina Island due to their position as apex predators, no data exists for the frequency with which small eels are consumed. Though seals and sea lions have been shown to feed on eels in other regions (Goodman-Lowe 1998, Berry et al. 2017), these marine mammals are not abundant around the Two Harbors area of Catalina Island, and they do not appear to feed on California morays (Shane 1994, LeBoeuf 2002). Sharks have also been observed feeding on eels in other areas (Béguer-Pon et al. 2012, Sears & Sikkel 2016). However, historical diet studies on 2 of the most likely shark predators, the leopard shark *Triakis semifasciata* and the blue shark *Prionace glauca* showed no indication that these species consume eels (Talent 1976, Tricas 1977, Smith 2001). While white sharks *Carcharodon carcharias* are known to visit Catalina Island (Jorgensen et al. 2012), only younger individuals are thought to predate upon bottom-dwelling fishes (Dewar et al. 2004), and no studies have reported eels in their diets. However, diet studies of sharks from the last 30 yr (the approximate lifespan of the California moray) are limited. While conspecific predation does occur, it makes up only a small percentage of moray diets (Higgins et al. 2018, Mehta et al. 2020). Increased trapping effort for smaller eels would provide more information on how coloration is established in earlier stages, particularly in post-settlement individuals.

4.4. Habitat self-selection

It is unlikely that California morays are self-selecting microhabitats within each site based on hue alone. First, California morays are probably colorblind, similar to other *Gymnothorax* species that have only one type of color-sensitive cone cell (Wang et al. 2011). The Kidako moray *G. kidako* and giant moray *G. javanicus* also have very small optic tectum volumes and unusual olfactory bulb structures, suggesting that these species hunt primarily by smell rather than sight (Yamamoto 2017, Iglesias et al. 2018). While California morays could theoretically still self-select habitat based on luminance, our results indicate that environmental characteristics associated with ambient light levels such as depth and rugosity were only weakly correlated with luminance.

Second, eels have very high site fidelity. Mehta et al. (2020) reported that of 1311 eels captured around

Santa Catalina from 2015–2018, only 17 individuals were captured in more than one cove. Thus, eels do not appear to be migrating between coves to find suitable habitat. This suggests that other mechanisms (such as mortality, predation, or post-settlement color changes) influence the establishment of coloration.

4.5. Conclusion

In summary, we found that there are differences in the coloration of individual California moray eels inhabiting the Two Harbors area of Catalina Island, California. Eels from Cat Harbor, a site characterized by sandy habitats with few hiding places, had the most distinct colorations. For a crevice-dwelling, nocturnal fish, we found a surprising correlation between hue and luminance and environmental characteristics of the habitat. Interestingly for a benthic fish whose body position in the water column is not static, morays exhibited countershading across their entire body surface, but most pronounced in the head and tail. Results indicated that coloration does not improve foraging success of adult eels, and we subsequently hypothesized that coloration has some advantage in early life stages.

Other benthic reef fishes in southern California waters do not exhibit the same suite of coloration characteristics as California morays. However, scorpionfishes *Scorpaena* spp. and cabezon *Scorpaenichthys marmoratus* qualitatively exhibit some degree of mottling and/or countershading. Other predatory fishes in California show distinctly different coloration patterns between the juvenile and adult stage, including the California sheephead *Semicossyphus pulcher* and giant sea bass *Stereolepis gigas*. Coloration may be a previously overlooked characteristic of importance for many nearshore fishes in California.

Acknowledgements. We thank the 2019 Mehta Lab moray trapping team (W. Moretto, C. Kintz, N. Castaneda, M. Miller, E. Pilch), the University of Southern California Wrigley Institute for Environmental Studies staff, and Research Experience for Undergraduates coordinators D. Kim and K. Heidelberg. We also thank 3 reviewers and editor D. Pittman for providing constructive comments. Funding was provided by National Science Foundation Award #OCE-1263356, the Hellman's Foundation Grant, the University of Southern California Wrigley Institute for Environmental Studies Summer Graduate Fellowship, and the University of California, Santa Cruz Giving Day 2019. Moray sampling was completed under California Department of Fish and Wildlife permit #S-190830002-19086-001.

LITERATURE CITED

Barbosa A, Mäthger LM, Buresch KC, Kelly J, Chubb C, Chiao CC, Hanlon RT (2008) Cuttlefish camouflage: the effects of substrate contrast and size in evoking uniform, mottle or disruptive body patterns. Vision Res 48: 1242–1253

Barry KL, Hawryshyn CW (1999) Effect of incident light and background conditions on potential conspicuousness of Hawaiian coral reef fish. J Mar Biol Assoc UK 79:495–508

Béguer-Pon M, Benchetrit J, Castonguay M, Aarestrup K, Campana SE, Stokesbury MJW, Dodson JJ (2012) Shark predation on migrating adult American eels (*Anguilla rostrata*) in the Gulf of St. Lawrence. PLOS ONE 7:e46830

Berry TE, Osterrieder SK, Murray DC, Coghlan ML and others (2017) DNA metabarcoding for diet analysis and biodiversity: a case study using the endangered Australian sea lion (*Neophoca cinerea*). Ecol Evol 7:5435–5453

Caballero L, Benítez M, Alvarez-Buyllla ER, Hernández S, Arzola A V., Cocho G (2012) An epigenetic model for pigment patterning based on mechanical and cellular interactions. J Exp Zool B Mol Dev Evol 318:209–223

Carleton KL, Escobar-Camacho D, Stieb SM, Cortesi F, Justin Marshall N (2020) Seeing the rainbow: mechanisms underlying spectral sensitivity in teleost fishes. J Exp Biol 223:jeb193334

Caro T (2005) The adaptive significance of coloration in mammals. Bioscience 55:125–136

Caro T, Beeman K, Stankowich T, Whitehead H (2011) The functional significance of colouration in cetaceans. Evol Ecol 25:1231–1245

Caro T, Stankowich T, Mesnick SL, Costa DP, Beeman K (2012) Pelage coloration in pinnipeds: functional considerations. Behav Ecol 23:765–774

Caves EM, Sutton TT, Johnsen S (2017) Visual acuity in ray-finned fishes correlates with eye size and habitat. J Exp Biol 220:1586–1596

Chen HM, Shao KT, Chen CT (1994) A review of the muraenid eels (family Muraenidae) from Taiwan with descriptions of twelve new records. Zool Stud 33:44–64

Cournoyer BL, Cohen JH (2011) Cryptic coloration as a predator avoidance strategy in seagrass arrow shrimp colormorphs. J Exp Mar Biol Ecol 402:27–34

Cuthill IC (2019) Camouflage. J Zool (Lond) 308:75–92

Cuthill IC, Allen WL, Arbuckle K, Caspers B and others (2017) The biology of color. Science 357:eaan0221

Dewar H, Domeier M, Nasby-Lucas N (2004) Insights into young of the year white shark, *Carcharadon carcharias* behavior in the Southern California Bight. Environ Biol Fishes 70:133–143

Donatelli CM, Summers AP, Tytell ED (2017) Long-axis twisting during locomotion of elongate fishes. J Exp Biol 220:3632–3640

Endler JA (1990) On the measurement and classification of colour in studies of animal colour patterns. Biol J Linn Soc 41:315–352

Eterovick PC, Figueira JEC, Vasconcellos-Neto J (1997) Cryptic coloration and choice of escape microhabitats by grasshoppers (Orthoptera: Acrididac). Biol J Linn Soc 61: 485–499

Fitch JE, Lavenberg RJ (1971) Marine food and game fishes of California. University of California Press, Berkeley, CA

Freiwald J, McMillan S, Abbott D, McHugh T, Kozma K (2019) Reef Check California instruction manual: a guide to monitoring California's kelp forests. Marina del Rey, CA

Froese R, Pauly D (2019) FishBase, version (08/2019). www.fishbase.org
Gilbert M, Rasmussen JB, Kramer DL (2005) Estimating the density and biomass of moray eels (Muraenidae) using a modified visual census method for hole-dwelling reef fauna. Environ Biol Fishes 73:415–426
Gilby BL, Mari RA, Bell EG, Crawford EW and others (2015) Colour change in a filefish (*Monacanthus chinensis*) faced with the challenge of changing backgrounds. Environ Biol Fishes 98:2021–2029
Goodman-Lowe GD (1998) Diet of the Hawaiian monk seal (*Monachus schauinslandi*) from the Northwestern Hawaiian Islands during 1991 to 1994. Mar Biol 132: 535–546
Gray SM, Hart FL, Tremblay MEM, Lisney TJ, Hawryshyn CW (2011) The effects of handling time, ambient light, and anaesthetic method, on the standardized measurement of fish colouration. Can J Fish Aquat Sci 68:330–342
Hartigan JA, Hartigan PM (1985) The dip test of unimodality. Ann Stat 13:70–84
Higgins BA, Mehta R (2018) Distribution and habitat associations of the California moray (*Gymnothorax mordax*) within Two Harbors, Santa Catalina Island, California. Environ Biol Fishes 101:95–108
Higgins BA, Law CJ, Mehta RS (2018) Eat whole and less often: ontogenetic shift reveals size specialization on kelp bass by the California moray eel, *Gymnothorax mordax*. Oecologia 188:875–887
Hyslop EJ (1980) Stomach contents analysis – a review of methods and their application. J Fish Biol 17:411–429
Iglesias TL, Dornburg A, Warren DL, Wainwright PC, Schmitz L, Economo EP (2018) Eyes wide shut: the impact of dim-light vision on neural investment in marine teleosts. J Evol Biol 31:1082–1092
Jerlov NG (1976) Marine optics, 2nd edn. Elsevier, Amsterdam
Johnsen S (2002) Cryptic and conspicuous coloration in the pelagic environment. Proc Biol Sci 269:243–256
Johnsen S, Sosik HM (2003) Cryptic coloration and mirrored sides as camouflage strategies in near-surface pelagic habitats: implications for foraging and predator avoidance. Limnol Oceanogr 48:1277–1288
Jorgensen S, Chapple T, Hoyos M, Reeb C, Block B (2012) Connectivity among white shark coastal aggregation areas in the Northeastern Pacific. In: Domeier ML (ed) Global perspectives on the biology and life history of the white shark, Chap 13. CRC Press, Boca Raton, FL, p 159–168
Josse J, Husson F (2016) MissMDA: a package for handling missing values in multivariate data analysis. J Stat Softw 70:i01
Kekäläinen J, Huuskonen H, Kiviniemi V, Taskinen J (2010) Visual conditions and habitat shape the coloration of the Eurasian perch (*Perca fluviatilis* L.): A trade-off between camouflage and communication? Biol J Linn Soc 99: 47–59
Kelsh RN (2004) Genetics and evolution of pigment patterns in fish. Pigment Cell Res 17:326–336
Lê S, Josse J, Husson F (2008) FactoMineR: an R package for multivariate analysis. J Stat Softw 25:i01
LeBoeuf BJ (2002) Status of pinnipeds on Santa Catalina Island. Proc Calif Acad Sci 53:11–21
Leclercq E, Taylor JF, Migaud H (2010) Morphological skin colour changes in teleosts. Fish Fish 11:159–193
Lefcheck JS (2016) PiecewiseSEM: piecewise structural equation modelling in R for ecology, evolution, and systematics. Methods Ecol Evol 7:573–579
Levine JS, MacNichol EF (1982) Color vision in fishes. Sci Am 246:140–149
Luckhurst E, Luckhurst K (1978) Analysis of the influence of substrate variables on coral reef fish communities. Mar Biol 49:317–323
Lythgoe JN (1980) The ecology of vision. Clarendon, Oxford
Marshall NJ (2000) Communication and camouflage with the same 'bright' colours in reef fishes. Philos Trans R Soc Lond B Biol Sci 355:1243–1248
Marshall JN, Vorobyev M (2003) The design of color signals and color vision in fishes. In: Collin SP, Marshall JN (eds) Sensory processing in aquatic environments. Springer-Verlag, New York, NY, p 194–222
Marshall NJ, Cortesi F, de Busserolles F, Siebeck UE, Cheney KL (2019) Colours and colour vision in reef fishes: past, present and future research directions. J Fish Biol 95:5–38
Martinez CM, Stiassny MLJ (2017) Can an eel be a flatfish? Observations on enigmatic asymmetrical heterenchelyids from the Guinea coast of West Africa. J Fish Biol 91: 673–678
McClure M, McCune AR (2003) Evidence for developmental linkage of pigment patterns with body size and shape in *Danios* (Teleostei: Cyprinidae). Evolution 57:1863–1875
Meakin CA, Qin JG (2012) Growth, behaviour and colour changes of juvenile King George whiting (*Sillaginodes punctata*) mediated by light intensities. NZ J Mar Freshw Res 46:111–123
Mehta RS, Dale KE, Higgins BA (2020) Marine protection induces morphological variation in the California moray *Gymnothorax mordax*. Integr Comp Biol 60:522–534
Montes-Hugo MA, Alvarez-Borrego SS, Giles-Guzman AD (2003) Horizontal sighting range and Secchi depth as estimators of underwater PAR attenuation in a coastal lagoon. Estuaries 26:1302–1309
Nemtzov SC, Kajiura SM, Lompart CA (1993) Diel color phase changes in the coney, *Epinephelus fulvus* (Teleostei, Serranidae). Copeia 1993:883
Olsson P, Lind O, Kelber A (2018) Chromatic and achromatic vision: parameter choice and limitations for reliable model predictions. Behav Ecol 29:273–282
Orton RW, McElroy EJ, McBrayer LD (2018) Predation and cryptic coloration in a managed landscape. Evol Ecol 32: 141–157
Pankhurst NW, Lythgoe JN (1982) Structure and colour of the integument of the European eel *Anguilla anguilla* (L.). J Fish Biol 21:279–296
Phillips GAC, How MJ, Lange JE, Marshall NJ, Cheney KL (2017) Disruptive colouration in reef fish: Does matching the background reduce predation risk? J Exp Biol 220: 1962–1974
Pignatelli V, Champ C, Marshall J, Vorobyev M (2010) Double cones are used for colour discrimination in the reef fish, *Rhinecanthus aculeatus*. Biol Lett 6:537–539
Pinheiro J, Bates D, DebRoy S, Sarkar D, R Core Team (2019) Nlme: linear and nonlinear mixed effects models. R package version 3.1-151. https://mran.microsoft.com/web/packages/nlme/index.html
R Core Team (2016) A language and environment for statistical computing. R Foundation for Statistical Computing, Vienna
Reimchen TE (1989) Loss of nuptial color in threespine sticklebacks (*Gasterosteus aculeatus*). Evolution 43:450–460

Risk MJ (1972) Fish diversity on a coral reef in the Virgin Islands. Atoll Res Bull 153:1–4

Rueden CT, Schindelin J, Hiner MC, DeZonia BE, Walter AE, Arena ET, Eliceiri KW (2017) ImageJ2: ImageJ for the next generation of scientific image data. BMC Bioinformatics 18:529

Ruxton GD, Speed MP, Kelly DJ (2004) What, if anything, is the adaptive function of countershading? Anim Behav 68:445–451

Schwassmann HO (1968) Visual projection upon the optic tectum in foveate marine teleosts. Vision Res 8:1337–1348

Sears WT, Sikkel PC (2016) Field observation of predation on an adult Caribbean purplemouth moray eel by a nurse shark. Coral Reefs 35:971

Shane SH (1994) Occurrence and habitat use of marine mammals at Santa Catalina Island, California from 1983–91. Bull South Calif Acad Sci 93:13–29

Shannon CE (1948) A mathematical theory of communication. Bell Syst Tech J 27:379–423

Siebeck UE, Wallis GM, Litherland L, Ganeshina O, Vorobyev M (2014) Spectral and spatial selectivity of luminance vision in reef fish. Front Neural Circuits 8:118

Sköld HN, Aspengren S, Cheney KL, Wallin M (2016) Fish chromatophores — from molecular motors to animal behavior. Int Rev Cell Mol Biol 321:171–219

Smith SE (2001) Leopard shark. In: Leet SW, Dewees DM, Klingbeil R, Larson EF (eds) California's marine living resources: a status report. California Department of Fish and Game, Davis, CA, p 252–254

Stevens M, Merilaita S (2009) Animal camouflage: current issues and new perspectives. Philos Trans R Soc Lond B Biol Sci 364:423–427

Talent LG (1976) Food habits of the leopard shark, *Triakis semifasciata*, in Elkhorn Slough, Monterey Bay, California. Calif Fish Game 62:286–298

The GIMP Development Team (2019) GNU image manipulation program. https://www.gimp.org/

Tricas TC (1977) Relationships of the blue shark *Prionace glauca* and its prey species near Santa Catalina Island, California. Fish Bull 77:175–182

Troscianko J, Stevens M (2015) Image calibration and analysis toolbox — a free software suite for objectively measuring reflectance, colour and pattern. Methods Ecol Evol 6: 1320–1331

Tyrie EK, Hanlon RT, Siemann LA, Uyarra MC (2015) Coral reef flounders, *Bothus lunatus*, choose substrates on which they can achieve camouflage with their limited body pattern repertoire. Biol J Linn Soc 114:629–638

Wang FY, Tang MY, Yan HY (2011) A comparative study on the visual adaptations of four species of moray eel. Vision Res 51:1099–1108

Watanabe M, Kondo S (2015) Is pigment patterning in fish skin determined by the Turing mechanism? Trends Genet 31:88–96

Watson AC, Siemann LA, Hanlon RT (2014) Dynamic camouflage by Nassau groupers *Epinephelus striatus* on a Caribbean coral reef. J Fish Biol 85:1634–1649

Weller HI, Westneat MW (2019) Quantitative color profiling of digital images with earth mover's distance using the R package colordistance. PeerJ 7:e6398

Westley PAH, Conway CM, Fleming IA (2012) Phenotypic divergence of exotic fish populations is shaped by spatial proximity and habitat differences across an invaded landscape. Evol Ecol Res 14:147–167

Whiteley AR, Bergstrom CA, Linderoth T, Tallmon DA (2011) The spectre of past spectral conditions: colour plasticity, crypsis and predation risk in freshwater sculpin from newly deglaciated streams. Ecol Freshwat Fish 20:80–91

Whitney JL, Donahue MJ, Karl SA (2018) Niche divergence along a fine-scale ecological gradient in sympatric color morphs of a coral reef fish. Ecosphere 9:e02015

Wilson RP, Ryan PG, James A, Wilson MPT (1987) Conspicuous coloration may enhance prey capture in some piscivores. Anim Behav 35:1558–1560

Wojan EM, Carreiro NC, Clendenen DA, Neldner HM, Castillo C, Bertram SM, Kolluru GR (2019) The effects of commonly used anaesthetics on colour measurements across body regions in the poeciliid fish, *Girardinus metallicus*. J Fish Biol 95:1320–1330

Yamamoto N (2017) Adaptive radiation and vertebrate brain diversity: cases of teleosts. In: Shigeno S, Murakami Y, Nomura T (eds) Brain evolution by design. Springer, Tokyo, p 253–271

Editorial responsibility: Simon Pittman, Oxford, UK
Reviewed by: C. Bergstrom and 2 anonymous referees

Submitted: January 20, 2021
Accepted: August 18, 2021
Proofs received from author(s): October 12, 2021

Chapter 4

Identifying mechanisms influencing Eastern Pacific ichthyoplankton abundances using a hierarchical Bayesian framework

Katherine E. Dale[1], Andrew R. Thompson[2], M. Tim Tinker[1]

[1]Department of Ecology and Evolutionary Biology, University of California, Santa Cruz, Santa Cruz, CA, USA

[2]NOAA Fisheries Service, Southwest Fisheries Science Center, La Jolla, California, USA

Abstract

Understanding how species distributions change through space and time is central to ecological studies. For marine fishes, continued dispersal or retention of larvae is important for population persistence and maintaining genetic connectivity. The survival and movement of fish in their early life history stage is strongly dependent on both environmental factors as well as species' characteristics, but it is not always clear how environmental variation influences species from diverse habitats. Many fisheries management plans and stock assessments for California fisheries do not account for spatial variation in larval abundance, so a spatially-explicit hierarchical model was developed to examine how larval abundances in the California Current region vary with environmental factors. We applied this model to five data-moderate, underassessed, cryptic, or threatened California fisheries: Pacific sanddab

(*Citharichthys sordidus*), California sheephead (*Semicossyphus pulcher*), cabezon (*Scorpaenichthys marmoratus*), rockfishes (*Sebastes* spp.) and sablefish (*Anoplopoma fimbria*). This showed that oceanographic conditions, particularly sea surface height, best describe larval abundances. Results support past studies examining environmental covariates of larval abundance in these species. Outputs from this model are highly interpretable and can provide estimates of larval abundances at specific spatial scales.

Introduction

The biodiversity of terrestrial and aquatic communities is driven by the ability of species to successfully reproduce and disperse to and persist in different habitats. For many marine fishes, dispersal occurs during a planktonic larval form that resides in the surface layer of the ocean for a period of days to months. Both extrinsic and intrinsic factors influence the dispersal and retention of propagules (Cowen and Sponaugle 2009; Llopiz et al. 2014). Extrinsic pressures include the strength and direction of oceanic currents (Shanks and Eckert 2005), oceanographic processes such as eddies, fronts, and rings (Limouzy-Paris et al. 1997), geographic features such as peninsulas (Ebert and Russell 1988), and large scale climate oscillations (i.e., Leising et al. 2015). Larval mobility may also be influenced by intrinsic factors such as pelagic larval duration time (Shanks 2009), swimming performance (Stobutzki & Bellwood 1997, Müller et al. 2008), ability to detect environmental cues (Gerlach et al. 2007; Naisbett-Jones et al. 2017), and growth rate (Wilson and Meekan 2002). The

interaction between these extrinsic and intrinsic factors may further impede or facilitate dispersal (e.g., Hunt von Herbing 2002).

Natural and anthropogenic climate patterns, coupled with a strong sea surface temperature gradient and complex oceanographic features, make the California Current ecosystem (CCS) a unique platform for examining population persistence, range expansion, and species invasions of fishes. Within the CCS, seasonal shifts during winter months can cause the southward-flowing California Current to move offshore and weaken, allowing the northward-flowing nearshore Davidson Current to dominate (Parrish et al. 1981; Shanks and Eckert 2005). Climate oscillations such as the El Niño Southern Oscillation (ENSO) have similar effects on current patterns and can cause net transport to temporarily turn northward (Lynn and Bograd 2002). Ongoing climate change is further altering current patterns worldwide (Harley et al. 2006), with some evidence suggesting that climate change will strengthen oceanographic processes off California such as upwelling (Snyder et al. 2003) and induce more frequent ENSO events (Timmermann et al. 1999). Environmental factors interact with biotic characteristics of larvae themselves, because the ability of some larvae to find food or reach preferred juvenile habitats may decline due to shifts in characteristics such as spawning timing or larval growth rates (Llopiz et al. 2014; Asch 2015).

Large-scale climate oscillations have previously been shown to transport fish and invertebrate species northward (Cowen 1985; Davis 2000; Lluch-Belda et al. 2005; Leising et al. 2015; Nielsen et al. 2021; Thompson et al. 2022), and can have

large impacts on the productivity of California's fisheries. Many past studies have examined the relationship between environmental variation on recruitment and abundance of larval fishes, but few have done so in a framework that explicitly accounts for spatial patterns and various sources of error. Spatial data are often complicated by various sources of sampling error, observation (or measurement) error, and spatial autocorrelation that can be difficult to account for in traditional modeling approaches (Latimer et al. 2006). Spatial autocorrelation (where points that are close together are more alike than those farther apart) violates a fundamental assumption of traditional statistics, which assumes that residuals are independent and identically distributed. Larval fish distributions likely have a high degree of spatial autocorrelation for various reasons: dispersal occurs from specific spawning locations, local current patterns entrap all larvae in one area, and fish tend to move to communal feeding patches, etc. In large part because of these data complexities and the challenges of addressing them within classical statistical methods, even management plans for economically important species are usually not spatially explicit. This omission is potentially problematic for managers: For example, in the CCS, assemblages vary latitudinally, and assemblage dynamics cannot be predicted for the entire region by examining a single spatial subset of the region (Thompson et al. 2014). This highlights the importance of accounting for spatial variation within the CCS.

Bayesian methods can easily incorporate multiple sources of error and correct for autocorrelation, while still providing interpretable estimates on parameter values.

Additionally, these methods are beneficial when working with species that are less frequently seen in surveys. Although past studies have used Bayesian hierarchical models to examine environmental predictors of recruitment in northeastern Pacific fishes, spatial autocorrelation was not formally accounted for (Stachura et al. 2014; Stawitz et al. 2015). Here, we combine empirical data from a long-term ichthyoplankton sampling program with robust Bayesian hierarchical models, explicitly incorporating (and thus controlling for) spatial autocorrelation, to identify the strength to which environmental variables influence larval distributions and how larval distribution shifts vary for diverse species. In addition to examining general trends for all fish larvae, we specifically examined trends for five case-study taxa that are of commercial importance (Fig. 4.1, Table 1.1): Pacific sanddab (*Citharichthys sordidus*), California sheephead (*Semicossyphus pulcher*), cabezon (*Scorpaenichthys marmoratus*), rockfishes (*Sebastes* spp.) and sablefish (*Anoplopoma fimbria*). These taxa represent a diverse array of life history strategies, from the deep-dwelling sablefish to nearshore kelp forest species such as cabezon and sheephead. These taxa are classified in prior state and federal stock assessments as data-moderate (sheephead), underassessed (Pacific sanddab, cabezon, sheephead), cryptic (sablefish), or a threatened (some rockfishes) (Cope and Key 2009; Dick and MacCall 2010; Loke-smith 2011; He et al. 2013; He and Field 2017; Haltuch et al. 2019). The most recent stock assessments for cabezon, sablefish, Pacific sanddab, and some rockfishes such as Bocaccio (*Sebastes paucispinis*) explicitly call for improved understanding of the interaction between the environment and recruitment and/or

region-specific data on life history traits (Fig. 4.1, Cope and Key 2009; He et al. 2013; He and Field 2017; Haltuch et al. 2019). For instance, the 2009 stock assessment for cabezon calls for a better understanding of the link between the El Nino Southern Oscillation and recruitment (Cope and Key 2009) and 2013 the stock assessment for Pacific sanddab calls for more data on reproductive biology in southern California (He et al. 2013). Other species, such as California sheephead, appear to move across the US-Mexico border, and represents a stock that should incorporate transboundary management (Cowen 1985; Bernardi et al. 2003; Loke-smith 2011).

Methods

The California Cooperative Oceanic Fisheries Investigations (CalCOFI) is a 70-year ichthyoplankton sampling program in the Eastern Pacific, primarily covering the California bight region (ref). Several types of nets have been used onboard over the history of the program. From 1951-1968, a 1-m ring net was used. Mesh sizes of the ring net varied from 550 µm-25 mm (1951-1969) and 505 µm (1969-1977). Since 1978, sampling has been completed with a 71-cm double bongo net (mesh size 505 µm) towed behind the ship at 1-2 knots. Sampling depth of ring nets or bongos is approximately 210 m. Additional surface tows were completed using a 505 µm manta net.

We extracted larval catch data for five case study taxa: Pacific sanddab, California sheephead, cabezon, rockfishes, and sablefish. Catch data were comprised

of both positive occurrences as well as "zero" stations where no larvae of the taxon were captured. All data are available for public use through the ERDDAP portal (https://coastwatch.pfeg.noaa.gov/erddap/index.html). Raw larval counts were standardized to larvae/10 m^2 by dividing by the percentage of the sample that was sorted and multiplied by the standard haul factor, a measure of the amount of water flowing through the net (Smith and Richardson 1977).

Environmental data waswere also obtained through ERDDAP and came from onboard measurements during CalCOFI sampling (dataset ID: erdNOAAhydros). We collated data on sea surface height, sea surface temperature, salinity, and dissolved oxygen. Three primary tools were used to evaluate environmental conditions: Surface-only measurements, a conductivity-temperature-depth sensor (CTD, implemented at all stations after 1992), and a 20-bottle hydro cast (discrete-depth bottle sampling, replaced by the CTD in 1993). For neuston tows at the surface, we averaged environmental data from all sources from depths ≤ 50 m. For bongo tows, we averaged data over depths ≤ 210 m. For each station, we also extracted the latitude and calculated the great-circle distance from nearest landmass. All covariates were centered and scaled.

The total geographic range of CalCOFI cruises encompasses a huge area, stretching from the US-Canada border to the Gulf of California and hundreds of km offshore. The five case study taxa had geographic ranges that represented only a subset of this range. Therefore, for each species we constructed a study area encompassing the convex hull of only positive stations where larvae of that taxon

were successfully caught. We overlaid a hexagonal grid over each sampling extent, resulting in *G* total grid cells, each with a diameter 1.5°.

The model was constructed in three parts: an observation model, a sampling model, and a correlative autoregressive model, to account for spatial autocorrelation (Fig. 4.2). The sampling model was constructed as a Bayesian implementation of a linear deterministic function, in which a vector of station-specific covariates *X* and a vector of grid-level covariates *W*, along with associated coefficients β and A, are related to the true count of larvae μ in grid cell *G*:

$$\mu_n = \beta_0 + \mathbf{X}_n\boldsymbol{\beta}_n + \mathbf{W}_g\mathbf{A}_g + \epsilon \quad (1)$$

Several options are available for accounting for spatial autocorrelation in a Bayesian framework (Banerjee et al. 2003). One of the most well-implemented techniques for grid-level data is the conditional autoregressive (CAR) model (Besag 1974). We chose to implement a Besag-York-Mollié 2 (BYM2) model due to its efficiency and interpretable parameters (Riebler et al. 2016). A random value ρ_n is drawn from a CAR distribution, which is dependent on the number of connected grid cells. Cells are considered neighbors if any of their borders intersect. The BYM2 model is defined as:

$$\epsilon = \left(\sqrt{1-\rho} * \theta + \sqrt{\frac{\rho}{s}} * \phi\right)\sigma \quad (2)$$

Where ρ models the spatial variance, , θ is the uncorrelated (i.e., non-spatial) random effect, *s* is the scaling factor computed such that the Var(φ) ≈ 1, and σ is the overall standard deviation of combined error terms. φ is the spatially-autocorrelated random

effect, where all values of phi are calculated as an ICAR multivariate normal with a correlation of 1 between adjacent cells. φ sums to 0 across all cells.

Observational (i.e., sampling) error can be quite substantial with regards to ichthyoplankton datasets. Null stations, where larvae of a certain species were not identified in the sample, are very common. This is due to the inherent difficulties in sampling for tiny, relatively mobile animals across a very large spatial region. There are two reasons why larvae may be absent from a sample. First, they may have been present, but sampling failed to catch them. Alternatively, fish could have been absent from the area entirely for some environmental or biotic reason. In light of this, observed larval count y_n was modeled using a zero-inflated gamma hurdle model. The observed larval abundance is represented by a gamma distribution incorporating both the "true" count μ_n, observer variance η_n, and z, a binary value indicating whether a larva was successfully caught (1) or missed (0):

$$p(y \mid z, \mu, \eta) = \begin{cases} (1 - z) + \overset{z}{gamma}\left(y \middle| \frac{\mu^2}{\eta^2}, \frac{\mu}{\eta^2}\right) \end{cases}$$

(3)

The full proportional posterior and likelihood are as follows. Terms in bold indicate vectors.

$$[\boldsymbol{\mu}, \eta, z, \beta_0, \mathbf{\beta}, \mathbf{W}, \rho, \boldsymbol{\phi}, \boldsymbol{\theta}, \sigma, \boldsymbol{\omega}, \boldsymbol{x}, p| \, y]$$

$$\propto \prod_{n}^{N} \prod_{k}^{K} \prod_{g}^{G} \left[y_n | \frac{\mu_n^2}{\eta^2}, \frac{\mu_n}{\eta^2}, z \right] \times$$

$$\times [z] \times [\eta] \times \left[\mu_n | f(x_{kn}, \omega_g, \beta_0, \beta_k, W_{k'g}, \phi_G, \theta_G, \rho) \right] \times [\rho] \times [\phi_G] \times [\theta_G]$$

$$\times [\beta_0] \times [\beta_k] \times [\sigma_G] \times [W_{k'g}]$$

(7)

Variables were assigned weakly informative priors as follows:

$$y \sim \text{Gamma}\left(\frac{\mu^2}{\eta^2}, \frac{\mu}{\eta^2}\right) \tag{8}$$

$$\eta \sim \text{Gamma}(0.01, 0.01) \tag{9}$$

$$z \sim \text{Beta}(0.5, 0.5) \tag{10}$$

$$\phi \sim -0.5 \times (\phi_{node1} - \phi_{node2}) \cdot (\phi_{node1} - \phi_{node2}) \tag{11}$$

$$\theta \sim \text{Normal}(0,1) \tag{12}$$

$$\rho \sim \text{Beta}(0.5, 0.5) \tag{13}$$

$$\sigma \sim \text{Cauchy}(0,1) \tag{14}$$

$$\beta \sim \text{Cauchy}(0,1) \tag{15}$$

$$\text{A} \sim \text{Cauchy}(0,1) \tag{16}$$

$$\eta \sim \text{Cauchy}(0,1) \tag{17}$$

We note that the prior for ϕ is not a true prior, as it is not a distribution; rather, the optimal value of ϕ minimizes the squared deviation between grid cells, ensuring that values for adjacent grid cells are as correlated as possible.

Model implementation was completed using Stan (Carpenter et al. 2017; Stan Development Team 2022). Stan is a Bayesian inference framework that estimates parameters using dynamic Hamiltonian Monte Carlo sampling. We used CmdStanR version 2.29.2 (https://mc-stan.org/cmdstanr/) to compile and run the model from R version 4.1.3.

Models were run with 3 chains for 4334 iterations (1000 of which were warmup) with an adapt delta of 0.9. Chain convergence was confirmed by examining $\widehat{R}$ values. Other convergence issues were checked using the 'check_hmc_diagnostics' in package RStan.

For each species and all fish larvae (n taxa = 517), we ran the model with four different sets of environmental covariates. First, we tested only geographic covariates (latitude and distance from shore). Second, we tested ENSO-related covariates (dynamic height and temperature). Third, we tested only oceanographic covariates (temperature, dynamic height, dissolved oxygen, and salinity). Finally, we ran a model that included all covariates (latitude, distance from shore, temperature, dynamic height, dissolved oxygen, salinity). We evaluated which of these model sets was the strongest predictor for each species using efficient leave-one-out cross-validation using Pareto-Smoothed Importance Sampling (PSIS), implemented in package 'loo' (https://mc-stan.org/loo/) (Vehtari et al. 2017). The model with the

highest estimated expected log pointwise predictive density (ELPD) value was considered the best model for describing each dataset.

Results

After removing any stations within the study area lacking environmental data, each taxon's dataset contained between 5,591 to 10,975 tows (Table 1.1). $\widehat{R}$ values were all < 1.1, indicating that chains mixed acceptably; this was also confirmed by visually examining trace plots. Diagnostic checks showed no divergences for any model. 21 of 24 models had fewer than 1% of iterations exceed a maximum tree depth of 10; California sheephead models 1 (geography), 2 (ENSO), and 3 (oceanography) had 21.6-40.4% of iterations exceed maximum tree depth. The CAR model satisfactorily accounted for spatial autocorrelation across sampling extents for all taxa (Fig. 4.3).

Model 3, with oceanographic variables as covariates (dissolved oxygen, sea surface height, salinity, and sea surface temperature), best predicted larval abundances across the three nearshore species (cabezon, California sheephead, and rockfishes) and all fish larvae (Fig. 4.4; Table 1.2). The two shelf/slope species were better described by ENSO conditions (Pacific sanddab) and geography (sablefish). However, the strength and predictive power of covariates varied across taxa (Table 1.2). Of the four environmental variables, sea surface height was the only covariate predictive factor for all taxa, with all but one species (Pacific sanddab) being more abundant in lower sea surface heights. Although positive sea surface temperatures

were correlated with higher abundances for general fish larvae, among case study species, sea surface temperature was a weak predictor only for Pacific sanddab. Similarly, dissolved oxygen was a positive predictor only for general larvae and rockfishes. Salinity was positively correlated only with cabezon and rockfishes.

Log-transformed latent larval abundances and standardized observed catches are shown in Fig. 4.5. In general, latent abundances were lower and more uniform than observed catches. Taxa with small sample sizes had the widest uncertainty intervals (Table 1.2, Fig. 4.6). Thus, although the model with only geographic covariates best described sablefish abundances, neither latitude nor distance from shore were strong predictors.

Discussion

This study used hierarchical modeling to examine environmental drivers of the abundance of primarily five taxa of larval fish in the Eastern Pacific. We found that oceanographic conditions (rather than geography, ENSO-related predictors, or all predictors) best predicted larval abundances across a diverse set of taxa. In particular, sea surface height emerged as a strong predictive variable. Sea surface height is a proxy for El Niño Southern Oscillation (ENSO) events, which lead to a "pile" of warm water in the Eastern Pacific. While sea surface temperature is an obvious related factor in ENSO events, sea surface height also appears to be correlated with decreased upwelling and stronger northward currents (Chelton et al. 1982; Kruse and Huyer 1983). Most of our five cast-study taxa had higher abundances in lower sea

surface heights. Our results support past work showing that both sablefish and rockfishes were associated with lower sea surface heights (Schirripa and Colbert 2006; Laidig et al. 2007; Ralston et al. 2013). Pacific sanddab was the only species that showed higher abundances in both higher sea surface heights and higher temperatures. High recruitment years for Pacific sanddab have previously been recorded throughout the California Current in pre-ENSO and marine heatwave conditions, possibly aided by high primary productivity as indicated by increased body condition in warm years, or larval transport over the shelf (Keller et al. 2013; Leising et al. 2014; Thompson et al. 2022). In turn, sanddab declines have been recorded following strong ENSO events, such as in 2016 (McClatchie et al. 2016). However, given past studies, the biological connection between sea surface height and abundance for other species is less clear. For instance, California sheephead larvae were historically thought to be advected northward from Mexico to southern California during ENSO events (Cowen 1985), but more recent work has countered this, finding no link between recruitment levels in southern California and ENSO for California sheephead (Selkoe et al. 2007). Output from our model demonstrates a different trend altogether, in which California sheephead larvae are more abundant in southern California in lower sea surface heights.

Sea surface temperature variations are frequently associated with ENSO/La Niña conditions. However, for species other than Pacific sanddabs, sea surface temperature was not a strong predictor of larval abundance. Despite the known effects of temperature on larval physiology and behavior (e.g., Rombough 1997; Hunt von

Herbing 2002), it appears that other changes related to regime shifts (such as prey availability or downwelling/upwelling) may be driving abundance fluctuations. For instance, rockfish recruitment is higher in cooler, fresher waters with higher oxygen concentrations (Schroeder et al. 2019). Although we did not find temperature to be a predictor of rockfish abundance, model output confirmed that rockfish larvae are more common in fresher waters with more dissolved oxygen.

Interestingly, geographic covariates of distance from shore and latitude were not important predictors for any fish. This may be due to the relatively constrained latitudinal range of most species and the strong associations with coastal or shelf habitats. It may also be due to a lack of data at offshore stations, which have been less frequently sampled over the course of the CalCOFI program. Bayesian methods are good at accounting for missing data or smaller datasets, and even with a small number of records. However, explanatory power was influenced by sample size (Fig. 4.6). Posterior uncertainty intervals were large for sablefish and California sheephead, which had the fewest positive stations and lowest number of overall tows. This indicates that this model may be most useful in examining populations at smaller spatial scales. Despite this, model output supports our current knowledge of the taxa examined. It also reinforces past work completed by Statchura et al. (2014), who used hierarchical modeling to examine environmental drivers of recruitment synchrony across the entire northeastern Pacific. That study found that sea surface height emerged as a major predictor of recruitment; however, they recognized that autocorrelation was not accounted for due to computational limitations. Our current

study incorporates spatial autocorrelation, which led to a more uniform larval distribution over the sampling area. Ichthyoplankton surveys have spatial heterogeneity and sampling error not typically corrected for (Hsieh et al. 2005); our model overcomes this obstacle.

One area for future application is examining interannual variations in larval abundance. Asch (2015) showed that a large percentage of offshore species fish species were advancing the timing of spawning while coastal species were delaying spawning. Stachura et al. (2014) did not find strong links between habitat groups in terms of the timing of spawning or other reproductive events. Adding a temporal component across years or seasons, along with appropriate corrections for temporal autocorrelation, is an important future direction.

Developing predictive frameworks, integrating multiple stressors, and examining effects of natural oscillations and anthropogenic climate change in a spatial context has been cited as an important area for early life history research (Llopiz et al. 2014). Our study examined how environmental covariates influence larval distributions over time, as well as provides estimates of larval abundance and environmental covariate coefficients at defined spatial locations. Past papers have highlighted the need for using long-term data to examine ecological and evolutionary trends in larval fishes (Llopiz et al. 2014); this work makes use of the extensive resource that is the CalCOFI dataset and provides support for the continued value of this long-term sampling program.

Acknowledgements

Thank you to C. Wilmers and P. Mattern for advice on model design, Bayesian statistical techniques, and RStan implementation. Funding was provided to KED through an Achievement Rewards for College Scientists (ARCS) Foundation fellowship and NMFS/Sea Grant Population and Ecosystem Dynamics Graduate Fellowship Award #NA20OAR4170467.

Tables & Figures

Taxon	Scientific name	Predictive model (highest ELPD)	Number of tows in study area	% tows with positive catches	Adult habitat
All fish larvae	–	Oceanographic environment	10,975		Various
Cabezon	*Scorpaenichthys marmoratus*	Oceanographic environment	9239		Nearshore, benthic
California sheephead	*Semicossyphus pulcher*	Oceanographic environment	6199		Nearshore, canopy
Pacific sanddab	*Citharichthys sordidus*	ENSO	10,312		Shelf/slope, benthic
Rockfishes	*Sebastes* spp.	Oceanographic environment	10,851		Various
Sablefish	*Anoplopoma fimbria*	Geography	5591		Shelf/slope

Table 1.1. Predictive models for each species, along with the number of tows with environmental data in the study area.

Taxon	Variable	Mean	Sd	2.5%	25%	75%	97.5%	N_{eff}	
All larvae	Sea surface temperature	0.03	0.01	0.02	0.03	0.03	0.04	1875.12	*
All larvae	Salinity	0.02	0.01	0.00	0.01	0.02	0.04	3022.85	
All larvae	Sea surface height	-0.13	0.01	-0.14	-0.13	-0.12	-0.11	3643.95	*
All larvae	Dissolved oxygen	0.12	0.01	0.10	0.12	0.13	0.14	3082.49	*
Cabezon	Sea surface temperature	-0.02	0.06	-0.13	-0.06	0.02	0.10	2617.68	
Cabezon	Salinity	0.18	0.05	0.07	0.14	0.21	0.27	3156.48	*
Cabezon	Sea surface height	-0.45	0.08	-0.62	-0.51	-0.39	-0.29	2851.80	*
Cabezon	Dissolved oxygen	0.05	0.04	-0.04	0.02	0.08	0.13	3065.55	
California sheephead	Sea surface temperature	0.09	0.16	-0.23	-0.02	0.20	0.41	1475.34	
California sheephead	Salinity	0.51	0.24	0.00	0.35	0.67	0.97	1433.23	
California sheephead	Sea surface height	-0.44	0.22	-0.89	-0.60	-0.28	-0.02	2563.02	*
California sheephead	Dissolved oxygen	-0.06	0.14	-0.32	-0.16	0.03	0.23	1904.25	
Pacific sanddab	Sea surface height	0.10	0.04	0.02	0.08	0.13	0.18	3060.14	*
Pacific sanddab	Sea surface temperature	0.07	0.03	0.01	0.05	0.09	0.13	3410.79	*
Rockfishes	Sea surface temperature	-0.03	0.02	-0.06	-0.04	-0.02	0.00	4093.68	
Rockfishes	Salinity	0.05	0.01	0.03	0.04	0.06	0.08	4989.81	*
Rockfishes	Sea surface height	-0.16	0.02	-0.19	-0.17	-0.15	-0.13	4914.39	*
Rockfishes	Dissolved oxygen	0.11	0.02	0.08	0.10	0.12	0.14	5484.94	*
Sablefish	Latitude	0.13	0.15	-0.05	0.02	0.21	0.49	260.07	
Sablefish	Distance from shore	0.04	0.42	-0.78	-0.24	0.30	0.91	980.90	

Table 1.2 Posterior distributions for the best-performing model for each taxon. Asterixes indicate covariates whose 2.5-97.5 percentiles do not include zero, and thus could be considered important predictors of larval abundance.

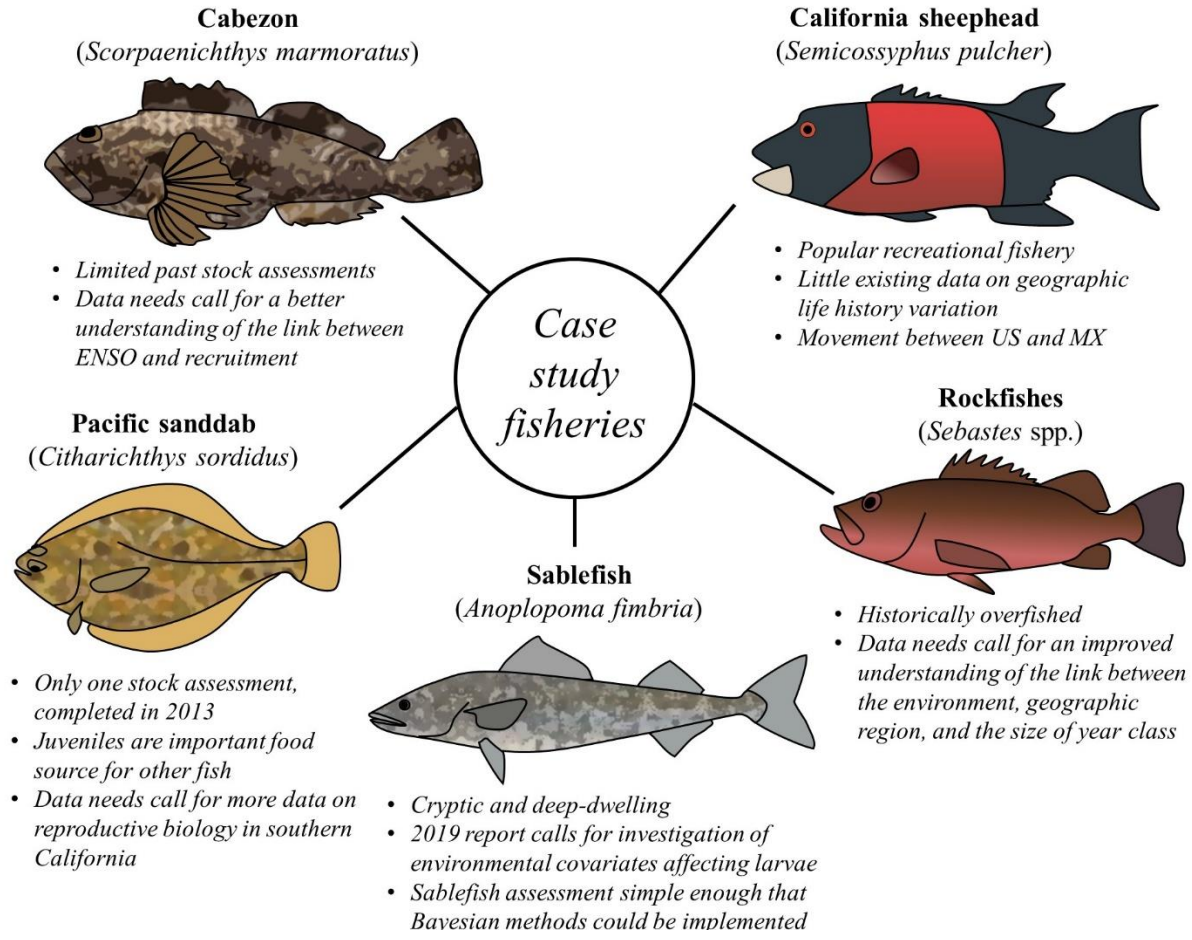

Figure 4.1. Illustration of the five case-study fisheries, listed with importance and knowledge gaps. This set of five species represent a diverse array of life histories, reproductive strategies, and adult habitats, and are all data-moderate, cryptic, threatened, or underassessed.

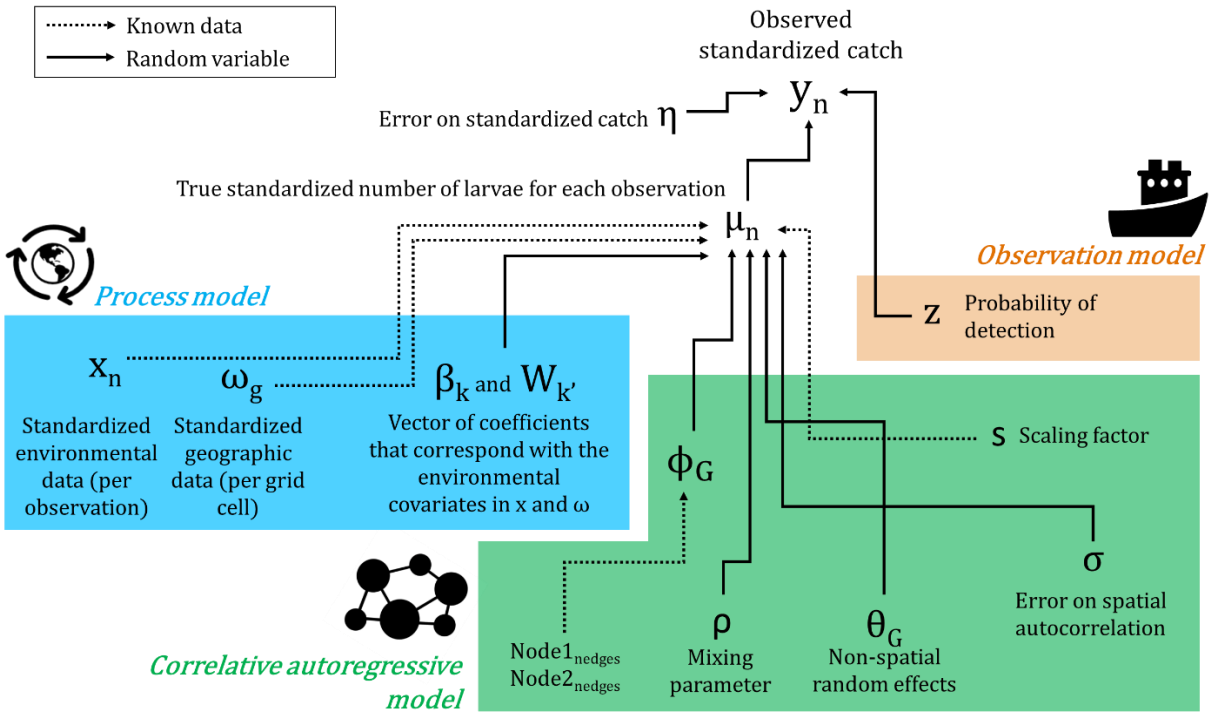

Figure 4.2 Bayesian directed acyclic graph (DAG) showing three-part model structure.

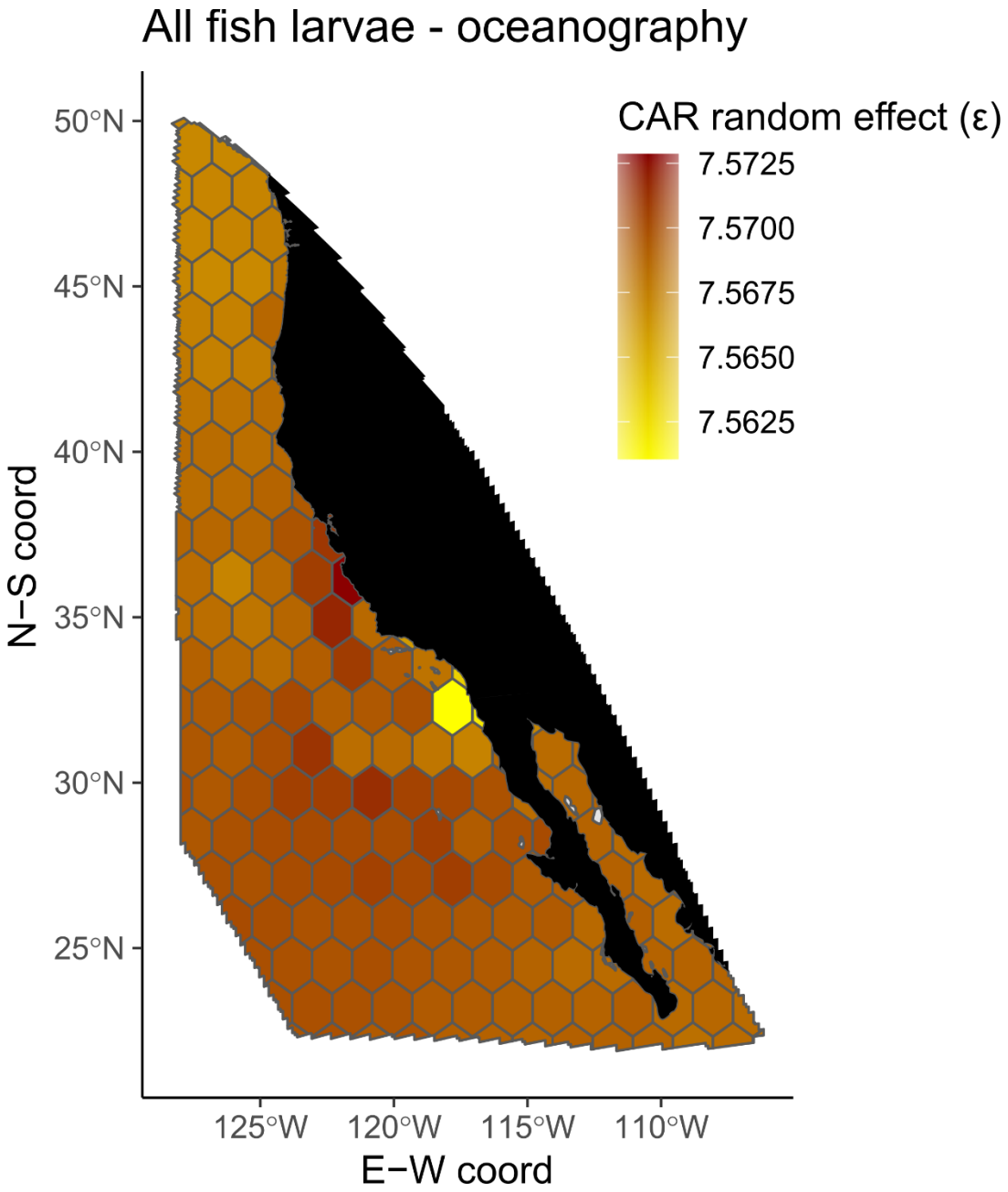

Figure 4.3 CAR model net random effect (ε), for all fish larvae, model 3 (oceanography). CAR random effect output for remaining models is similar to this example.

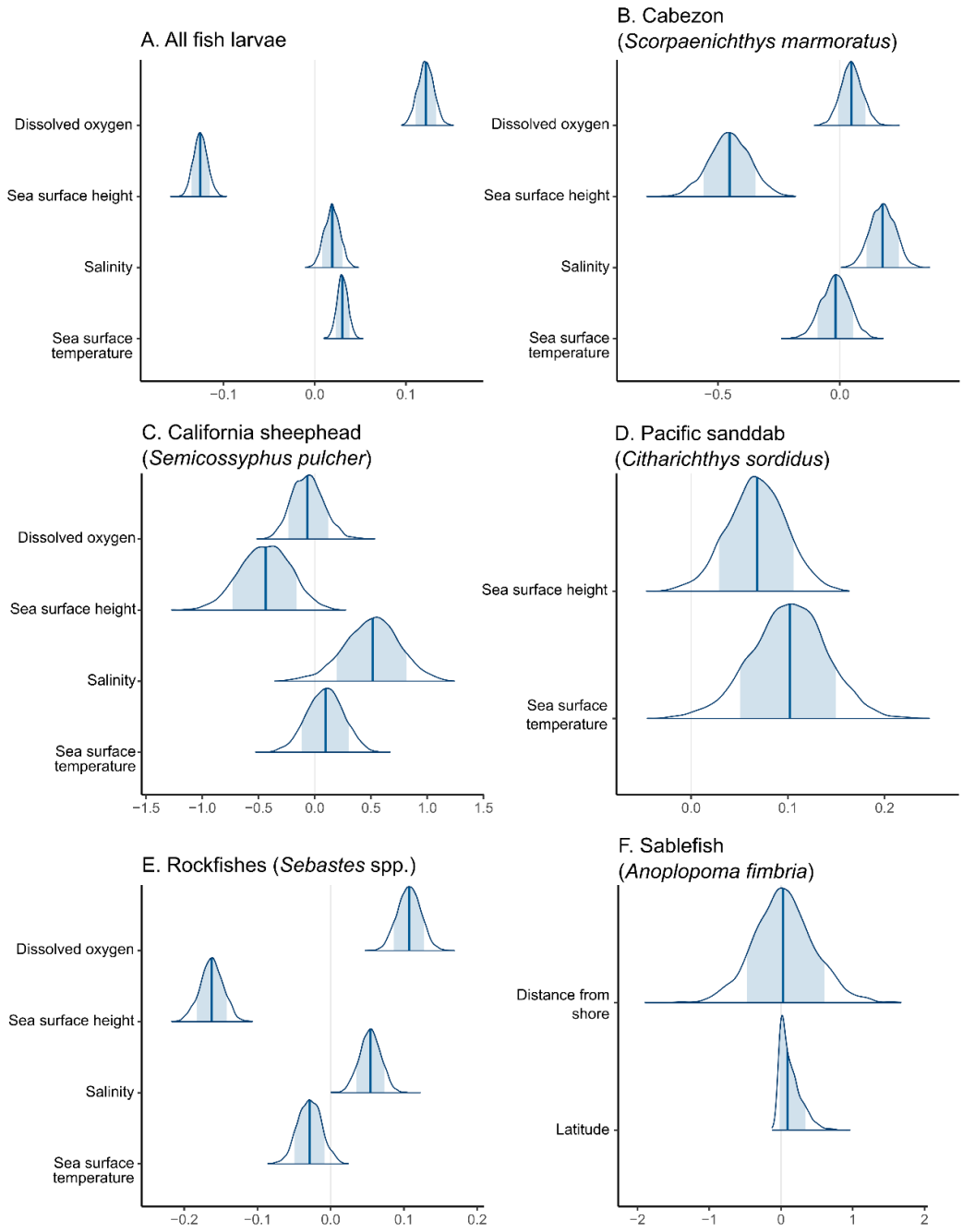

Figure 4.4 Posterior distributions for all larval fish (A) and the five case-study species (B-F). Results are shown only for the best-fitting model (see Table 1.1).

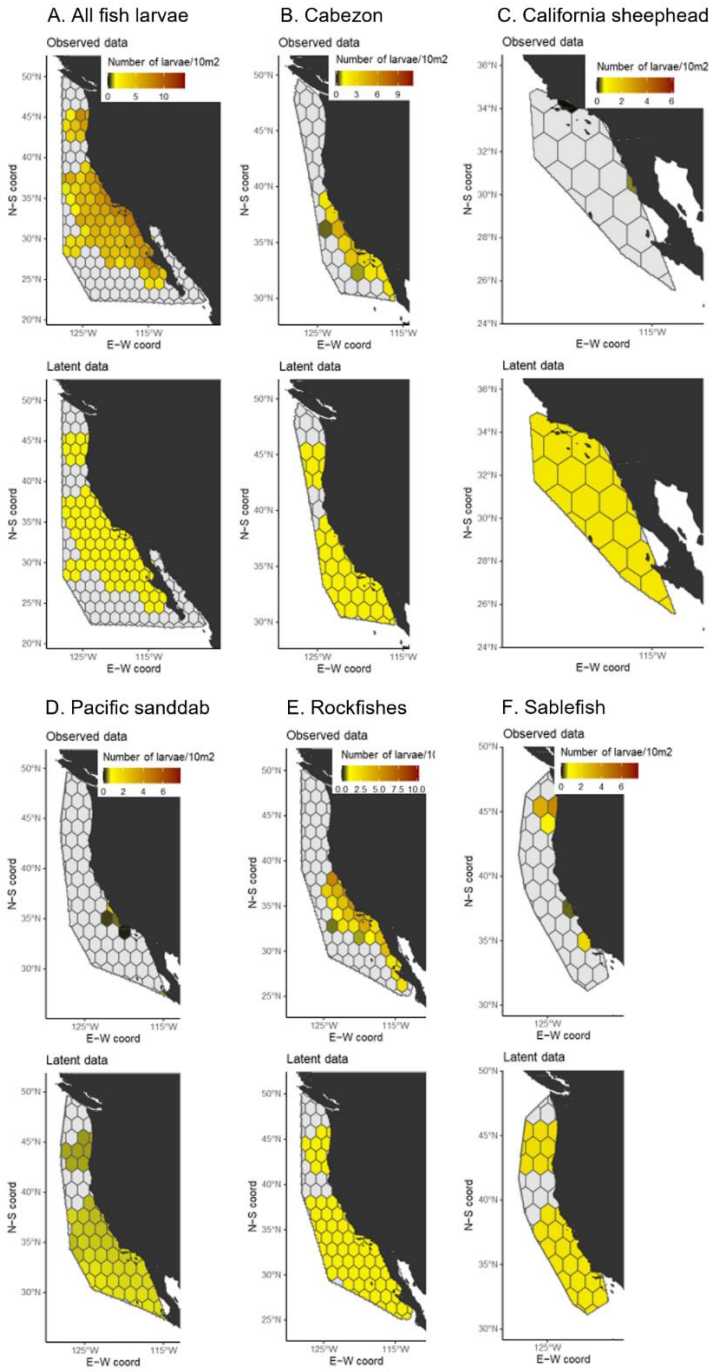

Figure 4.5 Observed and latent log-transformed larval abundances for all larvae (A) and five case study species (B-F). Model output predicts a more uniform and generally lower distribution of fish larvae than observed data.

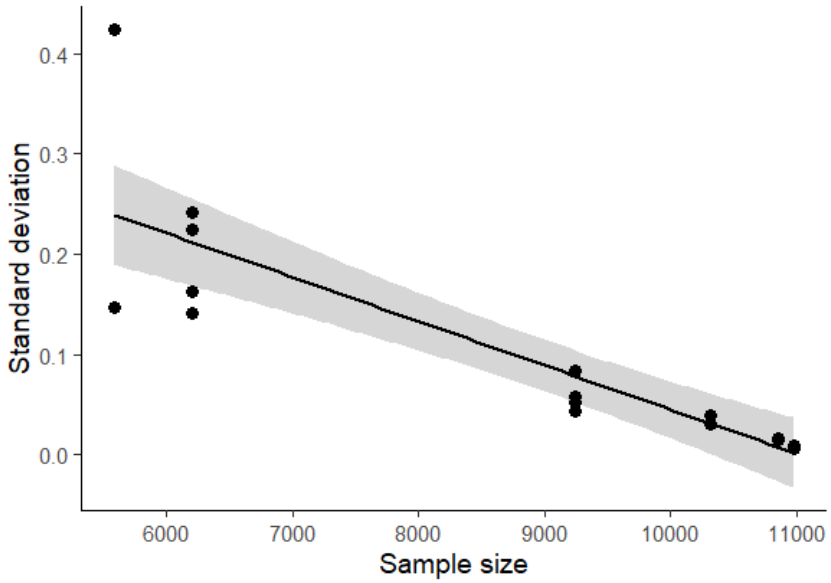

Figure 4.6 Standard deviations on posterior distributions decreased as sample sizes increased. R^2 adj. = 0.74, $p < 0.001$.

Stan code

Stan program

```
// Custom functions-------------------------------------------------
---------
functions {
  real hurdle_gamma_lpdf(real y, real alpha, real beta, real hu) {
    if (y == 0) {
      return bernoulli_lpmf(1 | hu);
    } else {
      return bernoulli_lpmf(0 | hu) +
      gamma_lpdf(y | alpha, beta);
    }
  }
}


// Data ------------------------------------------------------------
---------
data {
  int Nobs;                              // number observations (plank
ton tows)
  int N;                                 // number grid cells
  int<lower=0> N_edges;                  // number of "edges" (grid ce
ll boundaries)"
  int<lower=1, upper=N> node1[N_edges];// node1[i] adjacent to node2
```

```
[i]
  int<lower=1, upper=N> node2[N_edges];// and node1[i] < node2[i]
  int<lower=1> K;                      // number covariates
  matrix[Nobs,K] X;                    // covariate matrix
  vector[Nobs] Y;                      // observed variable: Standar
dized larvae count
  int<lower=1> G[Nobs];                // grid cell index for each o
bservation
  real<lower=0> scaling_factor;        // scales the variance of the
spatial effects
  int<lower=0> Nzeros;
}

// Transformed data ------------------------------------------------
---------
transformed data {
  real<lower=0> mean_y;
  real<lower=0> sd_y;

  mean_y = mean(to_vector(Y));
  sd_y = sd(to_vector(Y));
}

// The parameters accepted by the model----------------------------
```

```
parameters {
  real beta0;                              // intercept
  vector[K] betas;                         // covariates
  real<lower = 0> sigma;                   // std dev of mean expected
value (positive)
  real<lower=0,upper=1> rho;               // spatial autocorrelation
coefficient
  vector[N] theta;                         // heterogeneous random eff
ects
  vector[N] phi;                           // spatially autocorrelated
random effects
  real<lower=0,upper=1> detect;            // probability of detection
(0 to 1)
  real<lower=0> eta;                       // error on gamma (positive
)
}

// Transformed parameters-------------------------------------------
---------
transformed parameters {
  vector[N] eps;               // convolved random effect for each g
rid cell
  vector[Nobs] mu;             // mean number of larvae
```

```
  mu  = beta0 + X * betas;     // fixed-effects on larval abundance


  for (n in 1:N) {
    eps[n] = (sqrt(1 - rho) * theta[n] + sqrt(rho / scaling_factor)
* phi[n]) * sigma;
  }
}


// The model to be estimated----------------------------------------
---------
model {


  real alpha;
  real beta;


    for (n in 1:Nobs) {
      alpha = exp((mu[n] + eps[G[n]]))^2/eta^2; // moment matching
      beta = exp((mu[n] + eps[G[n]]))/eta^2;    // moment matching

      // gamma hurdle model
      target += hurdle_gamma_lpdf(Y[n] | alpha, beta, detect);

      }
```

```
    // Priors:
    target += -0.5 * dot_self(phi[node1] - phi[node2]); // prior for
phi
    beta0 ~ normal(0.0, 1.0);
    betas ~ normal(0.0, 1.0);
    theta ~ normal(0.0, 1.0);
    sigma ~ normal(0.0, 1.0);
    rho ~ beta(0.5, 0.5);
    detect ~ beta(0.5, 0.5);    // probability of detection, between
0 and 1
    eta ~ gamma(0.01,0.01);     // gamma error - always positive

    // soft sum-to-zero constraint on phi)

    // equivalent to mean(phi) ~ normal(0,0.001)
    sum(phi) ~ normal(0, 0.001 * N);

}
// Generated quantities-----------------------------------------
---------
generated quantities {
  vector[Nobs] log_lik;
  real y_rep[Nobs];
  real alpha;
```

```
  real beta;
  real<lower=0> mean_y_rep;
  real<lower=0> sd_y_rep;
  int<lower=0, upper=1> mean_gte;
  int<lower=0, upper=1> sd_gte;
  int<lower=0, upper=1> mean_gt;  // will have value 1 if the mean o
f the simulated data y_rep is >= the mean of Y
  int<lower=0, upper=1> sd_gt;


  for (n in 1:Nobs) {
      alpha = exp((mu[n] + eps[G[n]]))^2/eta^2; // moment matching
      beta = exp((mu[n] + eps[G[n]]))/eta^2;    // moment matching


    y_rep[n] = gamma_rng(alpha, beta) * bernoulli_rng(detect) ; // m
ay need to be edited?
    log_lik[n] = hurdle_gamma_lpdf(Y[n] | alpha, beta, detect); // l
og-likelihood for LOO
  }
  mean_y_rep = mean(to_vector(y_rep));
  sd_y_rep = sd(to_vector(y_rep));
  mean_gte = (mean_y_rep >= mean_y);
  sd_gte = (sd_y_rep >= sd_y);
  mean_gt = mean_y_rep > mean_y;
```

```
  sd_gt = sd_y_rep > sd_y;


}
```

Dashboard code

Load libraries, set working directory, optimize system

```
library(sp, quietly = TRUE)

library(sf, quietly = TRUE)

library(rstan, quietly = TRUE)

library(cmdstanr, quietly = TRUE)

library(posterior, quietly = TRUE)

library(loo)


library(parallel, quietly = TRUE)

library(tmap, quietly = TRUE)

library(plyr, quietly = TRUE)

library(dplyr, quietly = TRUE)

library(bayesplot, quietly = TRUE)


setwd("C://KDale/Projects/Bayesian Modeling/LarvalDispersal/")


# Run on multiple cores

options(mc.cores = parallel::detectCores())


# Automatically save a bare version of a compiled Stan program to th

e hard disk so that it does not need to be recompiled (unless you ch

ange it)
```

```
rstan_options(auto_write = FALSE)


options(mc.cores = parallel::detectCores())

install_cmdstan(cores = 2, overwrite = FALSE)

check_cmdstan_toolchain(fix = TRUE)
```

Define study area and create hex grid

```
# Load land shapefiles

spatialGridCreation <- function(data) {


northSouthAmerica <- st_read("Shapefiles/North_South_America.shp") %
>%
  st_union() %>% st_make_valid()


# Convert to multipoint, and get positive stations for convex hull

stations.sf <- st_as_sf(data, coords = c("longitude", "latitude"), c
rs = 4326)

stations <- st_cast(stations.sf, to = "MULTIPOINT") %>% st_combine(.
)

stations.positive <- subset(stations.sf, larvae_count>0) %>% st_cast
(., to = "MULTIPOINT") %>% st_combine(.)


# Create study area polygon (convex hull around positive tows)

studyArea <- st_convex_hull(stations.positive) %>% st_buffer(., dist
```

```
= 1000, singleSide = FALSE)


# Create hexagonal grid
hex <- st_make_grid(studyArea, crs = 4326, cellsize = 1.5, what = "p
olygons", square = FALSE) %>% st_make_valid() %>% st_difference(., n
orthSouthAmerica) %>% st_intersection(., studyArea)


# Add grid ID to stations
hex.sf = st_sf(hex) %>% mutate(., GridID = 1:length(hex))
stations.sf$distance_from_shore <- st_distance(stations.sf, northSou
thAmerica, by_element = TRUE) %>% scale()
stations.hex <- st_join(stations.sf, hex.sf)


return(list(hex.sf, stations.sf))
}
```

Setup Stan data

```
setupdata <- function(modelName) {


  ## Get data for Stan
  neighbors <- poly2nb(pl = hex.sf) # produces a list of neighbors f
or each hex
  source("nb2graph.R")
  grid <- nb2graph(neighbors)
```

```
  nCells <- grid$N # Number of grid cells
  nEdges <- grid$N_edges # Number of edges
  node1 <- grid$node1 # Node 1 of edges
  node2 <- grid$node2 # Node 2 of edges

  adjacency = nb2mat(neighbors, zero.policy = TRUE) # adjacency, sca
led by number of neighboring cells
  adjacency_identity = ceiling(adjacency)
  identity = diag(nCells)                       # Identity matrix
  sharedEdges = colSums(adjacency_identity)    # number shared edges
per cell
  rho = 0.95  # estimated value of rho for calculating scaling facto
r

  InvM = solve(identity-rho*adjacency)
  # Compute the geometric mean of the variances, on the diagonal of
Cov matrix; use this to calculate scaling factor for BYM2 model
  scaling_factor = exp(mean(log(diag(InvM))))

  # Number of total observations
  nObs = nrow(data)
  # Independent (predictor) variables for fixed effects
  if (modelName == "geography") {
```

```
    X = cbind(data$lat_standardized - mean(data$lat_standardized),
              data$distance_from_shore[,1])
    colnames(X) = c("latitude", "distance_from_shore")
  } else if (modelName == "enso") {
    X = cbind(data$meanTemp_standardized,
              data$meanDynamicHeight_standardized)
    colnames(X) = c("temperature", "dynamic_height")
  } else if (modelName == "oceanography") {
    X = cbind(data$meanTemp_standardized,
              data$meanSalinity_standardized,
              data$meanDynamicHeight_standardized,
              data$meanO2_standardized)
    colnames(X) = c("temperature", "salinity", "dynamic_height", "O2
")
  } else if (modelName == "allvars") {
    X = cbind(data$lat_standardized - mean(data$lat_standardized),
              data$meanTemp_standardized,
              data$meanSalinity_standardized,
              data$meanDynamicHeight_standardized,
              data$meanO2_standardized,
              data$distance_from_shore[,1])
    colnames(X) = c("latitude", "temperature", "salinity", "dynamic_
height", "O2", "distance_from_shore")
  }
```

```
K = ncol(X) # Number of predictor variables
G = data$GridID # Grid cell ID of each observation
W = cbind(data$ship_factor,
          data$net_type_factor,
          data$tow_type_factor)
K_obs = ncol(W)
Nzeros = length(subset(data, data$Y==0))
isnotzero = ifelse(data$Y==0,0,1)

# Define data
stan.data <-
  list(
    Nobs = nObs,
    N = nCells,
    N_edges = nEdges,
    node1 = node1,
    node2 = node2,
    K = K,
    X = X,
    Y = data$Y,
    G = G,
    scaling_factor = scaling_factor,
    Nzeros = Nzeros
```

```
    )
  return(stan.data)
}
```

Execute model

```
cmdstanrModel <- function(stan.data) {


  cores = detectCores()
  nc = min(20,cores-1)


  # Compile
  CAR_mod <- cmdstan_model(stan_file = "Models/CAR_modBYM2_gammaHurd
le.stan")


  # Run model
  fit <- CAR_mod$sample(
    data = stan.data,
    seed = 123,
    chains = 3,
    parallel_chains = 3,
    refresh = 50,
    adapt_delta = 0.9
  )
```

```
  fit$save_object(file = "fit.RDS")


  return(fit)


}
```

Import data and run models

```
files = list.files(path = "C://KDale/Projects/Bayesian Modeling/CalC
OFI_data/SpeciesCounts")
resultFiles <- list.files("Results/")
modelNames = c("geography", "enso", "oceanography","allvars")


for (i in 1:6) {


  ## Import data---------
  data = read.csv(file = paste0("C://KDale/Projects/Bayesian Modelin
g/CalCOFI_data/SpeciesCounts/", files[i]))


  species = strsplit(files[i], "_hydros.csv")[[1]]


  spatialSets <- spatialGridCreation(data) # Create hex grid


  hex.sf <- spatialSets[[1]]
  data <- spatialSets[[2]]
```

```
  # Remove stations without environmental data and those that are ou
tside the study area
  data <- subset(data, !is.na(data$meanTemp_standardized)& !is.na(me
anO2_standardized) & !is.na(meanDensity_standardized) & !is.na(meanS
alinity_standardized) & !is.na(meanDynamicHeight_standardized) & !is
.na(distance_from_shore))
  data <- subset(data, !is.na(GridID))

  # Standardize larval counts using % of sample sorted and standard
haul factor
  data$Y = data$larvae_count/(data$percent_sorted * data$standard_ha
ul_factor)

  for (j in 1:length(modelNames)) {

    modelName = modelNames[j]
    stan.data <- setupdata(modelName = modelNames[j])

    # Fit model
    fit <- cmdstanrModel(stan.data)

    # Evaluate model
    fitStan <- rstan::read_stan_csv(fit$output_files())
```

```
    sumstats = summary(fitStan)$summary


    mcmc2 <- as.matrix(fitStan)

    param.post.names = colnames(mcmc2)

    Nsims = nrow(mcmc2)


    loo <- fit$loo(variables = "log_lik", r_eff = TRUE)


    save(fitStan,mcmc2,param.post.names,sumstats,loo,file=paste0("Re
sults/",species,"_",modelNames[j],".rdata"))
  }
}
```

Conclusions & Future Directions

In this dissertation, I aimed to elucidate factors that affect fish dispersal, abundance, individual survival, and population persistence in the northeastern Pacific. I used a diverse array of lenses to examine these themes, including hierarchical modeling, morphology, genetics, and coloration.

Chapter 1 began by showing that morphology predicts dispersal distance. Specifically, morphological traits of intermediate-stage larvae predicted larval latitudinal range, as anguilliform leptocephali with larger relative predorsal body lengths and snout-to-anus lengths exhibited larger larval ranges. Surprisingly, body aspect ratio and maximum body length at transformation, two traits we initially hypothesized to be important, were not significant predictors of dispersal range. It appears that there may be a potential relationship between longer relative anterior body segments and improved swimming ability, where more elongate body parts may improve undulatory/anguilliform swimming ability by reducing drag and increasing body propulsion. Both offshore and coastal species with longer predorsal body lengths and snout-to-anus lengths had larger ranges, demonstrating that both offshore and coastal species conduct active larval movement to adult habitats. My work indicates that eel larvae do not appear to use body shape to enhance or impede passive transport; instead, morphology may be involved with active swimming. A future area of work could be examining the link between morphology and geographic range of other fish families or expanding this dataset to include anguilliform larvae from other basins, such as the NE Atlantic.

My work in Chapter 1 revealed that body shape might contribute to the large geographic ranges of Eastern Pacific leptocephali. Despite the potential for long-distance dispersal of Eastern Pacific muraenid larvae, the California moray is the only muraenid off southern California. The long-standing hypothesis has been that California morays in southern California are non-reproductive, with water temperature limiting gonadal development (McCleneghan 1973). This in turn would make southern California populations primarily recipient populations, though it was unclear where larvae may be arriving from. After examining larval dispersal in Chapter 1, I wanted to further examine population connectivity and evidence of local reproduction in California morays. **Chapter 2** revealed that while California morays have high gene flow, they are experiencing local adaptation on a small subset of loci. Though source populations are difficult to identify, a large proportion of hybrids in populations such as Catalina Island (Two Harbors) support the long-standing hypothesis that eels on the north side of Catalina Island are minimally reproductive and comprised mainly of first-generation hybrids. However, it remains unclear where propagules are arriving from, and the mechanisms behind successful spawning. Based on larval occurrence data, the presumed function of genes under selection, and correlations between environmental conditions at settlement and genetic diversity, , it appears that natural selection is strongest during the late larval or early juvenile period. Future work should continue to examine gene functions in teleosts, and particularly in eels. Additional areas of work include aging Baja California individuals and building population-specific growth curves; sequencing more of the

genome to quantify intrapopulation migration rates; sequencing additional individuals from below the Bahía Magdalena biogeographic break; and making efforts to sample for leptocephali, especially in southern California.

Chapters 1 and 2 examined factors related to larval dispersal and selective pressures during this early life history period. Chapter 3 also showed that California morays appear to be under different selective pressures in different parts of their range, even between locations that are geographically close. In **Chapter 3**, I further narrowed my geographic focus to Catalina Island, and found that the coloration of morays around the island is correlated with their habitats, a surprising trend for a temperate, cryptic fish that cannot rapidly change color. Eels were lighter and yellower in sandy, turbid habitats. It does not appear that coloration improves foraging success or adult survival, and eels do not appear to self-select their habitat when they are adults. Instead, similar to Chapter 2, we hypothesize that selection is primarily occurring during the early juvenile stage. Future work should focus on catching and quantifying coloration of early settlement and juvenile individuals, which our traps do not catch, as we hypothesize that either juveniles are either changing color during settlement or being predated upon if they have less-adaptive camouflage. It would be especially exciting to examine the function of loci under selection from Chapter 2 and find genes related to pigmentation or coloration.

After examining eels for the first three chapters, I was interested in broadening my focus to additional taxa while continuing to think about the effect of environmental factors on larval abundance. **Chapter 4** showed that the environmental

covariates that best describe larval abundance in California Current region vary across species, but that sea surface height was a strong predictor of larval abundance. In general, model results support what we know about the biology of the case-study taxa in question, better account for spatial autocorrelation, and provide interpretable output on larval abundance at specific spatial points. We hope to incorporate biological aspects of larvae (such as body shape, stemming from Chapter 1) in the future.

My conclusions suggest that previously-overlooked characteristics of fishes, such as larval body shape and the coloration of predators, may play a role in determining the geographic ranges and individual survival of Eastern Pacific Anguilliformes, and are worth additional study in other fishes. Although swimming ability is incorporated into some dispersal models, variation in swimming ability is not usually allowed for, much less variation based on body shape. We also have new insights into the lives of California morays. It appears that strong selection is occurring for California morays during their early life stage, either during the larval period of shortly thereafter. Intrinsic factors such as body shape, development, coloration, and swimming ability interact with environmental conditions appear to select for individuals of certain genotypes.

Chapter 4 showed that underutilized or novel tools, such as hierarchical models accounting for spatial autocorrelation, can provide new (and complementary) insights to what we know about the biology of species. Most modeling efforts are based around frequentist methods, R packages that aim to be as user-friendly as

possible, or point-and-click software that either has steep learning curves or a lack of flexibility. Although learning Bayesian statistics can be a hurdle, the amount of control that comes from writing one's own model is worth it.

My overarching research goal is to understand the mechanisms influencing the dispersal, biogeography, and ecology of fishes. Over the course of my PhD, I have worked towards answering questions related to these themes by learning and using a diverse set of quantitative tools, including morphology, genetics, phylogenetics, and statistical modeling. I am excited to continue to add to my toolbox in my next career step!

Appendix

Table S2.1. Summary of environmental covariate analysis. Environmental variables were used as predictors, and the first two axes from the DAPC analyses (without Todos Santos) were used as the response. Sea surface temperature anomaly was analyzed using a generalized additive model (GAM); degrees of freedom reported for the GAM are effective degrees of freedom.

Response variable	**Predictor variable**	**P**	**R^2 adj.**	**Slope**	**Df**	**Std err**
DAPC axis 1	Sea surface height	0.74	0.00	8.3	185	25.5
DAPC axis 2	Sea surface height	<0.001	0.18	-70.8	185	11.2
DAPC axis 1	Sea surface temperature	0.06	0.02	-1.02	217	0.55
DAPC axis 2	Sea surface temperature	<0.001	0.24	-1.91	217	0.23
DAPC axis 1	Sea surface temperature anomaly	0.42	0.003	--	1.9	--
DAPC axis 2	Sea surface temperature anomaly	0.004	0.05	--	2.0	--
DAPC axis 1	Magnitude of Ekman transport	<0.001	0.27	0.04	111	0.005
DAPC axis 2	Magnitude of Ekman transport	<0.001	0.09	0.01	111	0.002

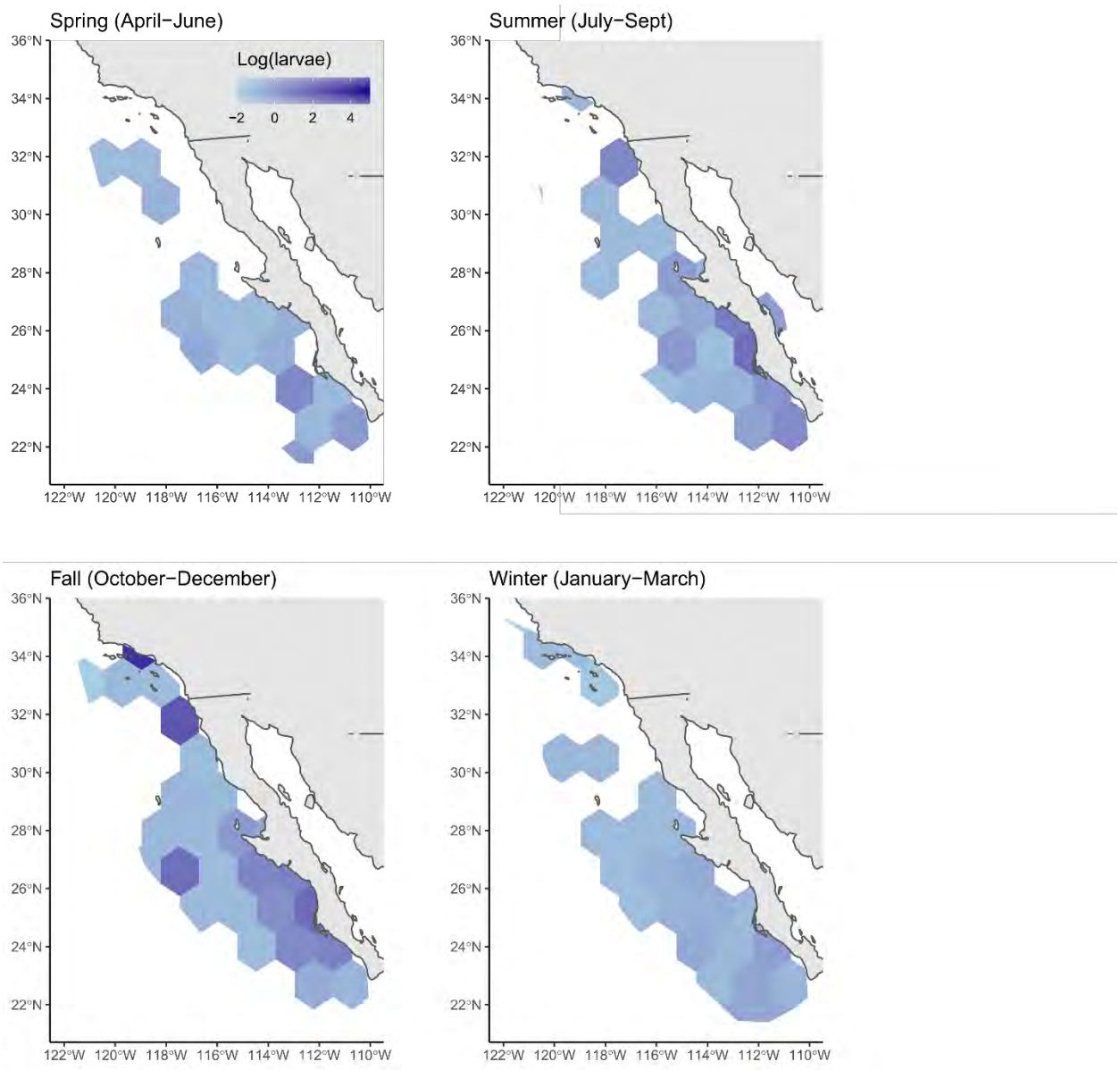

Figure S2.1. Heatmap of standardized larval counts for all unidentified Anguilliformes and muraenid larvae from, taken from the California Cooperative Oceanic Fisheries Investigation (1951-2021) and Investigaciones Mexicanas de la Corriente de California (1990-2020).

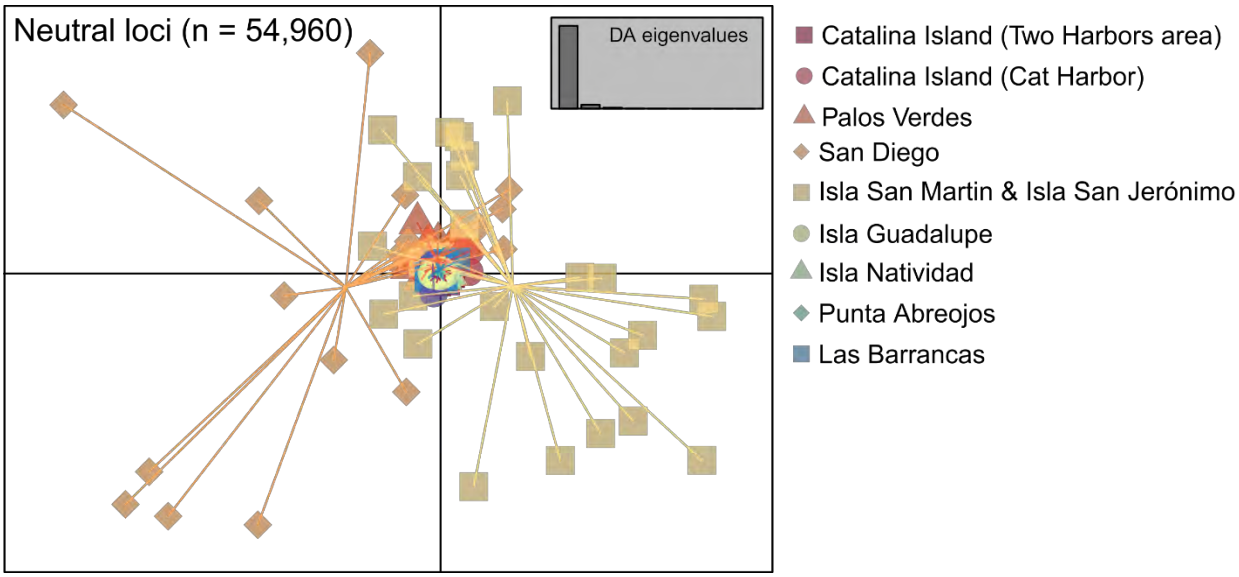

Figure S2.2. DAPC results for neutral loci (n = 54,960).

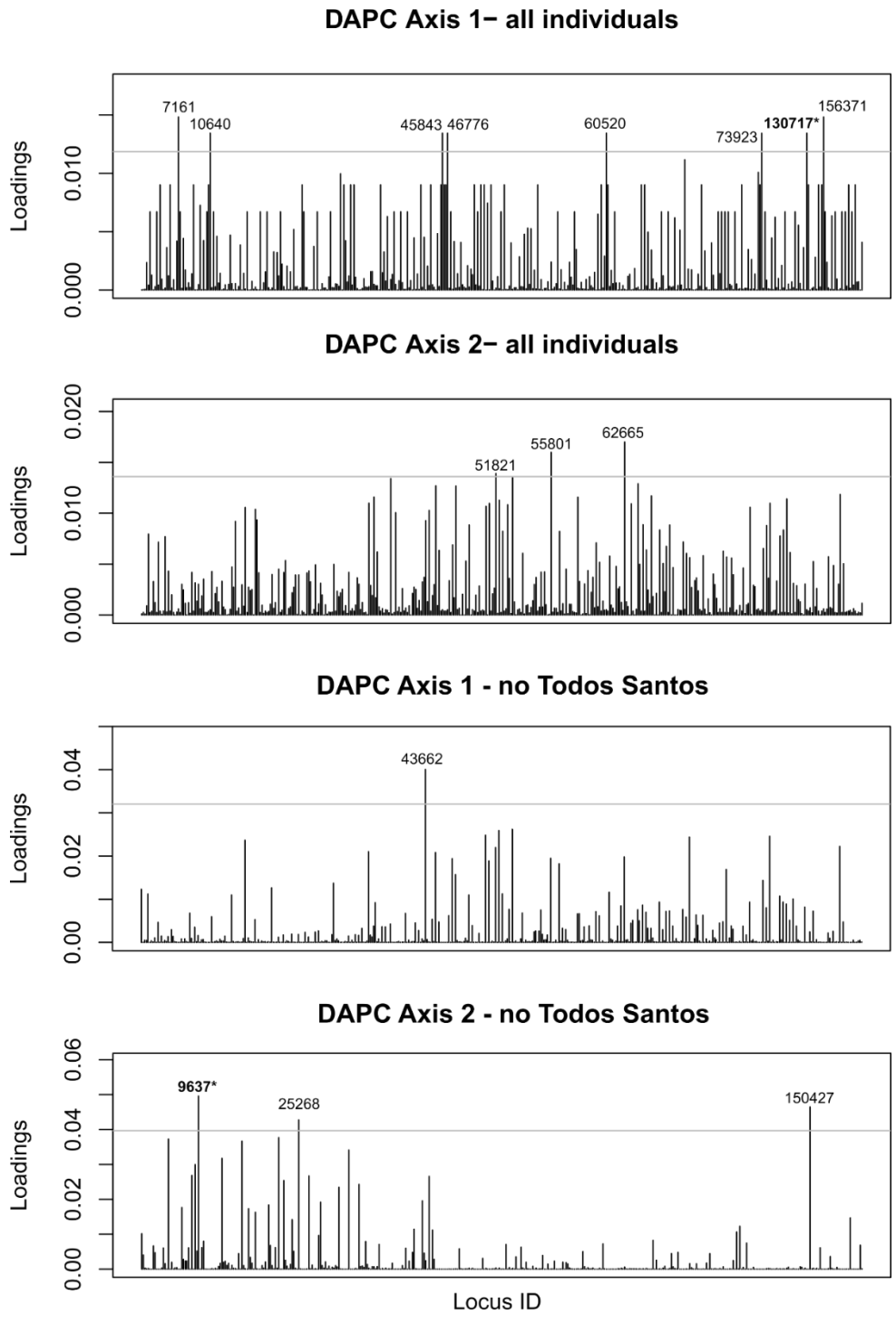
DAPC Axis 1− all individuals
Loadings
0.000
0.010
7161
10640
45843
46776
60520
73923
130717*
156371
DAPC Axis 2− all individuals
Loadings
0.000
0.010
0.020
51821
55801
62665
DAPC Axis 1 - no Todos Santos
Loadings
0.00
0.02
0.04
43662
DAPC Axis 2 - no Todos Santos
Loadings
0.00
0.02
0.04
0.06
9637*
25268
150427
Locus ID

Figure S2.3. Labeled loci are those that fell in the 80th percentile for variance explained along each DAPC axis. All plots are for DAPCs on loci under selection. Loci that are in bold had significant matches with annotated genes in BLAST.

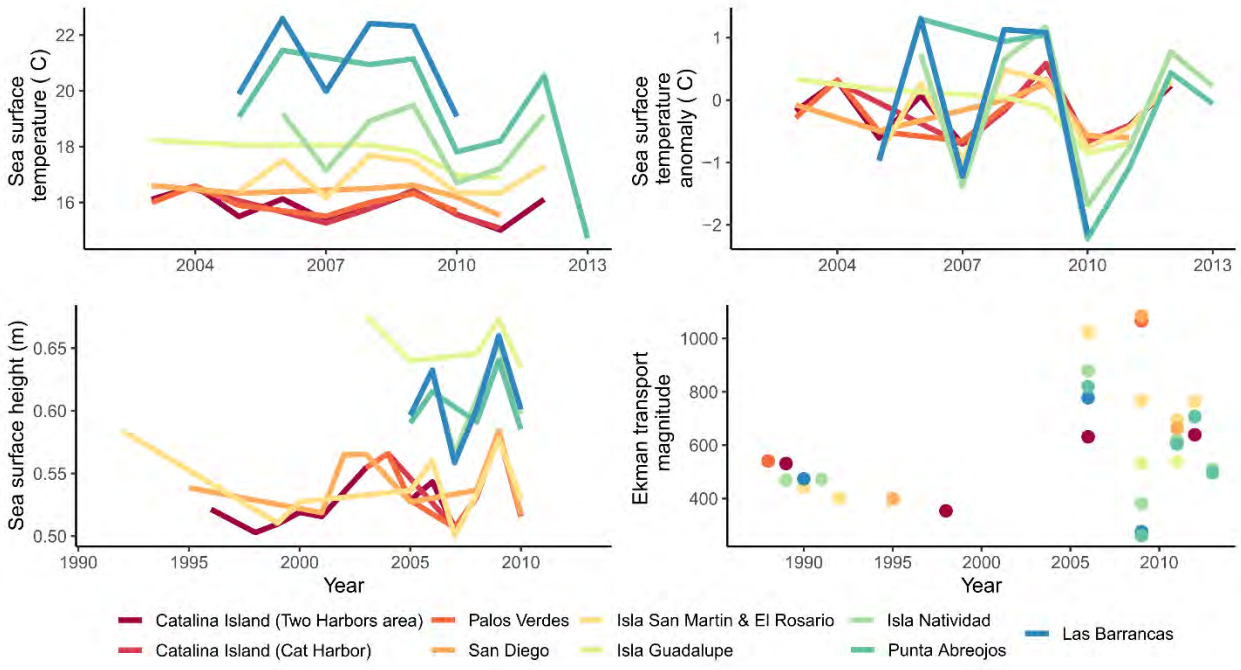

Figure S2.4. Yearly averages of sea surface temperature, sea surface temperature anomaly, sea surface height, and Ekman transport, used for testing if environmental covariates predict genetic diversity. Data were averaged over the period of July-December for each year, corresponding to when muraenid leptocephali are most common in waters off Baja, Mexico and southern California (Fig. S2.1).

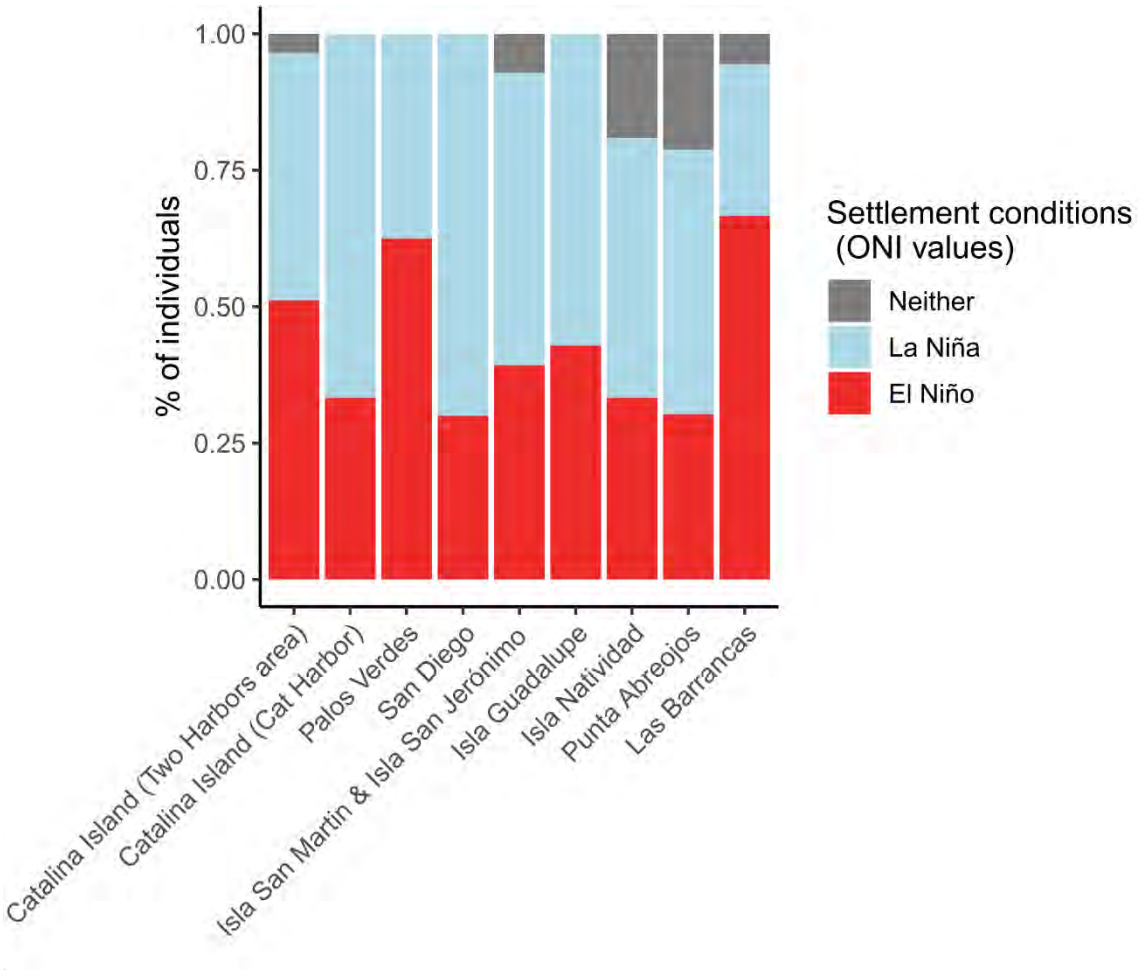

Figure S2.5. We calculated El Niño Southern Oscillation conditions at settlement using methods outlined in Higgins et. al. 2017, which considered ENSO events as being any 6-month period in which Oceanic Nino Index values remained above 0.5. La Niña events were considered any 6-month period where ONI values remained below -0.5. Years where neither condition were met were considered Neutral.

Bibliography

Anneser L, Alcantara IC, Gemmer A, et al (2020) The neuropeptide Pth2 dynamically senses others via mechanosensation. Nature 588:653–657. https://doi.org/10.1038/s41586-020-2988-z

Antao T, Lopes A, Lopes RJ, et al (2008) LOSITAN: A workbench to detect molecular adaptation based on a Fst-outlier method. BMC Bioinformatics 9:1–5. https://doi.org/10.1186/1471-2105-9-323

Asch RG (2015) Climate change and decadal shifts in the phenology of larval fishes in the California Current ecosystem. Proc Natl Acad Sci 112:E4065–E4074. https://doi.org/10.1073/pnas.1421946112

Babin C, Gagnaire PA, Pavey SA, Bernatchez L (2017) RAD-Seq reveals patterns of additive polygenic variation caused by spatially-Varying selection in the American eel (*Anguilla rostrata*). Genome Biol Evol 9:2974–2986. https://doi.org/10.1093/gbe/evx226

Baird NA, Etter PD, Atwood TS, et al (2008) Rapid SNP discovery and genetic mapping using sequenced RAD markers. PLoS One 3:e3376. https://doi.org/10.1371/journal.pone.0003376

Banerjee S, Gelfand AE, Carlin BP (2003) Hierarchical Modeling and Analysis for Spatial Data (Chapman & Hall/CRC Monographs on Statistics & Applied Probability)

Beato S, Toledo-Solís FJ, Fernández I (2020) Vitamin k in vertebrates' reproduction: Further puzzling pieces of evidence from teleost fish species. Biomolecules

10:1–26. https://doi.org/10.3390/biom10091303

Bernardi G, Findley L, Rocha-Olivares A (2003) Vicariance and dispersal across Baja California in disjunct marine fish populations. Evolution (N Y) 57:1599–1609. https://doi.org/10.1111/j.0014-3820.2003.tb00367.x

Besag J (1974) Spatial interaction and the statistical analysis of lattice systems. J R Stat Soc Ser B 36:192–236

Bishop RE, Torres JJ, Crabtree RE (2000) Chemical composition and growth indices in leptocephalus larvae. Mar Biol 137:205–214. https://doi.org/10.1007/s002270000362

Blaxter JHS (1975) The eyes of larval fish. In: Vision in fishes. Springer, Boston, MA, pp 427–443

Briggs JC, Bowen BW (2012) A realignment of marine biogeographic provinces with particular reference to fish distributions. J Biogeogr 39:12–30. https://doi.org/10.1111/j.1365-2699.2011.02613.x

Brothers EB, Thresher RE (1985) Pelagic duration, dispersal, and the distribution of Indo-Pacific coral-reef fishes. In: Reaka ML (ed) The Ecology of Coral Reefs. National Oceanic and Atmospheric Administration, Washington, D.C., pp 53–70

Burgess SC, Baskett ML, Grosberg RK, et al (2016) When is dispersal for dispersal? Unifying marine and terrestrial perspectives. Biol Rev Camb Philos Soc 91:867–882. https://doi.org/10.1111/brv.12198

Carpenter B, Gelman A, Hoffman MD, et al (2017) Stan: A probabilistic programming language. J Stat Softw 76:1–32.

https://doi.org/10.18637/jss.v076.i01

Catchen J, Hohenlohe PA, Bassham S, et al (2013) Stacks: an analysis tool set for population genomics. Mol Ecol 22:3124–40. https://doi.org/10.1111/mec.12354.Stacks

Catchen JM, Amores A, Hohenlohe P, et al (2011) Stacks: Building and genotyping loci de novo from short-read sequences. G3 Genes, Genomes, Genet 1:171–182. https://doi.org/10.1534/g3.111.000240

Chang X, Patiño R, Thomas P, Yoshizaki G (1999) Developmental and protein kinase-dependent regulation of ovarian connexin mRNA and oocyte maturational competence in Atlantic croaker. Gen Comp Endocrinol 114:330–339. https://doi.org/10.1006/gcen.1999.7262

Chelton DB, Bernal PA, McGowan JA (1982) Large-scale interannual physical and biological interaction in the California Current (El Niño). J Mar Res 40:1095–1125

Chen L, Hu J, Yun Y, Wang T (2010) Rab36 regulates the spatial distribution of late endosomes and lysosomes through a similar mechanism to Rab34. Mol Membr Biol 27:23–30. https://doi.org/10.3109/09687680903417470

Cope JM, Key M (2009) Status of Cabezon (*Scorpaenichthys marmoratus*) in California and Oregon Waters as Assessed in 2009

Cowen RK (1985) Large scale pattern of recruitment by the labrid, *Semicossyphus pulcher*: Causes and implications. J Mar Res 43:719–742. https://doi.org/10.1357/002224085788440376

Cowen RK, Sponaugle S (2009) Larval dispersal and marine population connectivity. Ann Rev Mar Sci 1:443–466. https://doi.org/10.1146/annurev.marine.010908.163757

Dale KE, Ramírez-Valdez A, McCosker JE, Love MS (2021) Revising geographic distributions of eastern Pacific moray eels. Bull Mar Sci 97:305–325. https://doi.org/10.5343/bms.2020.0060

Davis JLD (2000) Changes in a tidepool fish assemblage on two scales of environmental variation: Seasonal and El Niño Southern Oscillation. Limnol Oceanogr 45:1368–1379. https://doi.org/10.4319/lo.2000.45.6.1368

Deangelis MM, Wang DG, Hawkins TL (1995) Solid-phase reversible immobilization for the isolation of PCR products. Nucleic Acids Res 23:4742–4743. https://doi.org/10.1093/nar/23.22.4742

Dick EJ, MacCall AD (2010) Estimates of Sustainable Yield for 50 Data-Poor Stocks in the Pacific Coast Groundfish Fishery Management Plan

Diluzio AR, Baliga VB, Higgins BA, Mehta RS (2017) Effects of prey characteristics on the feeding behaviors of an apex marine predator, the California moray (*Gymnothorax mordax*). Zoology 122:80–89

Downie AT, Illing B, Faria AM, Rummer JL (2020) Swimming performance of marine fish larvae: review of a universal trait under ecological and environmental pressure. Rev Fish Biol Fish 30:93–108. https://doi.org/10.1007/s11160-019-09592-w

Durazo R (2015) Seasonality of the transitional region of the California Current

System off Baja California. J Geophys Res Ocean 120:1773–1196. https://doi.org/doi:10.1002/2014JC010405

Earl DA, vonHoldt BM (2012) STRUCTURE HARVESTER: A website and program for visualizing STRUCTURE output and implementing the Evanno method. Conserv Genet Resour 4:359–361. https://doi.org/10.1007/s12686-011-9548-7

Ebert TA, Russell MP (1988) Latitudinal variation in size structure of the west coast purple sea urchin: A correlation with headlands. Limnol Oceanogr 33:286–294

Fernández-Chacón R, Königstorfer A, Gerber SH, et al (2001) Synaptotagmin I functions as a calcium regulator of release probability. Nature 410:41–49. https://doi.org/10.1038/35065004

Gaggiotti OE, Smouse PE (1996) Stochastic migration and maintenance of genetic variation in sink populations. Am Nat 147:919–945

Garcia E, Simison WB, Bernardi G (2020) Patterns of genomic divergence and signals of selection in sympatric and allopatric Northeastern Pacific and Sea of Cortez populations of the sargo (*Anisotremus davidsonii*) and longjaw mudsucker (*Gillichthys mirabilis*). J Hered 111:57–69. https://doi.org/10.1093/jhered/esz071

Garrido S, Ben-Hamadou R, Santos AMP, et al (2015) Born small, die young: Intrinsic, size-selective mortality in marine larval fish. Sci Rep 5:1–10. https://doi.org/10.1038/srep17065

Gerlach G, Atema J, Kingsford MJ, et al (2007) Smelling home can prevent dispersal of reef fish larvae. Proc Natl Acad Sci 104:858–863.

https://doi.org/10.1073/pnas.0606777104

Goudet Jérôm (2005) hierfstat, a package for r to compute and test hierarchical F-statistics. Mol Ecol Notes 5:184–186. https://doi.org/10.1111/j.1471-8286.2004.00828.x

Haenisch C, Diekmann H, Klinger M, et al (2005) The neuronal growth and regeneration associated Cntn1 (F3/F11/Contactin) gene is duplicated in fish: Expression during development and retinal axon regeneration. Mol Cell Neurosci 28:361–374. https://doi.org/10.1016/j.mcn.2004.04.013

Haltuch MA, Johnson KF, Tolimieri N, et al (2019) Status of the sablefish stock in US waters in 2019

Harley CDG, Hughes AR, Hulgren KM, et al (2006) The impacts of climate change in coastal marine systems. Ecol Lett 9:228–241. https://doi.org/10.1111/j.1461-0248.2005.00871.x

Harrison JS, Higgins B, Mehta R (2017) Scaling of dentition and prey size in the California moray (*Gymnothorax mordax*). Zoology 122:16–26

He X, Field JC (2017) Stock assessment update: Status of Bocaccio, *Sebastes paucispinis*, in the Conception, Monterey and Eureka INPFC areas for 2017. Portland, OR

He X, Pearson DE, Field JC, et al (2013) Status of the U.S. Pacific sanddab resource in 2013. Santa Cruz, CA

Hickey BM (1979) The California current system—hypotheses and facts. Prog Oceanogr 8:191–279. https://doi.org/10.1016/0079-6611(79)90002-8

Higgins B, Pearson D, Mehta R (2017) El Niño episodes increase California moray recruits around Santa Catalina Island. J Fish Biol 90:1570–1583. https://doi.org/https://doi.org/10.1111/jfb.13253

Higgins BA, Law CJ, Mehta RS (2018) Eat whole and less often: Ontogenetic shift reveals size specialization on kelp bass by the California moray eel, *Gymnothorax mordax*. Oecologia 188:875–887. https://doi.org/https://doi.org/10.1007/s00442-018-4260-x

Higgins BA, Mehta RS (2018) Distribution and habitat associations of the California moray (*Gymnothorax mordax*) within Two Harbors, Santa Catalina Island, California. Environ Biol Fishes 101:95–108. https://doi.org/https://doi.org/10.1007/s10641-017-0684-0

Higgins BA, Mehta RS (2017) Distribution and habitat associations of the California moray (Gymnothorax mordax) within Two Harbors, Santa Catalina Island, California. J Environ Biol Fishes

Horn MH, Allen LG, Lea RN (2006) Biogeography. In: Allen LG, Horn MH (eds) The Ecology of Marine Fishes: California and Adjacent Waters. University of California Press, Berkeley, CA, pp 3–25

Hsieh CH, Reiss C, Watson W, et al (2005) A comparison of long-term trends and variability in populations of larvae of exploited and unexploited fishes in the Southern California region: A community approach. Prog Oceanogr 67:160–185. https://doi.org/10.1016/j.pocean.2005.05.002

Huang D, Bernardi G (2001) Disjunct Sea of Cortez-pacific ocean *Gillichthys*

mirabilis populations and the evolutionary origin of their Sea of Cortez endemic relative, Gillichthys seta. Mar Biol 138:421–428. https://doi.org/10.1007/s002270000454

Huang W, Chang J, Liao C, et al (2018) Pelagic larval duration, growth rate, and population genetic structure of the tidepool snake moray *Uropterygius micropterus* around the southern Ryukyu Islands, Taiwan, and the central Philippines. PeerJ 6:. https://doi.org/10.7717/peerj.4741

Hunt von Herbing I (2002) Effects of temperature on larval fish swimming performance: The importance of physics to physiology. J Fish Biol 61:865–876. https://doi.org/10.1006/jfbi.2002.2118

Iacchei M, Ben-Horin T, Selkoe KA, et al (2013) Combined analyses of kinship and FST suggest potential drivers of chaotic genetic patchiness in high gene-flow populations. Mol Ecol 22:3476–3494. https://doi.org/10.1111/mec.12341

Jombart T (2008) Adegenet: A R package for the multivariate analysis of genetic markers. Bioinformatics 24:1403–1405. https://doi.org/10.1093/bioinformatics/btn129

Keller AA, Bradburn MJ, Simon VH (2013) Shifts in condition and distribution of eastern North Pacific flatfish along the U.S. west coast (2003-2010). Deep Res Part I Oceanogr Res Pap 77:23–35. https://doi.org/10.1016/j.dsr.2013.03.003

Kitambi SS, Hauptmann G (2007) The zebrafish orphan nuclear receptor genes nr2e1 and nr2e3 are expressed in developing eye and forebrain. Gene Expr Patterns 7:521–528. https://doi.org/10.1016/j.modgep.2006.10.006

Kruse GH, Huyer A (1983) Relationships among shelf temperatures, coastal sea level, and the coastal upwelling index off Newport, Oregon. Can J Fish Aquat Sci 40:238–242. https://doi.org/10.1139/f83-034

Laidig TE, Chess JR, Howard DF (2007) Relationship between abundance of juvenile rockfishes (*Sebastes* spp.) and environmental variables documented off northern California and potential mechanisms for the covariation. Fish Bull 105:39–48

Latimer AM, Wu S, Gelfand AE, Silander, Jr. JA (2006) Building statistical models to analyze species distributions. Ecol Appl 16:33–50

Lawson DJ, van Dorp L, Falush D (2018) A tutorial on how not to over-interpret STRUCTURE and ADMIXTURE bar plots. Nat Commun 9:1–11. https://doi.org/10.1038/s41467-018-05257-7

Leggett WC, Deblois E (1994) Recruitment in marine fishes: Is it regulated by starvation and predation in the egg and larval stages? Netherlands J Sea Res 32:119–134. https://doi.org/10.1016/0077-7579(94)90036-1

Leis J (1991) The pelagic phase of coral reef fishes: Larval biology of coral reef fishes. In: The ecology of fishes on coral reefs. Academic Press, pp 183–230

Leis JM (2018) Paradigm lost: Ocean acidification will overturn the concept of larval-fish biophysical dispersal. Front Mar Sci 5:1–9. https://doi.org/10.3389/fmars.2018.00047

Leis JM, Caselle JE, Bradbury IR, et al (2013) Does fish larval dispersal differ between high and low latitudes? Proc R Soc B Biol Sci 280:1–9. https://doi.org/10.1098/rspb.2013.0327

Leising A, Schroeder I, Bograd S, et al (2014) State of the California Current 2013-14: El Niño looming. CalCOFI Reports 55:51–87

Leising AW, Schroeder ID, Bograd SJ, et al (2015) State of the California Current 2014-15: Impacts of the Warm-Water "Blob." CalCOFI Reports 56:31–68

Lester SE, Ruttenberg BI (2005) The relationship between pelagic larval duration and range size in tropical reef fishes: A synthetic analysis. Proc R Soc B Biol Sci 272:585–591. https://doi.org/10.1098/rspb.2004.2985

Li Y, Zhang L, Song P, et al (2021) Genetic homogeneity detectable in the sedentary moray eel *Gymnothorax minor* based on mitochondrial DNA analysis. Reg Stud Mar Sci 41:101504. https://doi.org/10.1016/j.rsma.2020.101504

Limouzy-Paris CB, Graber HC, Jones DL, et al (1997) Translocation of larval coral reef fishes via sub-mesoscale spin-off eddies from the Florida current. Bull Mar Sci 60:966–983

Llopiz JK, Cowen RK, Hauff MJ, et al (2014) Early life history and fisheries oceanography: New questions in a changing world. Oceanography 27:26–41

Lluch-Belda D, Lluch-Cota DB, Lluch-Cota SE (2005) Changes in marine faunal distributions and ENSO events in the California Current. Fish Oceanogr 14:458–467

Loke-smith KA (2011) Status of the Fisheries Report 2011: California sheephead, Semicossyphus pulcher

López-Martínez J, Herrera-Valdivia E, Rodríguez-Romero J, Hernández-Vázquez S (2010) Peces de la fauna de acompañamiento en la pesca industrial de camarón

en el golfo de california, México. Rev Biol Trop 58:925–942. https://doi.org/10.15517/rbt.v58i2.5255

López-Pérez RA, Calderon-Aguilera LE, Zepeta-Vilchis RC, et al (2013) Species composition, habitat configuration and seasonal changes of coral reef fish assemblages in western Mexico. J Appl Ichthyol 29:437–448. https://doi.org/10.1111/jai.12029

Lynn RJ, Bograd SJ (2002) Dynamic evolution of the 1997-1999 El Niño-La Niña cycle in the southern California Current System. Prog Oceanogr 54:59–75

Marshall DJ, Monro K, Bode M, et al (2010) Phenotype-environment mismatches reduce connectivity in the sea. Ecol Lett 13:128–140. https://doi.org/10.1111/j.1461-0248.2009.01408.x

McClatchie S, Goericke R, Leising A, et al (2016) State of the California current 2015-16: Comparisons with the 1997-98 El Niño. Calif Coop Ocean Fish Investig Reports 57:5–61

McCleneghan K (1973) The ecology and behavior of the California moray eel Gymnothorax mordax (Ayres, 1859) with descriptions of its larva and the leptocephali of some other East Pacific Muraenidae. University of Southern California

Mehta RS, Dale KE, Higgins BA (2020) Marine protection induces morphological variation in the California moray *Gymnothorax mordax*. Integr Comp Biol icaa061:522–534. https://doi.org/https://doi.org/10.1093/icb/icaa061

Mejía-ruíz P, Perez-enriquez R, Mares-mayagoitia JA, Valenzuela-quiñonez F (2020)

Population genomics reveals a mismatch between management and biological units in green abalone (*Haliotis fulgens*). PeerJ 1–23. https://doi.org/10.7717/peerj.9722

Mes D, Palstra AP, Henkel C V., et al (2020) Swimming exercise enhances brain plasticity in fish. R Soc Open Sci 7:. https://doi.org/10.1098/rsos.191640

Miller MJ (2009) Ecology of Anguilliform leptocephali: Remarkable transparent fish larvae of the ocean surface layer. Aqua-BioScience Monogr 2:1–94. https://doi.org/10.5047/absm.2009.00204.0001

Miller MJ (2002) Contrasting migratory strategies of marine and freshwater eels. Fish Sci 68:37–40

Miller MJ, Tsukamoto K (2020) The behavioral ecology and distribution of leptocephali: marine fish larvae with unforeseen abilities. Mar Biol 167:1–21. https://doi.org/10.1007/s00227-020-03778-8

Miller MR, Dunham JP, Amores A, et al (2007) Rapid and cost-effective polymorphism identification and genotyping using restriction site associated DNA (RAD) markers. Genome Res 17:240–248. https://doi.org/10.1101/gr.5681207

Muller UK, van den Boogaart JGM, van Leeuwen JL (2008) Flow patterns of larval fish: undulatory swimming in the intermediate flow regime. J Exp Biol 211:196–205. https://doi.org/10.1242/jeb.005629

Naisbett-Jones L, Putman N, Stephenson J, et al (2017) A magnetic map leads juvenile European eels to the Gulf stream. Curr Biol 27:1–5.

https://doi.org/10.1016/j.cub.2017.03.015

Nevárez-Martínez MO, Balmori-Ramírez A, Miranda-Mier E, et al (2008) Estructura de tallas, selectividad y composición específica de las capturas en trampas para peces marinos en el Golfo de California. Rev Biol Trop 56:1403–1417. https://doi.org/10.15517/rbt.v56i3.5718

Nielsen JM, Rogers LA, Brodeur RD, et al (2021) Responses of ichthyoplankton assemblages to the recent marine heatwave and previous climate fluctuations in several Northeast Pacific marine ecosystems. Glob Chang Biol 27:506–520. https://doi.org/10.1111/gcb.15415

Novembre J (2016) Pritchard, Stephens, and Donnelly on population structure. Genetics 204:391–393. https://doi.org/10.1534/genetics.116.195164

Olena AF, Rao MB, Thatcher EJ, et al (2015) MiR-216a regulates snx5, a novel notch signaling pathway component, during zebrafish retinal development. Dev Biol 400:72–81. https://doi.org/10.1016/j.ydbio.2015.01.016

Parrish RH, Nelson CS, Bakun A, et al (1981) Transport mechanisms and reproductive success of fishes in the California Current. Biol Oceanogr 1:175–203

Paterson CN, Chabot CL, Robertson JM, et al (2015) The genetic diversity and population structure of barred sand bass, *Paralabrax nebulifer*: A historically important fisheries species off southern and Baja California. Calif Coop Ocean Fish Investig Reports 56:1–13

Pavey SA, Gaudin J, Normandeau E, et al (2015) RAD sequencing highlights

polygenic discrimination of habitat ecotypes in the panmictic American eel. Curr Biol 25:1666–1671. https://doi.org/10.1016/j.cub.2015.04.062

Pinsky ML, Selden RL, Kitchel ZJ (2020) Climate-driven shifts in marine species ranges: Scaling from organisms to communities. Ann Rev Mar Sci 12:153–179. https://doi.org/10.1146/annurev-marine-010419-010916

Pritchard JK, Stephens M, Donnelly P (2000) Inference of population structure using multilocus genotype data. Genetics 155:945–959

Pujolar JM, Jacobsen MW, Als TD, et al (2014) Genome-wide single-generation signatures of local selection in the panmictic European eel. Mol Ecol 23:2514–2528. https://doi.org/10.1111/mec.12753

Ralston S, Sakuma KM, Field JC (2013) Interannual variation in pelagic juvenile rockfish (*Sebastes* spp.) abundance - going with the flow. Fish Oceanogr 22:288–308. https://doi.org/10.1111/fog.12022

Reece JS, Bowen BW, Joshi K, et al (2010) Phylogeography of two moray eels indicates high dispersal throughout the Indo-Pacific. J Hered 101:391–402. https://doi.org/10.1093/jhered/esq036

Reece JS, Bowen BW, Smith DG, Larson A (2011) Comparative phylogeography of four Indo-Pacific moray eel species (Muraenidae) reveals comparable ocean-wide genetic connectivity despite five-fold differences in available adult habitat. Mar Ecol Prog Ser 437:269–277. https://doi.org/10.3354/meps09248

Resendes RJ (2022) Spatiotemporal characterization of the prr12 paralogues in zebrafish. University of Western Ontario

Ribout C, Bech N, Briand MJ, et al (2018) A lack of spatial genetic structure of *Gymnothorax chilospilus* (moray eel) suggests peculiar population functioning. Biol J Linn Soc 125:142–151. https://doi.org/10.1093/BIOLINNEAN/BLY107

Riebler A, Sørbye SH, Simpson D, et al (2016) An intuitive Bayesian spatial model for disease mapping that accounts for scaling. Stat Methods Med Res 25:1145–1165. https://doi.org/10.1177/0962280216660421

Robertson DR (David R, Cramer KL (2009) Shore fishes and biogeographic subdivisions of the Tropical Eastern Pacific. Mar Ecol Prog Ser 380:1–17. https://doi.org/10.3354/meps07925

Rodríguez-Romero J, Palacios-Salgado DS, López-Martínez J, et al (2008) Composición taxonómica y relaciones zoogeográficas de los peces demersales de la costa occidental de Baja California Sur, México. Rev Biol Trop 56:1765–1783. https://doi.org/10.15517/rbt.v56i4.5758

Rombough PJ (1997) The effects of temperature on embryonic and larval development. In: Seminar Series-Society for Experimental Biology. Cambridge University Press, Cambridge, pp 177–224

Ruiz-Campos G, González-Guzmán S, Ramírez-Valdez A, et al (2010) Composition, density and biogeographic affinities of the rocky intertidal fishes on the western coast of the Baja California peninsula, Mexico. Calif Coop Ocean Fish Investig Reports 51:210–220

Sanford E, Holzman SB, Haney RA, et al (2006) Larval tolerance, gene flow, and the northern geographic range limits of fiddler crabs. Ecology 87:2882–2894.

https://doi.org/https://doi.org/10.1890/0012-9658(2006)87[2882:LTGFAT]2.0.CO;2

Sanford E, Roth MS, Johns GC, et al (2003) Local selection and latitudinal variation in a marine predator-prey interaction. Science (80-) 300:1135–1137

Santini F, Kong X, Sorenson L, et al (2013) A multi-locus molecular timescale for the origin and diversification of eels (Order: Anguilliformes). Mol Phylogenet Evol 69:884–894. https://doi.org/10.1016/j.ympev.2013.06.016

Schirripa MJ, Colbert J. J (2006) Interannual changes in sablefish (*Anoplopoma fimbria*) recruitment in relation to oceanographic conditions within the California Current System. Fish Oceanogr 15:25–36. https://doi.org/10.1111/j.1365-2419.2005.00352.x

Schroeder ID, Santora JA, Bograd SJ, et al (2019) Source water variability as a driver of rockfish recruitment in the california current ecosystem: Implications for climate change and fisheries management. Can J Fish Aquat Sci 76:950–960. https://doi.org/10.1139/cjfas-2017-0480

Schweitzer J, Gimnopoulos D, Lieberoth BC, et al (2007) Contactin1a expression is associated with oligodendrocyte differentiation and axonal regeneration in the central nervous system of zebrafish. Mol Cell Neurosci 35:194–207. https://doi.org/10.1016/j.mcn.2007.02.018

Selkoe KA, Toonen RJ (2011) Marine connectivity: a new look at pelagic larval duration and genetic metrics of dispersal. Mar Ecol Prog Ser 436:291–305. https://doi.org/10.3354/meps09238

Selkoe KA, Vogel A, Gaines SD (2007) Effects of ephemeral circulation on recruitment and connectivity of nearshore fish populations spanning Southern and Baja California. Mar Ecol Prog Ser 351:209–220. https://doi.org/10.3354/meps07157

Selkoe KA, Watson JR, White C, et al (2010) Taking the chaos out of genetic patchiness: Seascape genetics reveals ecological and oceanographic drivers of genetic patterns in three temperate reef species. Mol Ecol 19:3708–3726. https://doi.org/10.1111/j.1365-294X.2010.04658.x

Shanks AL (2009) Pelagic larval duration and dispersal distance revisited. Biol Bull 216:373–385. https://doi.org/10.2307/25548167

Shanks AL, Eckert GL (2005) Population persistence of California Current fishes and benthic crustaceans: A marine drift paradox. Ecol Monogr 75:505–524

Sifa L, Mathias JA (1987) The critical period of high mortality of larvae fish -A discussion based on current research. Chinese J Oceanol Limnol 5:80–96. https://doi.org/10.1007/BF02848526

Simon AM, Goodenough DA, Li E, Paul DL (1997) Female infertility in mice lacking connexin 37. Nature 385:525–526. https://doi.org/10.1038/385522a0

Sivasundar A, Palumbi SR (2010) Life history, ecology and the biogeography of strong genetic breaks among 15 species of Pacific rockfish, *Sebastes*. Mar Biol 157:1433–1452. https://doi.org/10.1007/s00227-010-1419-3

Smith PE, Richardson SL (1977) Standard techniques for pelagic fish egg and larva surveys. Rome

Snyder MA, Sloan LC, Diffenbaugh NS, Bell JL (2003) Future climate change and upwelling in the California Current. Geophys Res Lett 30:1–4. https://doi.org/10.1029/2003GL017647

Sotka EE (2012) Natural selection, larval dispersal, and the geography of phenotype in the sea. Integr Comp Biol 52:538–545. https://doi.org/10.1093/icb/ics084

Stachura MM, Essington TE, Mantua NJ, et al (2014) Linking Northeast Pacific recruitment synchrony to environmental variability. Fish Oceanogr 23:389–408. https://doi.org/10.1111/fog.12066

Stan Development Team (2022) Stan Modeling Language Users Guide and Reference Manual, version 2.29

Stawitz CC, Essington TE, Branch TA, et al (2015) A state-space approach for detecting growth variation and application to North Pacific groundfish. Can J Fish Aquat Sci 72:1316–1328. https://doi.org/10.1139/cjfas-2014-0558

Stobutzki I, Bellwood D (1997) Sustained swimming abilities of the late pelagic stages of coral reef fishes. Mar Ecol Prog Ser 149:35–41

Strathmann RR, Hughes TP, Kuris AM, et al (2002) Evolution of local recruitment and its consequences for marine populations. Bull Mar Sci 70:377–396

Takeuchi M, Inoue C, Goshima A, et al (2017) Medaka and zebrafish contactin1 mutants as a model for understanding neural circuits for motor coordination. Genes to Cells 22:723–741. https://doi.org/10.1111/gtc.12509

Taylor SM, Loew ER, Grace MS (2015) Ontogenic retinal changes in three ecologically distinct elopomorph fishes (Elopomorpha:Teleostei) correlate with

light environment and behavior. Vis Neurosci 32:1–13. https://doi.org/10.1017/S0952523815000024

Taylor SM, Loew ER, Grace MS (2011) A rod-dominated visual system in leptocephalus larvae of elopomorph fishes (Elopomorpha: Teleostei). Environ Biol Fishes 92:513–523. https://doi.org/10.1007/s10641-011-9871-6

Thompson AR, Auth TD, Brodeur RD, et al (2014) Dynamics of larval fish assemblages in the California Current System: A comparative study between Oregon and southern California. Mar Ecol Prog Ser 506:193–212. https://doi.org/10.3354/meps10801

Thompson AR, Ben-Aderet NJ, Bowlin NM, et al (2022) Putting the Pacific marine heatwave into perspective: The response of larval fish off southern California to unprecedented warming in 2014–2016 relative to the previous 65 years. Glob Chang Biol 28:1766–1785. https://doi.org/10.1111/gcb.16010

Timmermann A, Oberhuber J, Bacher A, et al (1999) Increased El Niño frequency in a climate model forced by future greenhouse warming. Nature 398:694–696. https://doi.org/https://doi.org/10.1038/19505

Vehtari A, Gelman A, Gabry J (2017) Practical Bayesian model evaluation using leave-one-out cross-validation and WAIC. Stat Comput 27:1413–1432. https://doi.org/10.1007/s11222-016-9696-4

Walker HJ, Hastings PA, Hyde JR, et al (2020) Unusual occurrences of fishes in the southern California Current system during the warm water period of 2014–2018. Estuar Coast Shelf Sci 236:106634.

https://doi.org/https://doi.org/10.1016/j.ecss.2020.106634

Wang R, Zhang Y, Liu S, et al (2014) Analysis of 52 Rab GTPases from channel catfish and their involvement in immune responses after bacterial infections. Dev Comp Immunol 45:21–34. https://doi.org/10.1016/j.dci.2014.01.026

Wang T, Liu F, Tian G, et al (2019) Lineage/species-specific expansion of the Mx gene family in teleosts: Differential expression and modulation of nine Mx genes in rainbow trout Oncorhynchus mykiss. Fish Shellfish Immunol 90:413–430. https://doi.org/10.1016/j.fsi.2019.04.303

Weersing K, Toonen RJ (2009) Population genetics, larval dispersal, and connectivity in marine systems. Mar Ecol Prog Ser 393:1–12. https://doi.org/10.3354/meps08287

Wilson DT, Meekan MG (2002) Growth-related advantages for survival to the point of replenishment in the coral reef fish *Stegastes partitus* (Pomacentridae). Mar Ecol Prog Ser 231:247–260. https://doi.org/10.3354/meps231247

Wittkopp N, Huntzinger E, Weiler C, et al (2009) Nonsense-mediated mRNA decay effectors are essential for zebrafish embryonic development and survival. Mol Cell Biol 29:3517–3528. https://doi.org/10.1128/mcb.00177-09

Xie S, Han S, Qu Z, et al (2019) Knockout of Nr2e3 prevents rod photoreceptor differentiation and leads to selective L-/M-cone photoreceptor degeneration in zebrafish. Biochim Biophys Acta - Mol Basis Dis 1865:1273–1283. https://doi.org/10.1016/j.bbadis.2019.01.022

Xu K, Xie X, Qi G, et al (2019) Grass carp STK38 regulates IFN I expression by

decreasing the phosphorylation level of GSK3β. Dev Comp Immunol 99:103410. https://doi.org/10.1016/j.dci.2019.103410

Yang Y, Enis D, Zheng H, et al (2015) Cell adhesion mediated by VCAM-ITGα9 interactions enables lymphatic development. Arterioscler Thromb Vasc Biol 35:1179–1189. https://doi.org/10.1161/ATVBAHA.114.304997

Yoo KW, Kim EH, Jung SH, et al (2006) Snx5, as a Mind bomb-binding protein, is expressed in hematopoietic and endothelial precursor cells in zebrafish. FEBS Lett 580:4409–4416. https://doi.org/10.1016/j.febslet.2006.07.009